UNIVERSIDADE DE SÃO PAULO

INSTITUTO DE ASTRONOMIA, GEOFÍSICA E CIÊNCIAS ATMOSFÉRICAS

DEPARTAMENTO DE GEOFÍSICA

PLINIO FRANCISCO JAQUETO

Speleothem magnetism: environmental and geomagnetic

records from Brazil

São Paulo

2021

PLINIO FRANCISCO JAQUETO

Speleothem magnetism: environmental and geomagnetic records from Brazil

Thesis to be presented to the Geophysics Department of Instituto de Astronomia, Geofísica e Ciências Atmosféricas from Universidade de São Paulo as requisite for the PhD title.

Versão Corrigida. O original encontra-se disponível na Unidade

Concentration area: Geophysics
Advisor: Prof. Dr. Ricardo Ivan Ferreira da Trindade

São Paulo

2021

This thesis is dedicated to Daniele, Guilherme
and my parents, who always gave me support
and love, the most important part of life.

Acknowledgments

I am grateful to Instituto Chico Mendes de Conservação da Biodiversidade (ICMBio) for providing permission to collect stalagmite samples.

I would like to thank my advisor, professor Ricardo Trindade, for the help throughout these years.

I'm grateful to professor Josh M. Feinberg, who supervised me at the IRM during my internship and always provided a good discussion on his research group about science and beyond.

This research could only happen because of the professors Francisco William da Cruz Jr. (Chico Bill) and Ivo Karmann from Instituto de Geociências. They always encourage and discuss the study with speleothem and provided free access to the karst lab.

From the speleothem research group, I'll be forever grateful to Valdir and Nicolás that joined me in this research subject and took me to caves around Brazil. Their support on discussion and queries changed my vision about science and how we can move forward with it.

I am grateful to the USPMag, especially Janine, Jhon, Filipe Temporim, Wilbor, Grasiane, Karine, Elder, Gelvam, Janine, Aruã, Rafael (Cabelo), Giovanni, Sônia, Filipe, Thiago and everyone that the names I cannot remember (feel included here).

I am also grateful to many researchers that I was able to meet throughout these years, and I won't be able to name all of them here, but I would like to say thanks for the fruitful discussions and papers that we published together.

I am very grateful for IAG Staff, especially Wellington, Márcio, Antônio, Roberto, Eliza and professors.

My friends that always understood when I needed to be focused and when we could have some good laughs.

My parents and family have always been an inspiration to me, and I will always be grateful for their support and care.

Daniele and Guilherme will always be part of my life, I love them and no words can express how much they changed me for good, with all the wisdom and patience that they have.

Abstract

Jaqueto, P. (2021). Speleothem magnetism: environmental and geomagnetic records from Brazil (PhD Thesis). Instituto de Astronomia, Geofísica e Ciências Atmosféricas, Universidade de São Paulo, São Paulo.

In the last decade, a revival in the use of stalagmites for paleomagnetic and environmental magnetism was observed. The advent of more sensitive magnetometers and a new generation of radiometric dating techniques made it possible to obtain high-resolution magnetic records in speleothems. In this thesis, both aspects of speleothem magnetism research were explored. First, a database of magnetic mineral properties from 22 caves in Brazil was built to comprehend the magnetic signal recorded in tropical-subtropical karst regions and how it relates to biomes and climate at different latitudes. This database has demonstrated the pervasive occurrence of low-coercivity magnetic minerals, without significant changes in magnetic mineralogy across the studied speleothem, all presenting pedogenic magnetite/maghemite (and sometimes goethite). Its concentration parameters presented some correlation with the local biome. These results reinforce the hypothesis that the soil's local dynamics above the cave control the magnetic signal recorded in speleothems. Then, two high-resolution records of the geomagnetic field were obtained from sites in western Brazil under the influence of the South Atlantic Anomaly. In this region, the geomagnetic field presents the lowest intensity value of the globe. Both sites provided coherent directional and relative paleointensity results. The last two millennia were investigated with two stalagmites from Pau d'Alho cave (15.21° S, 56.81° W) and revealed fast angular variations (> 0.10°/yr) for two distinct periods at 860 CE to 960 CE and 1450 CE to 1750 CE. These variations correspond to records obtained in South Africa with a westward time lag of ~200 years and express the recurrence of the South Atlantic Anomaly in the last two millennials in the southern hemisphere. This behavior is explained by the westward drift of reverse flux patches at the core-mantle boundary accompanied by their intensification and expansion. A stalagmite from Dona Benedita cave (20.57° S, 56.72° W) encompasses ~2100 years of record from mid-to-late Holocene. In contrast to the Pau d'Alho speleothems, the Dona Benedita speleothem revealed low angular variations below 0.06°/yr, expressing a low activity of non-dipolar sources in South America for this period, ultimately revealing that the South Atlantic Anomaly is an intermittent or absent feature whose expression depends on the non-dipole/dipole ratio of geomagnetic components and the density of reverse flux patches in the southern hemisphere. Therefore, the magnetic record of speleothems

provided key information for the reconstruction of soil dynamics and for tracking at high-resolution the evolution of the geomagnetic field in South America, where data is known to be scarce.

Resumo

Jaqueto, P. (2021). Magnetismo em espeleotemas: registros ambientais e geomagnéticos do Brasil (Tese de doutorado). Instituto de Astronomia, Geofísica e Ciências Atmosféricas, Universidade de São Paulo, São Paulo.

Na última década, um renascimento no uso de estalagmites para magnetismo paleomagnético e ambiental foi observado. O advento de magnetômetros mais sensíveis e uma nova geração de técnicas de datação radiométrica possibilitaram a obtenção de registros magnéticos de alta resolução em espeleotemas. Nesta tese, ambos os aspectos da pesquisa do magnetismo em espeleotemas foram explorados. Primeiramente, um banco de dados de propriedades de minerais magnéticos de 22 cavernas no Brasil foi construído para compreender o sinal magnético registrado em regiões cársticas tropicais-subtropicais e como ele se relaciona com biomas e clima em diferentes latitudes. Este banco de dados demonstrou a ocorrência de minerais magnéticos de baixa coercividade, sem alterações significativas na mineralogia magnética e todos apresentando magnetita/maghemita pedogênica (e às vezes goetita). A concentração de minerais magnéticos apresentou correlação com o bioma local. Esses resultados reforçam a hipótese de que a dinâmica local do solo acima da caverna controla o sinal magnético registrado nos espeleotemas. Em seguida, dois registros de alta resolução do campo geomagnético foram obtidos no Brasil central, uma área sob influência da Anomalia do Atlântico Sul. Nesta região, o campo geomagnético apresenta o menor valor do globo. Ambos os sítios forneceram resultados coerentes direcionais e de paleointensidade relativa. Os últimos dois milênios foram investigados com duas estalagmites da caverna Pau d'Alho (15,21° S, 56,81° W) e mostram variações angulares rápidas (> 0,10 °/ano) por dois períodos distintos em 860 AD a 960 AD e 1450 AD a 1750 AD. Essas variações correspondem aos registros obtidos na África do Sul com uma defasagem de tempo de ~ 200 anos e expressam a recorrência da Anomalia do Atlântico Sul para os últimos dois milênios no hemisfério sul. Estas variações podem ser explicadas pela deriva para oeste e lóbulos de fluxo reverso na interdace manto-núcleo acompanhadas por sua intensificação e expansão. Depois, uma estalagmite da caverna Dona Benedita (20,57 ° S, 56,72 ° W) abrange um período de 2100 anos de registro do Holoceno médio a tardio. Em contraste com os espeleotemas Pau d'Alho, a estalagmite da caverna Dona Benedita revelou baixas variações angulares, com valores menores que 0,06 °/ ano, expressando uma baixa atividade de fontes não-dipolares na América do Sul para este período. Esta baixa atividade mostra que a presença da Anomalia do

Atlântico Sul é intermitente ou ausente durante este período para esta região, cuja expressão depende da razão não-dipolar/ dipolar das componentes do campo geomagnético e da densidade dos lóbulos de fluxo reverso hemisfério sul. Portanto, podemos concluir que o registro magnético de espeleotemas forneceu informações essenciais para a reconstrução da dinâmica do solo e para o registros em alta resolução da evolução do campo geomagnético na América do Sul, onde os dados são sabidamente escassos.

Contents

Chapter 1   Introduction

Retrieving climate information through instruments is limited in time to the last four centuries. Information about the climate beyond the instrumental era is obtained indirectly from natural archives, where different types of "indicators" or "proxies" enable the reconstruction of the climate in the last thousands to millions of years. These paleoclimatic and paleoenvironmental "proxies" (e.g., concentration, types of deposited materials, gas concentration) need to be: sensitive to changes in the environment, preserved in time, and its relation to climate has to be understood. The natural archives' sensitivity and the proxies have to be understood in terms of global or local environmental variations (Ruddiman, 2008). Moreover, these proxies must be converted into parameters that can be incorporated into general circulation models to simulate global climate response at a particular time.

Paleoclimatic proxies are divided into four major categories: lithological/mineralogical, geochemical, geophysical, and paleontological (Ruddiman, 2008). Examples of lithological/mineralogical categories include indicators of glaciation, such as ice-rafted debris, moraines, varved sediments, indicators of warm climate, such as carbonates and evaporites, and indicators of paleoprecipitation, such as speleothems and paleosols loess deposits. With ice-cores and chemical sediments studies, the geochemical category includes stable isotopes like $^{18}O/^{16}O$, $^{13}C/^{12}C$, major and trace elements like iron, magnesium, and strontium. The geophysical category includes dating and rapid climate oscillations accessed through paleomagnetism and electrical conductivity studies. The paleontological category includes tree rings, planktonic and benthic foraminifera, pollen, and others (Gornitz, 2009), which provide estimation of age, paleotemperature, paleoclimate, and ocean productivity.
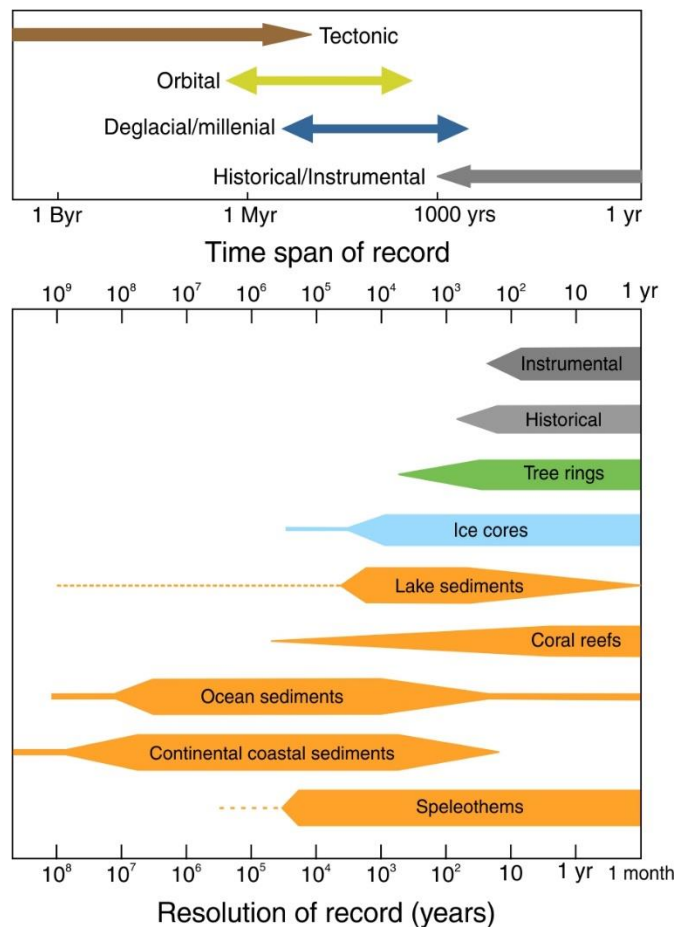
Figure 1-1: Resolution of climate records. (*Upper*) A time span of the processes that are present in the climate information. (*Lower*) Types of climate archives and resolution. (Figure modified with the addition of speleothem records (Ruddiman, 2008)).

The duration and resolution of each record will allow the comprehension of different processes and the effects of specific forcings (Figure 1-1). Among the terrestrial records, speleothems are one of the most used archives for paleoclimatic information. Speleothems are secondary carbonate deposits formed in caves (see section 1.2) and have the advantage that their location tends to be sheltered from perturbation and changes in reducing conditions with a stable climate over some time (Fairchild et al., 2006). One of the strengths of speleothem-based studies is the chronological control made through Uranium-series dating, which provides very precise dating back to 800,000 years (Cheng et al., 2013) (Figure 1-1). Studies of oxygen and carbon isotopes in stalagmites have documented climatic changes associated with Heinrich events, East-Asian monsoon intensity, shifts in Intertropical Convergence Zone, atmospheric CO_2, and regional relative proportions C_3 and C_4 vegetation (Fairchild and Baker, 2012; Meyer et al., 2014).

A proxy that has also been used in speleothems to assess paleoclimate is their magnetism (Hatfield, 2014). Magnetic properties are usually sensitive to the presence of iron. Iron is the fourth most abundant element in the crust and is commonly combined with oxygen and sulfur through inorganic or biological mediated processes. They form iron oxides and iron hydroxides when combined with oxygen and iron sulfides with sulfur. Studying these magnetic minerals, their concentration in rocks and sediments, how they are formed, transported, deposited, and related to climatic conditions constitutes a research topic called 'environmental magnetism' (see section 1.1).

1.1 Environmental magnetism

The field of 'environmental magnetism' started effectively in the early 20th century with the study of Quaternary Swedish varved lake sediments by Gustaf Ising (Maher, 1998). It comprises the measurement of magnetic susceptibility and natural remanent magnetization of the layered sediments. It has shown a yearly periodicity in magnetic properties, with varves deposited during spring being more magnetic than those from the winter.

Information about the magnetic minerals assembly focuses primarily on three broad questions: (1) composition, (2) concentration, and (3) size of magnetic particles (Evans and Heller, 2003). Information provided by these parameters is intimately linked to the iron cycle. This cycle operates at different scales, including global iron connections (desert dust, ocean biochemistry, and climate) and local or *in situ* transformation of iron oxides and iron sulfides.

Environmental magnetism is broadly used in paleoclimatic reconstructions. Wind-blown dust (loess) deposits have been a subject of intense investigation through the past decades (Maher, 2011). The north-central Chinese loess plateau covers the last three million years of Earth's history. It is composed of layers of paleosols (fossil soils) and wind-blown dust, where magnetic susceptibility tracks monsoonal variation. The layers more enriched in nanoscale magnetic grains reflect warmer interglacial and wetter climates, whereas weakly magnetic dust layers correspond to drier, colder glacial periods (Ahmed and Maher, 2018; Maher, 1998; Maher and Thompson, 1999). These results have been correlated with marine oxygen isotope changes (Figure 1-2) and interpreted as the strong coupling between the Asian monsoon system and global glacial cycles (Evans and Heller, 2003). The causes of the magnetic enhancement in loess soils were also extensively investigated. The magnetic minerals in these soils

comprise a mixing of iron-hydroxides, maghemite and magnetite. The enrichment is closely connected to well-drained, oxidizing soils, where the pedogenic formation of magnetite is induced by rainfall variation, soil wetness and local redox conditions (Ahmed and Maher, 2018). The ultrafine magnetite formed in the range size of superparamagnetic (SP) to a stable single domain (SSD, ~50 nm) will undergo slow oxidation forming a thin maghemite rim that depends on pH and temperature and can take millions of years to fully oxidize into maghemite (Ahmed and Maher, 2018).
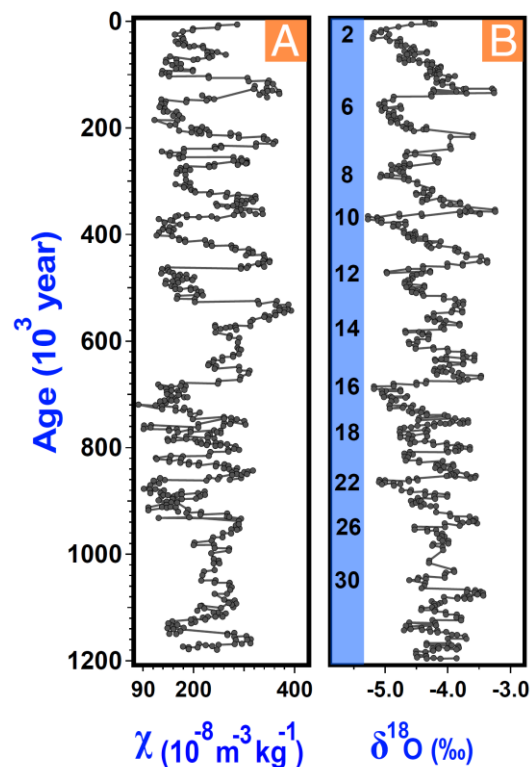

Figure 1-2: (a) Magnetic susceptibility results from wind-blown deposits in the Chinese loess plateau and (b) marine benthic oxygen isotope from the eastern equatorial Pacific (ODP site 677) (Ahmed and Maher, 2018).

These environmental changes recorded by magnetic minerals in sediments, wind-blown deposits, lakes, and speleothems occur in two ways. Magnetic minerals have already been originated elsewhere and then are transported (detrital) or created/transformed in situ (authigenic). The process of in-situ transformation can occur via inorganic chemical reactions or be biologically mediated (Evans and Heller, 2003). These pathways of transformation are of interest in soil science, environmental magnetism, and paleoclimate science, especially concerning rainfall and the magnetic enhancement in soils (Figure 1-3) (Balsam et al., 2011; Heslop and Roberts, 2013; Maxbauer et al., 2016a). Despite the long efforts to understand magnetic

enhancement, no general theory was provided yet, due to the complexity, diversity, and interaction of processes involved (Evans and Heller, 2003; Jordanova, 2017; Maxbauer et al., 2017).

Five mechanisms have been proposed to explain the magnetic enhancement in soils:

(1) 'fermentation' process (Maher and Taylor, 1988), in which redox oscillation of wet/dry cycles promote the formation of very fine-grained magnetite; this 'fermentation' process under anoxic condition is often coupled to the microbial reduction of Fe^{3+} in a process called dissimilatory iron reduction (DIR) mediated by *Geobacter metallireducins*. It is generally assumed that this bacteria plays an essential role in magnetic mineral production (Maxbauer et al., 2016a).

(2) organic process through magnetotactic bacteria and their magnetofossils (Fassbinder et al., 1990).

(3) burning produces small particles, limited to specific locations varying with iron content, organic matter, the temperature of burn, and soil porosity (Maher, 1998).

(4) dehydration of lepidocrocite (relevant in gley soils), also related to burning at temperatures higher than 200 °C (Maher, 1998).

(5) atmospheric fallout minerals composed of magnetic spherules are characterized by dissociation from clay fraction in soils (Maher, 1998; Maher and Thompson, 1999).
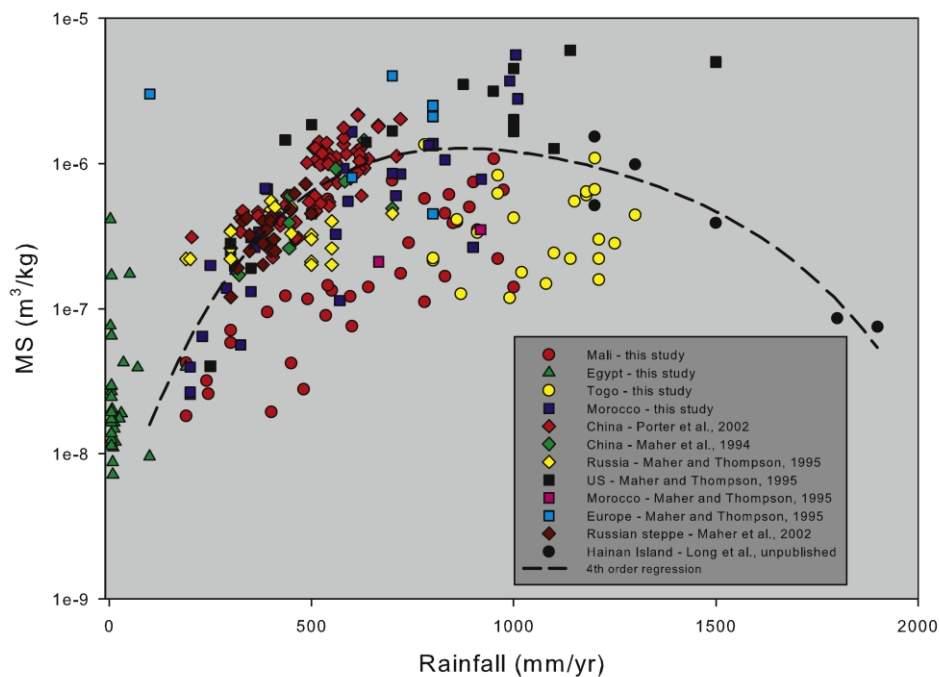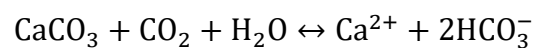
Figure 1-3: Magnetic susceptibility results from soil samples in 272 localities by rainfall (mm/yr), showing the increase of magnetic mineral concentration until a value of ~1000 (mm/yr), then the dissolution of magnetic minerals occur and reduce the concentration (Balsam et al., 2011).

Understanding these pathways of soil-forming magnetic minerals is essential to understand deposits that occur in natural archives, such as marine and continental records. One of the most studied records for paleoclimate reconstruction is speleothems. These secondary carbonate deposits have been studied in environmental magnetism with two main objectives: (1) paleoclimate reconstruction in regional and local climatic scales, soil dynamics in the epikarst, local hydrological conditions, and long-term changes in precipitation (Bourne et al., 2015; Jaqueto et al., 2016; Lascu and Feinberg, 2011); (2) depositional processes inside the cave, involving the transport of the magnetic mineral from the epikarst/karst system to the tip of the stalagmite, focused on the deposition process and the reliability of the geomagnetic record in these samples (Lascu et al., 2016). For this reason, the karst system and the speleothem formation will be briefly introduced and how the magnetic minerals are present in these records.

1.2 Karst environment and isotopic studies

The karst system is characterized by the feedbacks of climate, hydrology, biology, and geology, where speleothems (secondary carbonate deposits) are used as an archive to understand past climate changes because their composition allow the simultaneous use of carbon and oxygen stable isotopes and their content of U, Th and Pb allow precise dating, allowing sub-annual resolution analysis (Hartmann and Baker, 2017). Its development starts with the dissolution of carbonate rock at the surface through the reaction:

Equation 1-1

$$CaCO_3 + CO_2 + H_2O \leftrightarrow Ca^{2+} + 2HCO_3^-$$

which is characterized by strong water-rock interaction at long timescales, resulting in calcium (Ca^{2+}) and bicarbonate ($2HCO_3^-$) as a solution. This reaction occurs in both directions; in the vadose zone (unsaturated zone), the dissolution of soluble rocks prevails (mainly limestone), while for the speleothem, it occurs in the opposite direction by the precipitation of calcite ($CaCO_3$).

The soil horizon and the epikarst constitute dissolution regions. Epikarst or subcutaneous zone is defined as the uppermost layer of the carbonate rock, it develops close to the topography surface through rapid dissolution working as storage, and further concentration of the downward flow routed karst conduits and flow paths development. The soil on epikarst plays an essential hydrological role as it stores precipitation. The capacity depends on physical properties, depth, soil clay, and organic matter. Because of the surface heterogeneity, the soil may present high variability resulting in preferential lateral pathways for the downward stream or diffuse flow (Hartmann and Baker, 2017).

The process begins with the CO_2 in the water from the atmosphere (~400 ppm) and a large extent, to the biological process in soil, like plant root respiration and decomposition, often ranging from 5,000 ppm to 50,000 ppm (Hartmann et al., 2014). So, as the water interacts with the upper epikarst and soil, high pressure of CO_2 in an aqueous solution descends until it reaches the cave. In the cave environment (Figure 1-4), a degassing occurs since the pressure of CO_2 in the cave is lower, and calcite will precipitate (according to the equation above). The most important variable for this effect is the CO_2 at the cave atmosphere, although some

temperature variation for the high latitude caves and uncommon not saturated humidity may occur.
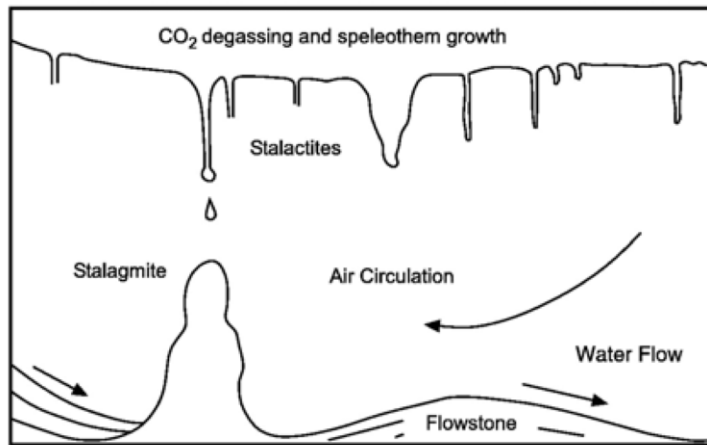

Figure 1-4: Chemical sediments formation through CO2 degassing (Fairchild et al., 2006).

Precipitation of secondary carbonate deposits occur in three different main speleothems (Figure 1-4): (1) *Flowstone*, which is a generic term for a laminated deposit originated from flowing water associated with strong water flows from fissures and conduits; (2) *Soda-straw* stalactites, formed on cave ceiling; (3) *Stalagmites*, originated from ground growth, usually cylindrical type, depending mainly from drip-water flow rate, water supersaturation and drop fall height (Fairchild et al., 2006). This heterogeneous flows and storage behavior results in different drip-rate flow characteristics: (1) drips solely fed by fissure matrix; (2) matrix and enlarged fissures or cracks; (3) by water routed through a reservoir while traveling through matrix and conduits; (4) exclusively by water passed through overflow storage that has fill before the water reaches the drip (soil, depression in fissures) (Hartmann and Baker, 2017; Hartmann et al., 2014).

The majority of paleoclimate studies in stalagmites are done through stable oxygen-isotope (Lachniet, 2009). Stable oxygen-isotope in speleothem is a terrestrial alternative to marine/ice cores bolstered by observing that caves can reflect mean annual temperature and/or precipitation. Oxygen is the second most abundant gas (O_2) in the atmosphere. It occurs in nature as three isotopes. The lighter ^{16}O accounts for almost 99.76 % of the total, ^{17}O corresponds to only 0.04 %, and the heavier ^{18}O accounts for 0.2 %. Individual measurements of the $^{18}O/^{16}O$ ratio in natural materials report as departures in parts per mil (‰) from the value of a standard:

Equation 1-2

$$\delta^{18}O_{(in\ ‰)} = \frac{(^{18}O/^{16}O)_{sample} - (^{18}O/^{16}O)_{standard}}{(^{18}O/^{16}O)_{standard}} \times 1000$$

where samples with positive $\delta^{18}O$ values are said to be ^{18}O enriched in (compared to ^{16}O), and samples with negative $\delta^{18}O$ values are said to be ^{18}O depleted. The heavier the oxygen isotope, the more rapidly it is removed from the atmosphere when condensation and precipitation occur. Repeated cycles of evaporation and precipitation through time leave the water vapor progressively more enriched in ^{16}O (Lachniet, 2009).

Another used proxy in stalagmites is the stable carbon isotopes ($\delta^{13}C$). This proxy can provide information about climate and vegetation, but the interpretation is not straightforward. The signal obtained can be related to complex mixed-signal (interdependent), derived from the atmosphere, soil, epikarst, and cave, and be site-specific and even unique of each stalagmite record of reservoir mixtures and different flow paths (Baldini et al., 2021; Fohlmeister et al., 2020). The carbon transfer dynamic into the cave is influenced by the soil gas CO_2 (soil respiration), with a signal derived from the density of the dominant photosynthetic pathways (C3, C4, and CAM plants). This CO_2 gas will be incorporated in the percolating water (solution) and temperature-dependent, that late will be introduced to the carbon isotope that will be recorded in the stalagmite (Fohlmeister et al., 2020; Novello et al., 2021). Also, "in cave" effects like cave ventilation can increase the $\delta^{13}C$ values due to the changes in pCO_2 and seasonal related, that can obscure the vegetation signal (Wong and Breecker, 2015).

A stalagmite from Pleistocene to the Holocene from southern Brazil shows values of $\delta^{18}O$ and $\delta^{13}C$ (Figure 1-5) that allowed us to interpret the primary supply of carbon originated from biogenic CO_2 from the soil. The soil is linked to the summer and winter extratropical circulation pattern, paced by the obliquity of the Earth (Figure 1-5), that will impact the biological processes (Cruz et al., 2006). Also, high-resolution stalagmite records from Brazil for the last two millennia (Novello et al., 2021) showed $\delta^{13}C$ values related to the C3 photosynthetic pathway, and it is in agreement with the higher concentration of CO_2 in the atmosphere since the transition from the Last Glacial Maximum (Novello et al., 2019).

The complexity in interpreting the stable isotopes is reduced with a multiproxy approach (Baldini et al., 2021). Examples of other proxies to be combined with stable carbon and oxygen isotopes are trace elements (e.g., Mg/Ca, Sr/Ca) and environmental magnetism (Jaqueto

et al., 2016). In a multiproxy study using $\delta^{13}C$, $\delta^{18}O$, and rock magnetism, a higher amount of magnetic minerals with less negative values of $\delta^{18}O$ and less negative $\delta^{13}C$ values (C4 photosynthetic pathway) was observed at a multidecadal scale, allowing an interpretation where increased soil biomass associated with denser vegetation retains the magnetic minerals in the soil, reducing the flux of these minerals into the cave (Jaqueto et al., 2016).
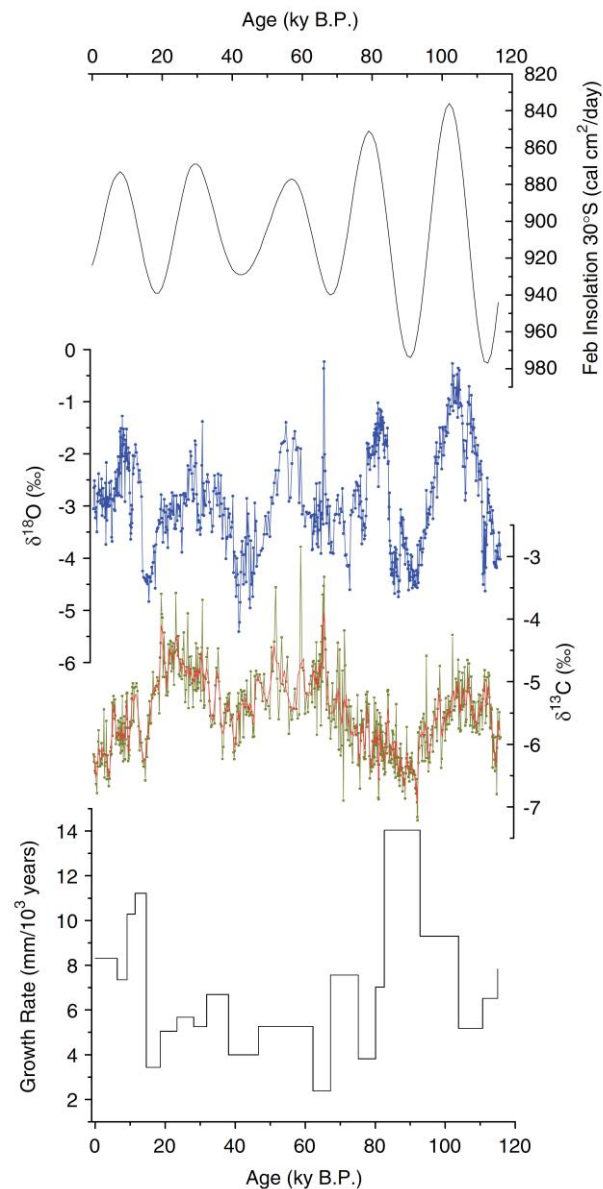

Figure 1-5: Stable isotopes (oxygen and carbon) and growth-rate records from a stalagmite from southern Brazil, compared to summer insolation (Cruz et al., 2006).

1.3 Speleothem magnetism

The first rock magnetic study in stalagmites was carried out in English caves at the end of the 1970s (Latham et al., 1979). The beginning of this research topic research focuses on the geomagnetic secular variation recorded in these samples (Inokuchi et al., 1981; Latham et al., 1989; Latham et al., 1980, 1986a, b; Morinaga et al., 1985, 1986, 1989). The choice of stalagmites was intended as an alternative to sedimentary records for the Brunhes epoch, avoiding bioturbation, depositional and post-depositional processes. Also, the correspondent age data in sedimentary records from lakes and ocean sediments could not be the same as the magnetization lock-in, whereas for stalagmites they could be well-constrained using U-Th dating (limited to < 350 ka). Another significant development of the rock magnetism community was the introduction of cryogenic magnetometers, providing the necessary sensitivity (~10^{-11} Am²) to measure samples with low magnetic content (Goree and Fuller, 1976). One of the drawbacks of the first studies was that the U-Th dating in speleothems was at its first stages of development. The errors were close to ~1000 years, attributed to the presence of ^{232}Th isotope (originated in soil and not from radioactive decay) (Latham et al., 1979), therefore hampering the reconstruction of the geomagnetic secular variation with a proper resolution. So, this topic of research stayed dormant for several decades waiting for new experimental developments (Lascu and Feinberg, 2011).

In the 1990s, some few studies in secular variation continued to be published (Lean et al., 1995; Openshaw et al., 1997), but were mostly focused on the magnetic mineralogy of stalagmite samples (Perkins, 1996; Perkins and Maher, 1993) and conducted by research groups with a strong background on environmental magnetism (Maher and Thompson, 1999). The combination of rock magnetism, x-ray diffraction, and electron microscopy, allowed the researchers to distinguish three-grain morphologies and different origins for the natural remanence carriers in speleothems: (1) 'Abraded grains' interpreted as detrital origin composed mainly of magnetite (Fe_3O_4) and hematite (Fe_2O_3) with less contribution of titanomagnetite (Fe_2TiO_4), ranging from 0.01 µm to 10 µm. These grains have their origins on flood streams or from overlying strata and soil via drip water. (2) 'Regular grains' with crystalline morphology, probably composed of magnetite. Two subgroups were identified, one with uniformly sized grains (0.05 µm to 0.1 µm) that resembles bacterial magnetite, and a second group composed of inorganic authigenic magnetite ranging from 0.01 µm to 0.1 µm. (3) 'Needle-like'

morphology, associated with goethite, with grains smaller than 2 µm, but their origin was still unknown (Perkins, 1996).

Over the past ten years (Lascu and Feinberg, 2011), there has been a revival of speleothem magnetism research for different reasons: (1) The accurate U-Th dating obtained with less amount of material promoted by a change from alpha spectrometry to the convergence of Thermal Ionisation Mass Spectrometry (TIMS) (Edwards et al., 1987a), and ultimately to multi-collector inductively coupled plasma mass spectrometry (MC-ICP-MS) that permitted extraordinarily robust (precise and accurate) chronological control with ages less than 800 ka (Baldini et al., 2021; Cheng et al., 2013). (2) A new generation of DC squid magnetometers allowed measurements of magnetization lower than 10^{-12} Am² (Lascu and Feinberg, 2011). (3) Magnetic microscopy techniques applied to stalagmites provide magnetic measurements at the same resolution as trace-elements studies (Feinberg et al., 2020; Fu et al., 2021; Fukuyo et al., 2021).

The new advances in instrumentation allowed studies of speleothem magnetism as a climate archive and as geomagnetic secular variation in high spatial and temporal resolution. Some of these advances will be summarized below.

1.3.1   Speleothem magnetism as a climate archive

The environmental significance of the magnetic signal recorded in speleothem depends on the age resolution of the stalagmite and the hydrological setting of the karst system. The processes that affect the magnetic mineralogy can be related to the atmosphere (rainfall, temperature, monsoon dislocation), the epikarst (soil formation, vegetation photosynthetic pathways change, soil pCO_2, rate of carbonate dissolution, colloid solution), the allochthonous input of magnetic particles (flooding events, soil-washdown, or wind-blown particles), and also the authigenic formation of magnetic minerals *in situ*.

The primary interpretation of environmental magnetism parameters in speleothems is a correspondence between higher magnetic mineral concentration and wet periods related to detrital inputs in episodic wet events at millennial-scale, as observed in speleothems from China and USA (Bourne et al., 2015; Xie et al., 2013; Zhu et al., 2017). Also, in a stalagmite from China that encompasses the Marine Stage Isotope 5a/4 transition, the solar activity was observed in a

power spectrum of the saturation magnetization, expressing the correlation of this parameter with precipitation.

In tropical sites and at the multidecadal scale, a detailed study was performed on a stalagmite, the soil above the cave, and in sediments inside the cave (Jaqueto et al., 2016). The unmixing of isothermal remanent magnetization and anhysteretic remanent magnetization were used to identify the origin of the magnetic minerals. The magnetic carrier in this stalagmite is magnetite (~90 %), with a magnetic fingerprint in the detrital + extracellular and pedogenic fields of the Egli's (2004) diagram (Figure 1-6). This cluster formed from the analysis of unmixing IRM and ARM acquisition curves points that magnetite was produced in the soil, opposing the idea that these minerals are only incorporated on flood events, where higher coercivities were expected (allochthonous origin). So, the proposed model combined magnetic properties, $\delta^{18}O$ and $\delta^{13}C$, to relate the vegetation cover type, soil erosion, and rainfall amount to the concentration of magnetic minerals in the speleothem. It showed that the less stable soils in the Medieval Climate Anomaly (less rainfall), resulted in higher fluxes of magnetic minerals through the drip water. Conversely, during the higher rainfall typical of the Little Ice Age in these latitudes, a denser vegetation (C_4) inhibited the input of magnetic minerals (Jaqueto et al., 2016). So, a strong regional climate component must be considered when interpreting the magnetic mineralogy.
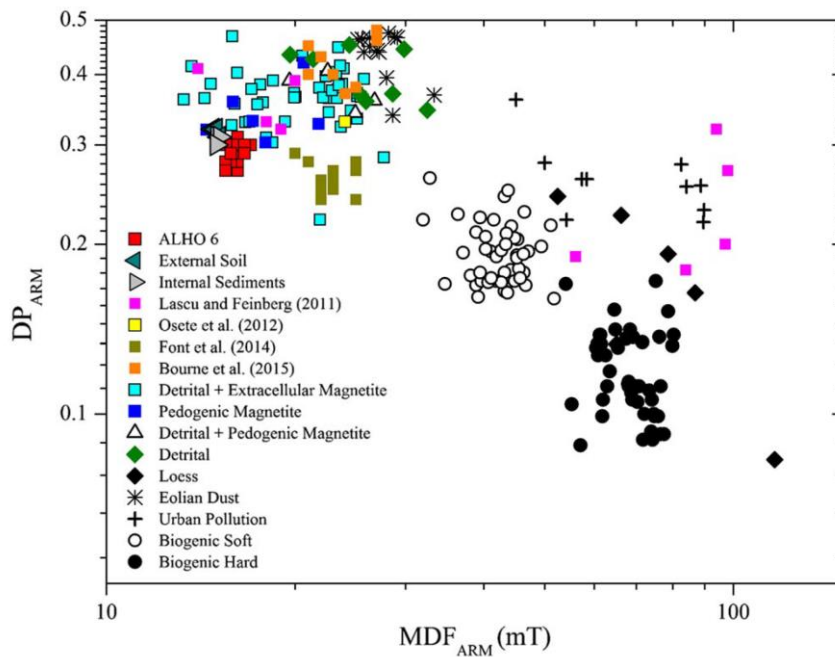
Figure 1-6: Magnetic fingerprints identified from speleothems, soil, and internal sediments from Pau d'Alho cave (Jaqueto et al., 2016).

1.3.2 Speleothem magnetism as geomagnetic recorder

In the past years, several new geomagnetic field records from speleothems (stalagmites and flowstones) were published but most of them limited to the Northern Hemisphere (Chou et al., 2018; Lascu et al., 2016; Osete et al., 2012; Ponte et al., 2018; Ponte et al., 2017; Pozzi et al., 2019; Zanella et al., 2018). The combination of high-resolution dating, annual layer counting, and paleomagnetic data better determined the age and duration of the Laschamp geomagnetic excursion (Lascu et al., 2016). This geomagnetic excursion was dated between 42.25-39.70 ka B.P., its main phase encompassing 700 yrs, where the virtual geomagnetic pole was located in a latitude of -30° (Figure 1-7). This result agrees with cosmogenic nuclide production rates and better defines the main phase of the excursion (Brown et al., 2018).
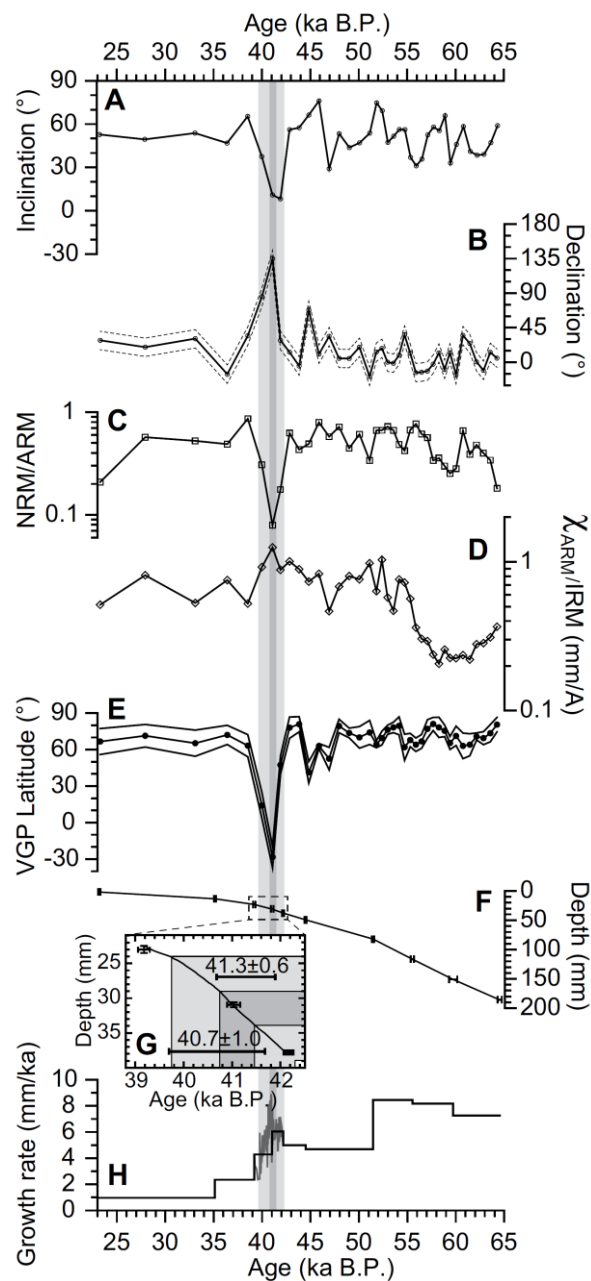
Figure 1-7: Paleomagnetic results from a stalagmite in North America. (a) Magnetic inclination record, (b) Magnetic declination record, (c) relative paleointensity record, (d) Magnetic grain size parameter, (e) Virtual geomagnetic pole from the stalagmite record, (f) U-Th dating points, (g) close up on the thickness of the magnetic excursion event, (h) growth-rate of the speleothem derive from the U-Th dating (Lascu et al., 2016).

The use of speleothems as geomagnetic records has several advantages over other sedimentary archives. The requirements for an excellent paleomagnetic record are (1) uniform magnetic mineralogy over the same sample, (2) uncomplicated behavior when defining the magnetic vector through principal component analysis, (3) no coherence between the relative paleointensity data and changes in magnetic mineralogy and (4) agreement in different relative paleointensity normalizers (Korte and Constable, 2006). On Holocene stalagmites, a good

agreement with geomagnetic field models that only accounts for lava flow and archeological artifacts was demonstrated (Ponte et al., 2018; Zanella et al., 2018). So, speleothems can expand the Holocene records to places where archeological artifacts are limited to the Age of Exploration (15th to the 18th century). This demand for new continuous records has been addressed in global Holocene field models that stated that regional field variations in the southern hemisphere could not be accessed without sediments (Panovska et al., 2015).

1.4 Thesis outline

The following chapters of this thesis represent a collection of papers and results obtained using mostly magnetic techniques applied to the study of speleothems. The main objective of this thesis was to determine a framework for the speleothem magnetism research topic, expanding the comprehension of the environmental significance of magnetic parameters in this kind of material and its use as a magnetic recorder of the Earth's magnetic field. The content of each chapter is outlined below.

- **Chapter 2**: A speleothem magnetism database is presented, this work was recently published (Jaqueto et al., 2021), and it was the first paper that encompassed a wide range of latitudes. Then a comparison of magnetic parameters with different biomes was made to understand their impact on the variability of the magnetic signal.

- **Chapter 3**: This chapter focuses on the depositional processes of the magnetic minerals encapsulated in stalagmites and their reliability is recording the Earth's magnetic field recorded. It comprises two papers covering the last 6000 yr. The first one, already published (Trindade et al., 2018), comprises the record of the last 1500 yr and demonstrates the recurrence of the South Atlantic Anomaly, whereas the second one, recently submitted (Jaqueto et al., submitted) reveals that this feature is intermittent or absent during the mid-to-late Holocene.

- **Chapter 4**: Concluding remarks are presented, focusing on the results obtained in the thesis and how future work could be developed on this research topic.

Chapter 2   Speleothem Magnetism database

The following chapter was published in "Frontiers in Earth Science"; the supplementary material can be found on the online version of the following paper.

2.1 Magnetic mineralogy of speleothems from tropical-subtropical sites of South America

2.1.1   Abstract

Fe-bearing minerals are a tiny fraction of the composition of speleothems. They have their origin in the karst system or are transported from the drainage basin into the cave. Recent studies on the magnetism of speleothems focused on the variations of their magnetic mineralogy in specific time intervals, and are usually limited to a single sample. In this study, we describe a database of environmental magnetism parameters built from 22 stalagmites from different caves located in Brazil (South America) at different latitudes, comprising different climates and biomes. The magnetic signal observed in these stalagmites is dominated by low-coercivity minerals (~20 mT) whose magnetic properties resemble those of magnetite formed in pedogenic environments. Also, a comparison with few samples from soils and the carbonate from cave's walls shows a good agreement of the magnetic properties of speleothems with those of soil samples, reinforcing previous suggestions that in (sub-)tropical regimes the dominant magnetic phase in speleothems is associated to the soil above the cave. Spearman's rank correlation points to a positive strong correlation between magnetic concentration parameters (mass-normalized magnetic susceptibility, natural remanent magnetization, anhysteretic remanent magnetization and isothermal remanent magnetization). This implies that ultrafine ferrimagnetic minerals are the dominant phase in these (sub-)tropical karst systems, which extend across a diverse range of biomes. Although the samples are concentrated in the savannah biome (Cerrado) (~70%), comparison with other biomes shows a higher concentration of

magnetic minerals in speleothem underlying savannahs and lower concentration in those underlying moist broadleaf forests (Atlantic and Amazon biome) and dry forests (Caatinga). Thus, rainfall, biome, and epikarst dynamics play an important role in the concentration of magnetic minerals in speleothems in (sub-)tropical sites and indicate they can be an important target for paleoenvironmental research in cave systems.

2.1.2   Introduction

Speleothems, together with ice-cores, are among the best continental records used in paleoclimate and paleoenvironment reconstruction thanks to their precise chronology, widespread geographic distribution and continuous growth. Environmental magnetic studies of speleothems show variations in magnetic mineral concentrations that correlate to decadal to millennial-scale climate fluctuations at regional and/or global scales (Table 1) (Bourne et al., 2015; Chen et al., 2019; Jaqueto et al., 2016; Regattieri et al., 2019; Xie et al., 2013; Zhu et al., 2017). The magnetic mineral assemblage and the relative concentration of different magnetic phases in speleothems can be interpreted in terms of (Figure 2-1): (i) atmospheric processes (rainfall, temperature), (ii) epikarst processes (soil formation, vegetation change, soil pCO_2, rate of carbonate dissolution), (iii) allochthonous detrital input, including flooding events or wind-blown particles, and (iv) modification of the magnetic mineralogy in-situ, in the speleothem.

Precipitation is a major factor in speleothem formation. The karst system encompasses dissolution and precipitation regimes related to the carbonate-water interactions (Fairchild et al., 2006). The dissolution phase operates as a cascading system, comprising the atmosphere, the soil-ecosystem, the epikarst, and the cave system itself (Fairchild and Baker, 2012). It involves the transformation of carbon dioxide gas ($CO_{2(g)}$) that dissolves into water to form the species ($CO_{2(aq)}$) reacting with water to form carbonic acid (H_2CO_3). This 'weak' acid will progressively dissolve the limestone ($CaCO_3$) and this reaction will produce calcium (Ca^{2+}) and bicarbonate (HCO_3^-). At the precipitation phase, in the cave system, a degassing of CO_2 will occur (when the solution is in contact with the cave atmosphere) and the secondary carbonate will form ($CaCO_3$), mainly calcite. The kinetics of the degassing reaction during calcite precipitation usually lasts from minutes to hours (Dreybrodt, 1999; Dreybrodt et al., 1997; Dreybrodt and Scholz, 2011), and favors the acquisition of detrital remanent magnetization. Furthermore, the absence of postdepositional perturbation, like bioturbation or

compaction, helps conserve the magnetic remanence and allows the speleothem to retain reliable directional and paleointensity data (Lascu et al., 2016; Trindade et al., 2018; Zanella et al., 2018).

Soils play an important role in speleothem formation since soil's microbial activity and root respiration are the main factors controlling the pCO_2 in the solution, which in turn will drive carbonate dissolution (epikarst). In karst environments, soils are generally classified as Rendzina soils (Leptsols developed in carbonates (Jordanova, 2017)). They develop over 10 to 100 years with a thin humic (A) horizon, overlying an incipient illuvial (B) horizon or the bedrock itself, and are often well-drained with good aeration and a brown-to-black soil color (Jordanova, 2017). The combination of well-drained soil together with a large amount of organic and enhanced biological activity will promote an active pedogenesis producing fine-grained pedogenic iron oxides (SP/SSD magnetite fraction) with the magnetic enhancement of the soil relative to the host carbonate (Figure 2-1). So, the synthesis of pedogenic magnetite/maghemite via an abiotic route or via iron-reducing bacteria will be controlled by the biome's characteristics and by the wetting and drying cycles in the soil (Jaqueto et al., 2016; Jordanova, 2017; Maxbauer et al., 2016a)

Transport of small-sized detrital particles derived from the soil into the cave system will occur through diffusive infiltration (Figure 2-1) along rock's fissures. These particles will be incorporated into the speleothem after reaching the top of the stalagmite by dripwater (Bosch and White, 2004; Bosch and White, 2018; Bourne et al., 2015; Font et al., 2014; Fu et al., 2021; Jaqueto et al., 2016; Regattieri et al., 2019; Zhu et al., 2017). Alternatively, detrital particles may reach the speleothems from sinking streams, from detrital material stored in the conduit system, or result from flooded surface steams and episodic storm flows (Bosch and White, 2004; Feinberg et al., 2020). Also, detrital input close to cave entrances can be derived from wind-blown material (pollen, dust) (Fairchild et al., 2006). Finally, authigenic formation cannot be ruled out in some cases with the formation of goethite needles and biogenic magnetite at the precipitation site (Perkins, 1996; Strauss et al., 2013).
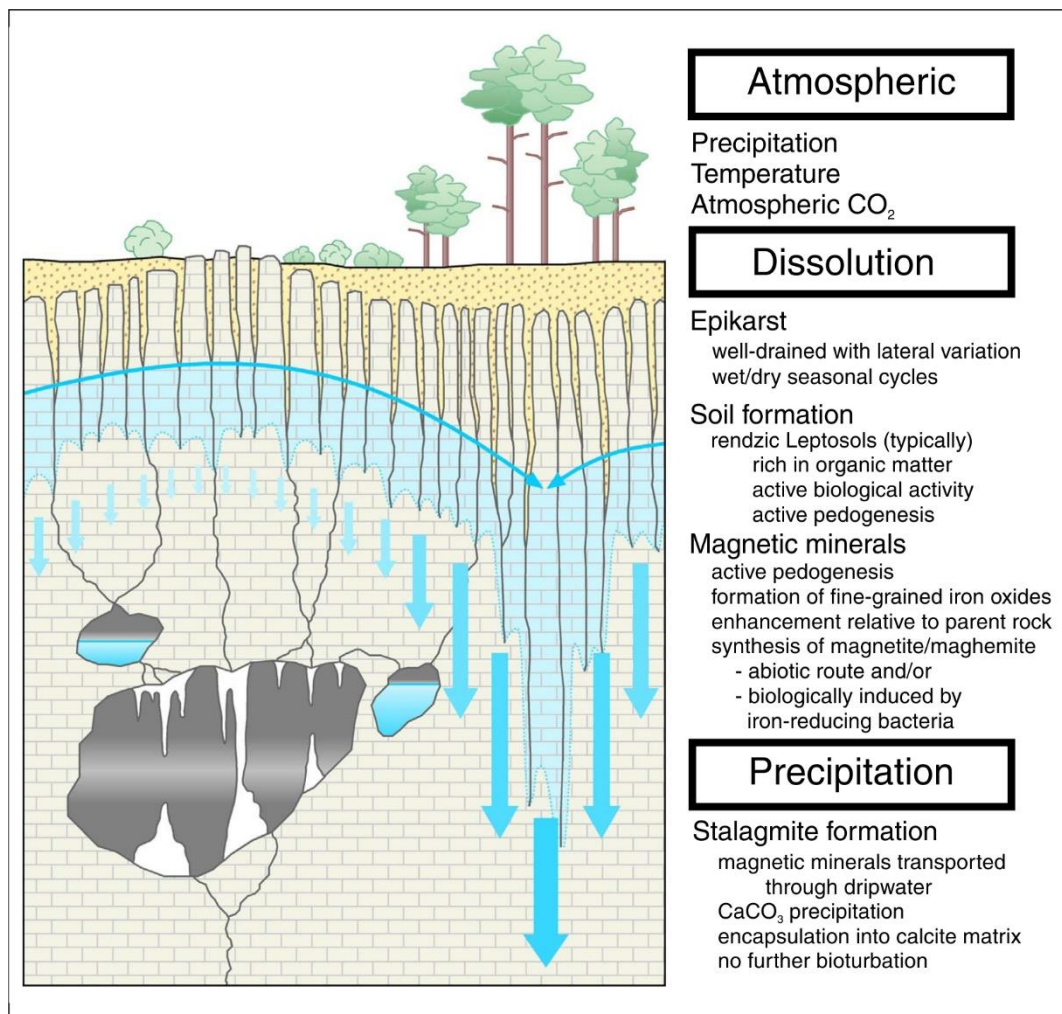
Figure 2-1: Schematic description of the karst vadose zone (Hartmann and Baker, 2017), with processes that are related to the speleothem magnetism.

Most studies dealing with the environmental magnetism of speleothems interpret the variations in magnetic mineral concentration as a proxy for paleoprecipitation (Table 1). For example, Xie et al. (2013), Zhu et al. (2017) and Bourne et al. (2015) show a millennial-scale correlation between magnetic parameters and proxies for paleoprecipitation in China and the southwest United States. Chen et al. (2019) used saturation magnetization (Ms) to track rainfall variation during MIS5a/4 transition and the power spectrum of Ms showed that solar activity plays an important role in precipitation variation in southern China. More recently, Reggatierri et al. (2019) linked climate proxies (with stable oxygen and carbon isotope) soil stability and evolution (magnetic parameters), and land-use on a Holocene speleothem from Northern Italy.

In tropical sites, Jaqueto et al. (2016) suggested an inverse correlation at the multidecadal scale between paleoprecipitation and magnetic mineral concentration in a speleothem from western Brazil. In their model, the concentration of magnetic minerals in the stalagmite was governed

by soil erosion and vegetation cover. A period of less rainfall (compared to the average) would be associated with less stable soils, resulting in higher fluxes of magnetic minerals into karst systems. Conversely, wetter periods would be associated with denser vegetation that inhibits the flux of the soil's detritic material into the cave. In this case, the relation between paleoprecipitation and magnetic mineral concentration is not a direct one and depends on the soil dynamics and the vegetation cover in addition to the regional climate.

In the present study, we will explore the variations of magnetic mineralogy through different biomes in South America through a large speleothem magnetism database covering a wide range of latitudes (4°S to 24°S). Also, we present two detailed case-studies where the magnetic signal of the speleothems is compared to the soil above the cave and the host carbonate to constraint the source of magnetic minerals inside the speleothems.

Table 2-1: Speleothem magnetism studies and their respective resolution and interpretation

Study	Location	Climatology	Cave	Sample	Timespan	Average sample resolution	Magnetic parameter	Comparison	Interpretation
Xie et al., 2013	China	Monsoonal, warm-wet summer and a cool-dry winter.	Heshang Cave	HS4	0.15 ka - 7.10 ka (6.94 ka)	74 years	ARM/SIRM	Peatlands Hopanoids	Heavy rainfall resulted in the enhanced transport of coarse magnetic particles to the cave.
Zhu et al., 2017	China	Eastern Asian and Indian monsoon systems	Heshang Cave	HS4	0.15 ka - 7.10 ka (6.94 ka)	74 years	IRMsoft_flux	$\delta13C$, Peatlands Hopanoids, ENSO variability, stalagmite BA03 - $\delta18O$ and core V21-30 - $\delta18O$ foraminifera	Flux of soil-derived magnetic minerals correlate with rainfall amount and intensity.
Bourne et al., 2015	USA	Humid, temperate climate, and well-developed, midlatitude seasonality.	Buckeye Creek Cave	BCC-010	58.71 ka - 125.21 ka (66.49 ka)	2015 years	IRMsoft, SIRM, IRMhard, S-ratio, IRM0.3T	$\delta13C$, $\delta18O$, Antarctic ice core CO2, Vostok ice core CO2	Changes in magnetite concentration as reflecting variations in local pedogenic processes, controlled by changes in regional precipitation.
Jaqueto et al., 2016	Brazil	South America Summer Monsoon with 90% of this amount falling	Pau D'Alho Cave	ALHO06	1891 CE - 535 CE (1.35 ka)	40 years	NRM, ARM, SIRM, HIRM, IRM_soft, S-ratio, ARM/SIRM	$\delta13C$, $\delta18O$	Concentration of magnetic minerals in the stalagmite is governed by soil erosion above the cave.
Chen et al., 2019	China	Subtropical monsoon climate, more than 65% rainfall falls during the monsoon season	Tangnei Cave	TN-1	77.9 ka to 82.3 ka (3.04 ka)	15 years	Ms and Hc	$\delta13C$, $\delta18O$, solar variability	Magnetic property in speleothems is interpreted to be related to regional precipitation.
Regattieri et al., 2019	Italy	Alpine climate, with precipitation correlated with southern Europe	Rio Martino Cave	RMD1	0.4 ka to 9.7 ka (9.3 ka)	60 years	Magnetic susceptibility	$\delta13C$, $\delta18O$, Growth rate, lake level	Magnetic susceptibility concentration and carbon stable isotope ratio related to soil stability and pedogenesis.

2.1.3   Regional Setting

The central part of South America is dominated by warm and humid conditions, where the South America Summer Monsoon (SASM) is responsible for 70% of the rainfall from November to February (Campos et al., 2019; Garreaud et al., 2009). Present-day interannual climate variability is controlled by El-Niño Southern Oscillation associated with warmer and rainfall below average on the Northern part and wetter conditions on the Southeastern part. Decadal and interdecadal variability is also present and forced by Pacific Decadal Oscillation with smaller amplitudes (Garreaud et al., 2009), while paleoclimate reconstitution of the SAMS based in δ^{18}O of speleothems showed strong centennial variability linked to solar cycles (Novello et al., 2016).

The biomes at each karst system have different biodiversities like plant structure (trees vs grasses), leaf type (broad vs needles), plant spacing (forest vs savannah), and climate that controls the organism type. Four main biomes are present in the main karst areas in Brazil (Figure 2-2) (Olson et al., 2001; Ribeiro et al., 1983; Whitmore and Prance, 1987):

1. Amazon biome (moist broadleaf forest), located in the north and northwestern part of Brazil, is characterized by low variability in temperature with a higher precipitation amount between 1800 mm/year to 2200 mm/year. Its ecoregion is classified as Neotropical, with high biodiversity, forest composition dominated by evergreen with a dense high canopy, and the transition on its border is characterized by less dense understory.

2. Cerrado biome (savannah), located in the Central part of Brazil, is characterized by seasonal rainfall, with a dry period during winter and a humid period in summer with average precipitation between 1000 mm/year to 1500 mm/year. Its ecoregion is classified as Neotropical and it has a border with other biomes (Amazon, Atlantic, Caatinga). The vegetation has characteristics of nutrient-poor, deep and well-drained soils. Forest composition varies from an open field to a tall closed forest, which gives a distinctive biota feature in a mosaic fashion.

3. Caatinga biome (dry forest), located in the northeastern part of Brazil, is characterized by a hot and dry climate with a precipitation amount between 700 mm/year to 750 mm/year (6 to 11 dry months). Its ecoregion is classified as Neotropical, forest

composition is considered heterogeneous, sparse, and diverse ranging from low shrubby to tall caatinga forest.

4. Atlantic biome (moist broadleaf forest), located in the southwestern part of Brazil along the southern coast, is characterized by high levels of rainfall between 1600 mm/year to 1800 mm/year. Its ecoregion is classified as Neotropical, with outstanding biodiversity in endemism. Forest ranges from coastal plains to the highest mountains, creating a vegetational gradient from shrubs to montane forests.

2.1.4   Material and Methods

South American caves occur over a wide range of latitudes and the speleothems within them act as climate archives extending back hundreds of millennia (Cruz et al., 2005). The choice of selected caves for this study was based on the availability of speleothems held at the Instituto de Geociências from Universidade de São Paulo and also the aim to sample different biomes (Figure 2-2, Supplementary Figure S1). In general, four specimens of each stalagmite were prepared with ~7.5 mm of diameter and ~10 mm of height (Supplementary Figures S2-S5) (specimens do not have a radiometric age control). The resulting speleothem database (Figure 2-2) consists of 139 specimens (Supplementary Table), where 90 specimens were prepared from 22 different speleothems, 34 specimens from soil samples from the epikarst for 4 caves, and 15 specimens from the host carbonate from 2 different caves. In two specific sites (pink squares, Figure 2-2, Jaraguá Cave (21.09° S, 56.58° W) and Lapa dos Anjos (15.44° S, 44.40° W), the samples consist of the stalagmite, soil, and carbonate.
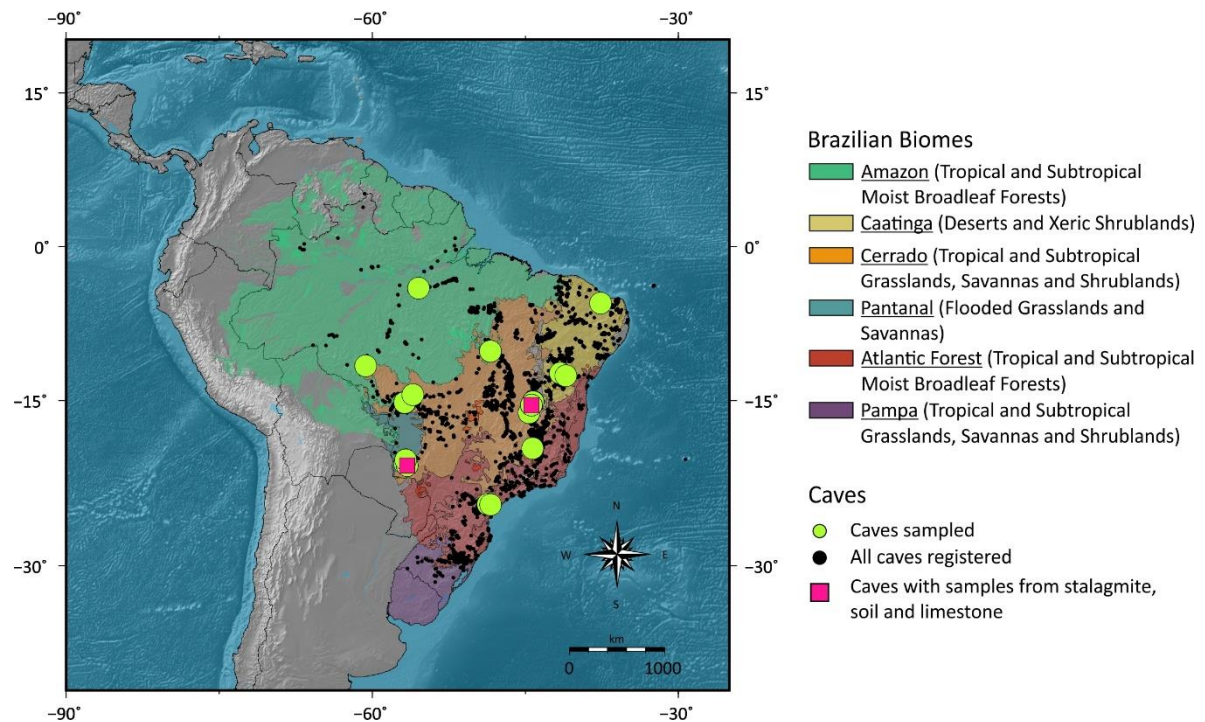
Figure 2-2: Map of South America, with Brazilian caves (black dots), the speleothems sampled (white circles), and the caves with samples from a stalagmite, soil, and carbonate (pink squares) for rock magnetic characterization in different biomes (Cerrado, Caatinga, Amazon, Atlantic Forest, Pantanal, Pampa) (Olson et al., 2001).

2.1.5   Rock Magnetic Parameters

Rock magnetism techniques are commonly used in environmental studies aiming to understand three different parameters: composition, concentration and granulometry (Evans and Heller, 2003). Magnetic concentration parameters include mass-normalized values of magnetic susceptibility (χ), natural remanent magnetization (NRM), anhysteretic remanent magnetization (ARM), isothermal remanent magnetization (IRM). Although they are referred to concentration dependent, each of these parameters different segments of the grainsize distribution and magnetic mineralogy in a sample. Magnetic susceptibility is the induced magnetization created by a small applied field, and in case of speleothems it is influenced by ferromagnetic minerals, diamagnetic carbonates, and paramagnetic minerals from clays and silts. NRM is the total natural remanence held by low coercivity minerals (10s of mT by (titano)-magnetite/maghemite), as well as by from high coercivity minerals (100s to 1000s of mT by hematite and goethite). Laboratory induced remanences are useful for tracking a variety of other characteristics. ARM is the magnetization acquired during the application of a small DC field superimposed over an alternating field (AF) demagnetization step. ARM activates only

those grains whose coercivities are less than the peak field reached during the AF step, and are usually lower coercivity minerals such as magnetite and maghemite. IRM is the magnetization acquired after the application of a strong DC pulsed field. Depending on the strength of the pulsed field, IRMs may include the saturation remanence of all low coercivity minerals, and portions of the hematite grain size distribution (which typically requires field up to ~5 T to saturate). Goethite has a coercivity of >57 T (Rochette et al., 2005) and therefore its remanence is not included in an IRM. Generally, IRM is interpreted as an indicator of magnetic mineral concentration. The ratio of ARM to IRM is often used as a granulometric tool, where higher ratios suggest a higher fraction of fine grained, low coercivity minerals capable of carrying a stable remanence (Maher, 2011). Another grain size dependent parameter is the median destructive field of ARM and IRM demagnetization curves, where higher values suggest smaller average grain sizes (Maher, 2011)

The S-ratio is a parameter used to quantify the fraction of an IRM that is held by low coercivity minerals. (Bloemendal et al., 1992) defined the S-ratio as

$$Sratio = \frac{1}{2}\left(\frac{IRM_{@1T} - IRM_{@0.3T}}{IRM_{@1T}}\right)$$

where values close to 1 indicate that minerals with coercivities <300 mT dominate the remanence, while lower values suggest increasing contributions from higher coercivity minerals. Also, the remanence held by the high coercivity fraction is termed the "Hard-Isothermal Remanent Magnetization" (HIRM) and is calculated by multiplying the complement of the S-ratio by the IRM_{1T} value (Maxbauer et al., 2016a).

2.1.6   Methods

2.1.6.1 Rock magnetism concentration parameters

Rock magnetic measurements were performed on bulk specimens. Measurements of magnetic susceptibility (χ), NRM, ARM, IRM were conducted in a magnetically shielded room with an ambient noise field less than 500 nT at the Laboratório de Paleomagnetismo at Universidade de São Paulo (USPMag).

The magnetic susceptibility of each specimen was measured ten times at low frequency (F1: 976 Hz) in a Kappabridge MFK1 by AGICO ltd. Remanence measurements were carried out using a 2G Enterprises superconducting rock magnetometer (RAPID) (noise level $< 5 \times 10^{-12}$ Am²). The IRM consisted of applying two different fields using a pulse magnetizer by 2G enterprise (model 2660). The pulse-field was applied along the Z-axis for all specimens in fields of 1000 mT, and a back-field of -300 mT. At least two measurements were carried out in the RAPID magnetometer at each step.

2.1.6.2 Unmixing of magnetic remanence

Analyses of the coercivity distribution are regularly applied in environmental magnetism studies to identify different magnetic populations in natural sediments (Heslop, 2015; Roberts et al., 2019). The protocol for measuring ARM (incorporated into the RAPID system) was to apply a direct DC field of 0.03 mT superposed by an alternating field of 300 mT in the Z-axial coil at least two times, followed by a 300 mT demagnetization field in the quartz tube, and then an alternating field with 76 steps was performed, following a detailed stepwise demagnetization procedure (Egli, 2004a). The demagnetization of IRM was done in two of four specimens for each stalagmite and followed the same steps as the ARM demagnetization (76 steps). Soil IRM intensities were close to the upper limit of the superconducting rock magnetometer ($> 10^{-5}$ Am²) causing higher standard deviations in the magnetization readings. For this reason, for these samples, we used the back-field IRM curves obtained in a vibrating sample magnetometer (VSM) by Princeton Measurements Corporation (model 3900) at the Institute for Rock Magnetism at Univervisity of Minnesota. To comprehend the magnetic subpopulations and their differences in the varying latitudes and biomes, the skewed generalized Gaussian (SGG) functions were analyzed using the software MAX UnMix (Maxbauer et al., 2016b).

2.1.7   Results

2.1.7.1 Rock Magnetism concentration parameters

Magnetic susceptibility was used to understand the contribution of different types of magnetic carriers in the karst system. The specimens were mass normalized, rather than volume normalized to avoid issues arising from varying porosities. Speleothems and carbonates show similar low magnetic susceptibility values (Figure 2-3). These low values are due to the the diamagnetic contribution from the calcite matrix and their low concentration of ferromagnetic material. The reference value of susceptibility for pure calcite is -4.46×10^{-9} m³/kg (Schmidt et al., 2006). The median value found for the stalagmites is -2.00×10^{-9} ($\pm 6.78 \times 10^{-8}$) m³/kg, pointing to the calcite matrix. The median value for the carbonates is 6.71×10^{-9} ($\pm 6.48 \times 10^{-9}$) m³/kg. The soil has a magnetic susceptibility median value of 6.92×10^{-6} ($\pm 3.12 \times 10^{-6}$) m³/kg, which is 3 to 4 orders of magnitude higher than that of calcite and carbonate (Supplementary Table1).
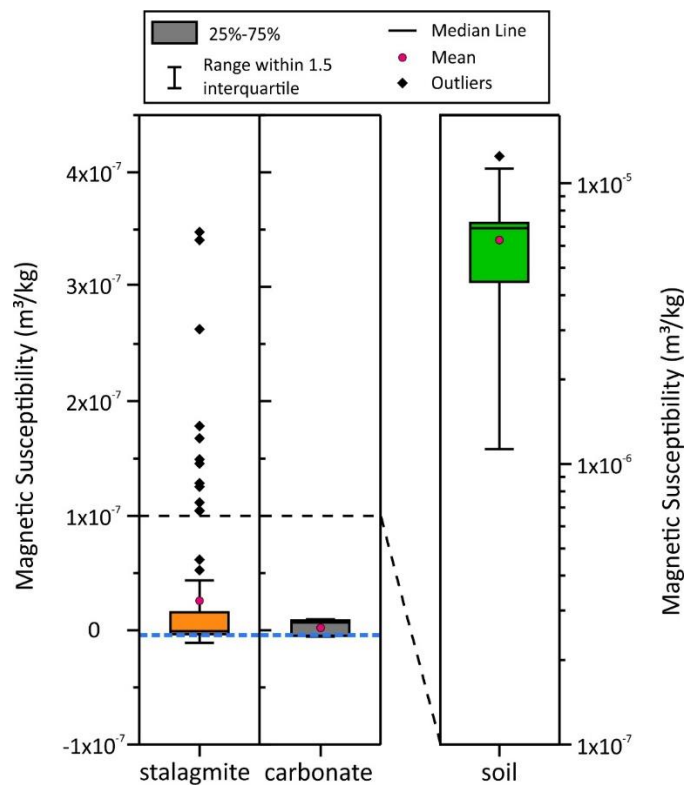

Figure 2-3: Box-plot of magnetic susceptibility results from stalagmite (orange), carbonate (gray), and soil (green), blue dashed line represent the pure calcite value (Schmidt et al., 2006).

The NRM, ARM, and IRM of all samples are shown in Figure 2-4. These results also indicate the contrast between the soil and the speleothems and the host carbonate, with lower median values from stalagmites NRM_{stal}: 1.10×10^{-7} $\pm 1.48 \times 10^{-5}$ Am²/kg; ARM_{stal}: 1.61×10^{-7} $\pm 2.21 \times 10^{-5}$ Am²/kg; IRM_{stal}: 7.48×10^{-6} $\pm 3.50 \times 10^{-4}$ Am²/kg, a similar value for the carbonates NRM_{carb}: 1.60×10^{-7} $\pm 1.45 \times 10^{-7}$ Am²/kg; ARM_{carb}: 3.07×10^{-7} $\pm 3.97 \times 10^{-7}$ Am²/kg; IRM_{carb}: 2.93×10^{-5} $\pm 3.14 \times 10^{-5}$ Am²/kg, and values of two to four orders of magnitude higher in the soil, with median values of NRM_{soil}: 1.22×10^{-5} $\pm 5.88 \times 10^{-5}$ Am²/kg; ARM_{soil}: 2.11×10^{-3} $\pm 8.46 \times 10^{-4}$ Am²/kg; IRM_{soil}: 2.52×10^{-2} $\pm 8.96 \times 10^{-3}$ Am²/kg.
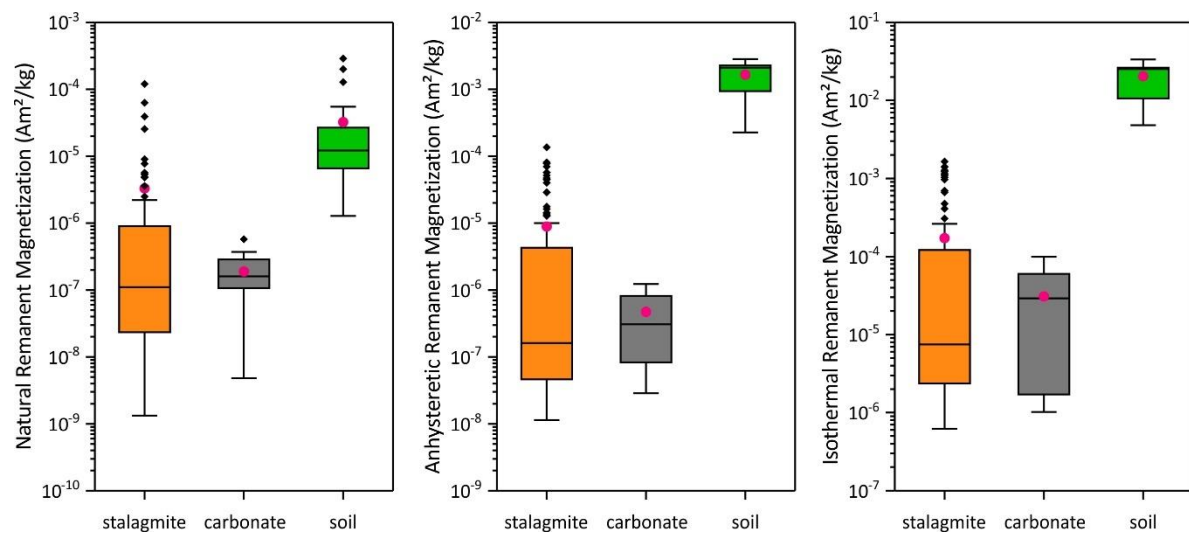

Figure 2-4: Box plot of remanent magnetization of stalagmites (orange), carbonates (grey) and soil (green), for natural remanent magnetization (NRM), anhysteretic remanent magnetization (ARM) and isothermal remanent magnetization (IRM).

2.1.7.2 S-ratio and HIRM

The distributions of S-ratio (Figure 2-5) show a distinctive grouping behavior when compared to the concentration parameters. Soil and speleothems show a predominance of low coercivity phases (stalagmite with median S-ratio: 0.97 ±0.07; soil with median S-ratio: 0.99 ±0.01) and a high coercivity contribution being more prominent in the carbonate (median S-ratio: 0.70 ±0.15). The HIRM that is the concentration of high coercivity minerals shows that these minerals are present with median values from stalagmites of 7.0×10^{-6} $\pm 1.9 \times 10^{-5}$ Am²/kg, carbonates 1.0×10^{-5} $\pm 1.1 \times 10^{-5}$ Am²/kg and for soil 2.7×10^{-4} $\pm 1.6 \times 10^{-4}$ Am²/kg (Figure 2-5).

Although for soil the values are higher in content than carbonate and speleothems, they only represent ~1% of the total IRM@1T, whereas for carbonate they represent 30% and for stalagmites 3% of the total IRM@1T.
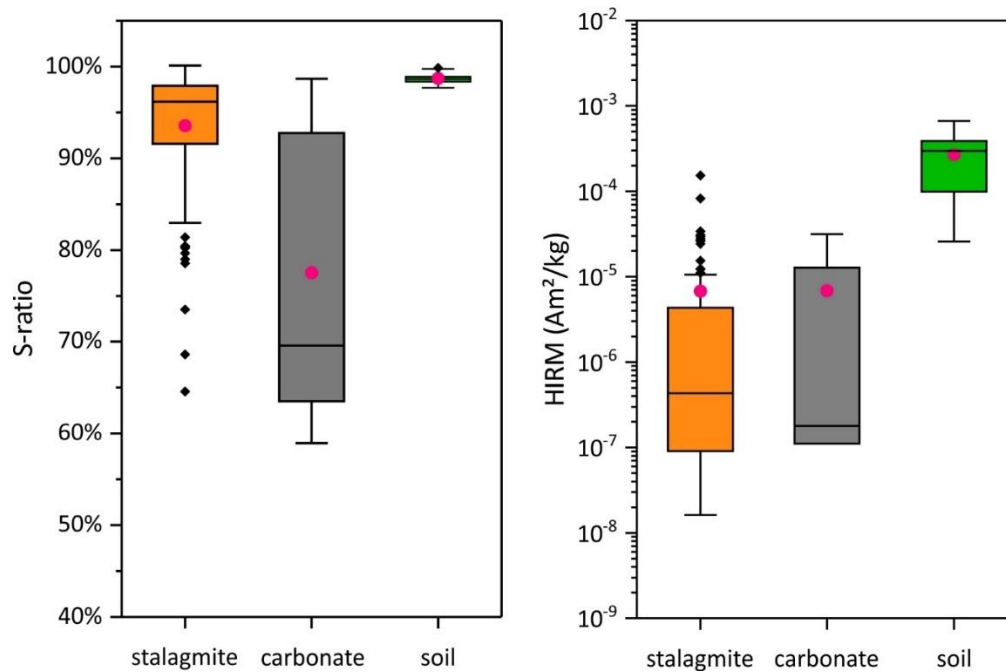

Figure 2-5: Environmental magnetic parameters showing the fraction of remanence held by grains with coercivities <300 mT (S-ratio) and the remanence held by high-coercivity minerals (HIRM) for stalagmites (orange), carbonate (gray) and soil (green).

2.1.7.3 Median destructive field of ARM and IRM

Demagnetization curves from stalagmites, carbonate, and soil indicate the presence of a low-coercivity magnetic phase in all specimens. Results from ARM have higher noise for stalagmites and carbonate due to the low-magnetization values close to the magnetometer noise level (5×10^{-12} Am²), where only 63% of the stalagmite specimens could be analyzed. The IRM demagnetization curves also show the presence of a low coercivity magnetic phase in all stalagmites and soil samples (Figure S6). Conversely, the carbonate presents higher coercivities.

Unmixing of the demagnetization curves of ARM and IRM was done using the MAX UnMix software (Maxbauer et al., 2016b), except when the noise dominates the signal. Only one component was fit for the whole dataset. Stalagmite and soil have similarly low values in

coercivity (Figure 2-6) (stalagmite: MDF$_{ARM}$: 18.8 ±1.1 mT; MDF$_{IRM}$: 20.3 ±1.0 mT, soil: MDF$_{ARM}$: 17.7 ±1.0 mT; MDF$_{IRM}$: 14.8 ±1.0) and dispersion (stalagmite, DP$_{ARM}$: 0.29 ±0.02; DP$_{IRM}$: 0.39 ±0.02; soil: DP$_{ARM}$: 0.28 ±0.01; DP$_{IRM}$: 0.37 ±0.01). The carbonate has median values of MDF$_{ARM}$: 37.6 ±1.1 mT; MDF$_{IRM}$: 32.2 ±1.1 mT; DP$_{ARM}$: 0.37 ±0.04; DP$_{IRM}$: 0.49 ±0.03. The results obtained of the median coercivity from both ARM and IRM measurements (Figure 2-6 and Figure 2-7) indicate that the magnetic signal of stalagmites is similar to that of the respective soil, and contrasts with that of the host carbonate.
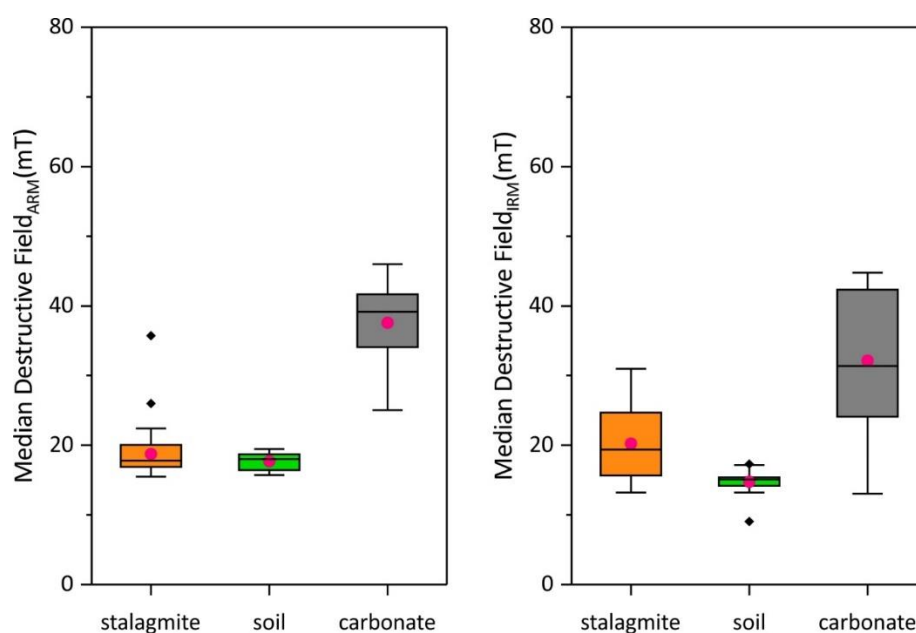

Figure 2-6: Magnetic coercivity results from the adjustment of skewed generalized Gaussian (SGG) functions from the detailed demagnetization curves of ARM and IRM for stalagmites (orange), soil (green) and carbonate (gray).

All speleothems irrespective of their location have coercivity values close to the detrital and pedogenic (plus extracellular) magnetite fields shown in Figure 2-7. The biplot of magnetic properties K$_{ARM}$/IRM by the median destructive field of ARM (MDF$_{ARM}$) also show an agreement with fingerprint components: detrital pedogenic, detrital, detrital and extracellular magnetite and pedogenic (DP, D, D+EX, PD) (Egli, 2004b), supporting the soil-derived origin of the recorded magnetic signal. The results for carbonate data are not in agreement with the magnetic behavior of the speleothems and soil, and are instead related to the magnetic mineral assemblage associated with their Neoproterozoic origin. Previous studies in stalagmites also found the same detrital/pedogenic magnetic component (Bourne et al., 2015; Jaqueto et al., 2016; Zhu et al., 2017), but they used median destructive field (ARM and IRM) and

dispersion parameters instead of K_{ARM}/IRM. The K_{ARM}/IRM parameter was preferred instead of the dispersion parameter that does not have a clear physical meaning (Egli, 2004b).
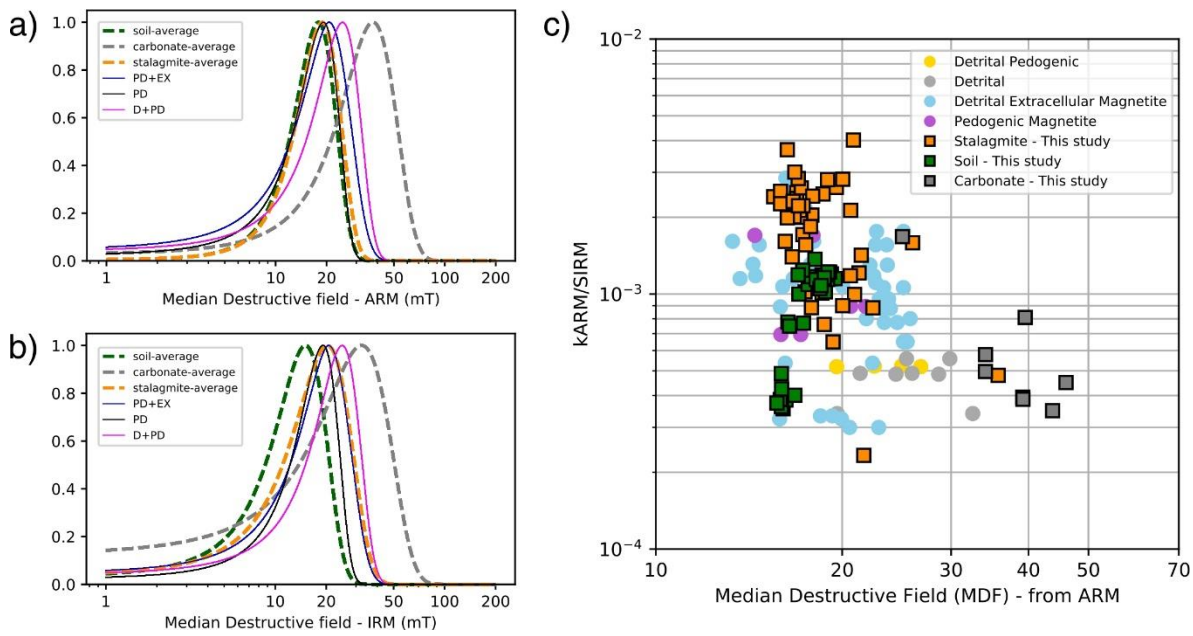

Figure 2-7: (a) Average coercivity distribution of anhysteretic remanent magnetization (ARM) and (b) isothermal remanent magnetization (IRM) of stalagmite (dashed orange), soil (dashed green) and carbonate (dashed gray) obtained from skewed generalized Gaussian (SGG) function (Max Unmix). Reference values of pedogenic + extracellular magnetite (PD+EX) (blue), pedogenic (PD) (black) and detrital + pedogenic (pink) retrieved from average values of ARM analysis by Egli (2004b). (c) Biplot of K_{ARM}/IRM and median destructive field (MDF) of ARM from stalagmites (orange squares), soil (green squares) and gray (carbonate squares). Magnetic properties taken from Egli (2004) represent detrital pedogenic (yellow), detrital (light gray circles), detrital extracellular magnetite (light blue circles) and pedogenic magnetite (purple circles).

2.1.7.4 Two case studies: Jaraguá and Lapa dos Anjos caves

Two sites containing stalagmite, carbonate and soil samples were chosen to refine this analysis. Lapa dos Anjos cave (15.44° S, 44.40° W) and Jaraguá cave (21.09° S, 56.58° W) are both located in the Cerrado biome. The average annual precipitation from 1979 to 2016 is 993.3 mm/year and 1402.7 mm/year, respectively (Figure S1, Cerrado East#2 and Cerrado West #2). Both sites show a similar mean temperature of 23.0 °C.

Stalagmites from both caves are considered 'clean' (without 'dirty' layers) (Supplementary Figure S2) and their median IRM values are 1.58×10^{-6} Am²/kg (Lapa dos Anjos) and 3.20x10⁻

[6] Am²/kg (Jaraguá cave) (Figure 2-8). Their host carbonates correspond to the Neoproterozoic formations of Sete Lagoas (Lapa dos Anjos) and Bocaina (Jaraguá cave) and their median IRM values are 5.06×10^{-5} Am²/kg and 1.71×10^{-6} Am²/kg, respectively. The soil has median IRM values of 2.59×10^{-2} Am²/kg and 2.96×10^{-2} Am²/kg, respectively. Stalagmites and soil at both sites show high S-ratios consistent with magnetic mineral assemblages dominated by low coercivity phases, with median values of 0.98 and 0.99 for Lapa dos Anjos cave and 0.97 and 0.99 for Jaraguá cave, respectively (Figure 2-8). By comparison, the carbonates at each site show greater remanence contributions from high coercivity minerals with S-ratios at Lapa dos Anjos of 0.64 and Jaraguá cave of 0.93.

The IRM demagnetization curves for stalagmites and soil yield lower median destructive fields, again showing the important role of lower coercivity minerals. The median MDF values for Lapa dos Anjos cave are 23.9 ±3.1 mT and 15.1 ±4.0 mT for stalagmites and soil, and for Jaraguá cave the median MDF values are 19.7 ±3.2 mT and 15.7 ±1.3 mT. In contrast, the carbonate bedrocks for Lapa dos Anjos and Jaraguá caves have median MDF values of 43.4 ±2.1 mT and 24.2 ±5.9 mT, respectively (Figure 2-8). The coercivity values for stalagmite and soil from both caves have their magnetic properties in the same cluster as detrital, detrital pedogenic and detrital extracellular magnetite (Figure 2-7). These results indicate that the dominant magnetic minerals in tropical stalagmites are mainly derived from overlying soils. Although magnetic minerals from host carbonate may be present, overall, they have a low contribution to the magnetic signal.
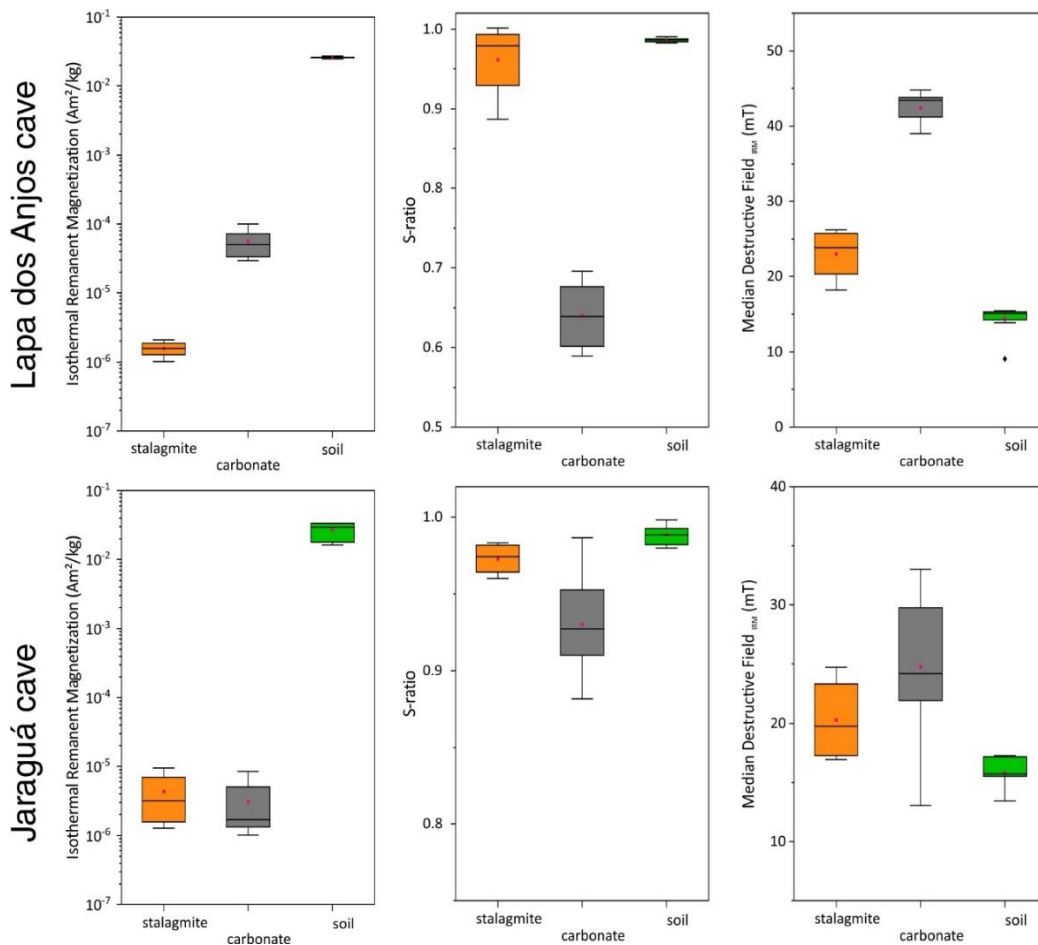
Figure 2-8: Magnetic properties of the caves: Lapa dos Anjos (upper) and Jaraguá (bottom). (*First column*) Isothermal remanence magnetization (IRM) after a pulse-field of 1T. (*Second column*) S-ratio shows the presence of the low coercivity phase. (*Third column*) Median destructive field from IRM demagnetization.

2.1.8   Magnetic Parameters and Biomes

2.1.8.1 Spearman's rank correlation

To compare the results obtained within the database we calculated the Spearman's rank correlation coefficients for 54 stalagmites specimens where IRM demagnetization was performed. The following magnetic properties (Section 2.1.5) were considered in the analysis: concentration parameters (magnetic susceptibility, NRM, ARM, IRM), composition parameter (S-ratio), granulometry parameters (χ_{ARM}/SIRM, MDF_{IRM}), (Figure 2-9). Spearman's correlation is recommended to avoid a linear relationship since most magnetic parameters have non-Gaussian distributions (Hu et al., 2019).
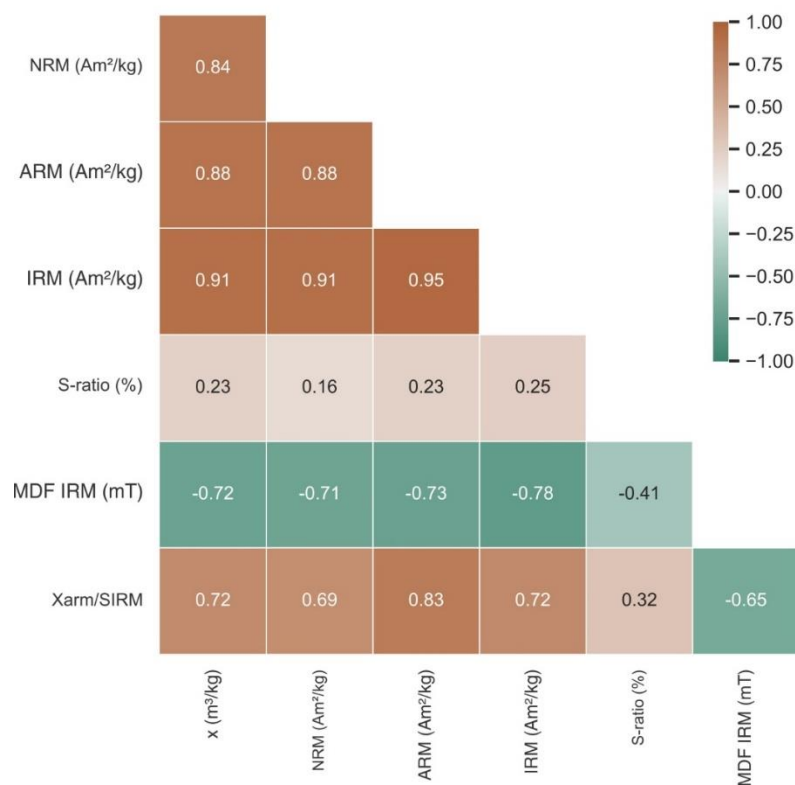
Figure 2-9: Spearman rank correlation of magnetic properties of speleothems (Susceptibility, Natural Remanent Magnetization (NRM), Anhysteretic Remanent Magnetization (ARM), Isothermal Remanent Magnetization (IRM), S-ratio, Median Coercivity Field of IRM and Susceptibility of ARM by IRM).

In the speleothems, a strong correlation (>0.84) is found among the magnetic concentration parameters (Susceptibility, NRM, ARM and IRM) (Figure 2-9). This result supports the idea that the different magnetic concentration parameters (Table 2.1) are essentially recording the same signal, with a predominance of ultrafine magnetite/maghemite in (sub-)tropical karst system. The strong correlation found using diverse rock magnetic parameters that responds different to concentration, granulometry, types of magnetization and magnetic mineralogy (Section 2.1.5), shows that previous interpretations of the pedogenic origin of magnetic grains prevails tropical in karst systems and can be used to interpret local soil dynamics and rainfall regimes (Fu et al., 2021; Jaqueto et al., 2016).

The proportion of low-coercivity minerals indicated by S-ratio have a weak correlation coefficient (0.16 to 0.25) with magnetic concentration parameters. Antiferromagnetic minerals have been previously reported in stalagmites, mainly goethite and hematite (Font et al., 2014; Lascu and Feinberg, 2011; Strauss et al., 2013), this positive weak correlation with S-ratio

could indicate that the concentration parameters favor the input of low-coercivity minerals (magnetite, maghemite) and the changes observed in concentration parameters can be associated with a detrital concentration in dripwater, instead of changes in mineralogy. So, changes in mineralogy tracked by S-ratio that correlate with magnetic concentratrion parameters would mean a more complex dynamics in karst system with changes of the dominant magnetic mineral phase, which is not found in (sub-)tropical regimes.

Coercivity parameters (MDF_{IRM}) have a strong negative correlation (0.71 – 0.78) with magnetic concentration parameters (Figure 2-9). This could indicate a better selection of magnetic mineral grain-size and/or changes in soil oxidation reaction (Ge et al., 2014). This is also evidenced by a negative moderate correlation (-0.41) with S-ratio, where a high coercivity could mean the presence of weathering (carbonate), detrital flood grains, and hematite (stable 'old' soils). Granulometry parameter (χ_{ARM}/SIRM) has a moderate negative correlation with MDF_{IRM} (-0.65) and could be related to magnetic interaction between grains (Egli and Lowrie, 2002).

2.1.8.2 The influence of biomes on magnetic mineral formation

Biomes are defined by climate, leaf structure, leaf type, and plant spacing (Fairchild and Baker, 2012). In karst systems, the most common soils are Rendzina soils, with a characteristic of few centimeters and with relatively permeable bedrock, which allows the free drainage of soil profiles and anaerobic conditions. So, we grouped the samples by their biomes (Figure 2-2, Figure S1) (Olson et al., 2001), compared with a magnetic concentration parameter (IRM) and coercivity to test for any correlation with different biomes (Figure 2-10). We chose these parameters based on the correlation between concentration parameters and coercivity due to their similarity with soil values.

The results from IRM grouped by biome (Figure 2-10) show a lower concentration in the Amazon, Atlantic and Caatinga biome, and higher concentrations and higher dispersions for the Cerrado biome. The coercivity values show a higher value for Amazon, Atlantic and Caatinga biomes and lower values for Cerrado. Interestingly, these results are exactly consistent with the soil study of (Maxbauer et al., 2017), which examined magnetic properties of modern soils as a function of grassland (savannah) and forest biomes in mid-latitude Minnesota. The

coherence observed between speleothem coercivity and IRM with the biomes may simply be a further expression of the close relationship between pedogenic processes at the surface and incorporation of pedogenic minerals into underlying karst features. Thus, in tropical settings such as Brazil, the magnetic mineral assemblages in speleothem may best be interpreted within the context of pedogenic processes.

- Cerrado biome (savannah shrubland): a high concentration of magnetic minerals (median IRM of 1.40×10^{-4} Am²/kg) and low coercivity (median MDF_{IRM} ~18.4 mT) suggests a greater flux of magnetic minerals from the epikarst than other biomes.

- Caatinga (dry forest): higher coercivity (median MDF_{IRM} ~24.4 mT) observed may be indicative of maghemitization (partial oxidation of magnetite) (Ozdemir and Dunlop, 2010) due to fewer dry/wet cycles, thereby inhibiting magnetic enhancement. Lower magnetic mineral concentrations are observed (median IRM of ~7.17×10^{-6} Am²/kg).

- Amazon and Atlantic biomes (moist broadleaf forest): lower IRM values (median IRM of ~4.28×10^{-6} Am²/kg and ~5.05×10^{-6} Am²/kg, respectively) compared to Cerrado, and higher coercivity values (median MDF_{IRM} ~27.7 mT and 23.9 mT respectively). Two processes may explain this behavior: enhanced maghemitization may increase the coercivity, while the prevalence of waterlogged soils and the concomitant dissolution of magnetic minerals could lower their concentration and diminish the transport of magnetic minerals to the cave system.
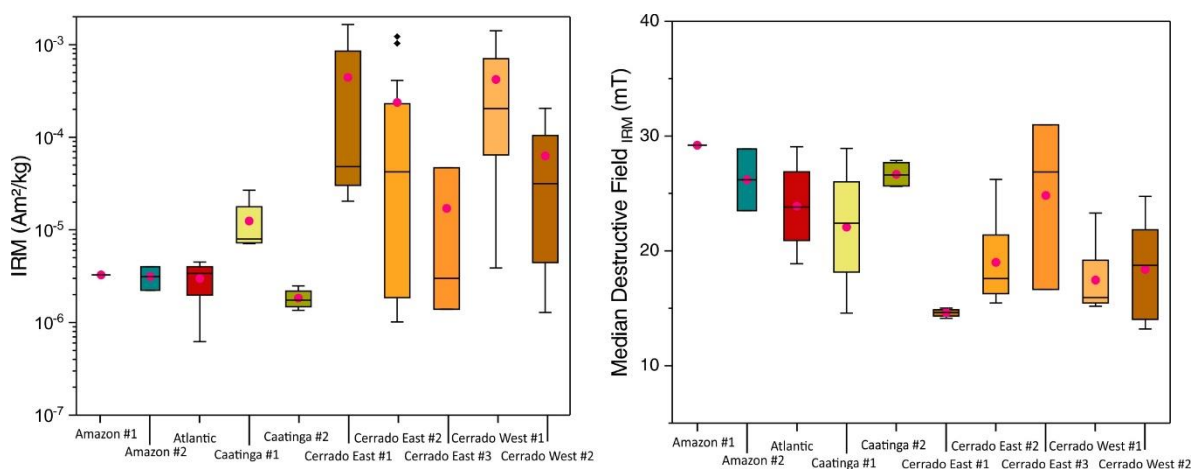

Figure 2-10: Magnetic properties of the stalagmites organized by their respective biomes. (left) Isothermal remanent magnetization and biomes; (right) Median destructive field of adjusted from IRM demagnetization curve

and its values by each biome. Amazon biome (greens), Atlantic biome (red), Caatinga biome (yellows) and Cerrado biome (oranges).

2.1.9   Summary and Conclusions

This study presents a database of stalagmite magnetic properties, including parameters related to magnetic mineral composition and concentration and grain size. In two instances we compared these values to those of overlying soil and host carbonate. These results expand our knowledge of speleothem magnetic properties in tropical-subtropical regimes far beyond what could be achieved through the examination of one or more speleothems from a single cave. Additionally, this database provides robust evidence that the main magnetic component in Brazilian stalagmites is derived from soils overlying karst systems and that processes affecting pedogenic enhancement are reflected in these speleothems. The presence of low coercivity magnetic minerals is pervasive across different latitudes and biomes. Median destruction field values from the demagnetization of IRMs show similarities between stalagmites and soil, whereas host carbonates showed consistently higher values. The fraction of remanence held by low-coercivity magnetic minerals as observed via the S-ratio (>90%) also shows this relationship.

Statistical analysis of stalagmite magnetic properties using Spearman's correlation shows a high correlation among rock magnetism concentration parameters (susceptibility, NRM, ARM, IRM). Thus, although different parameters have been reported in literature, they are essentially recording the same phenomena within (sub-) tropical zones. The weak correlation between magnetic concentration values with coercivity values shows that changes in mineralogy are not the main control in the karst system.

When compared within the four different biomes, the Cerrado biomes have a high concentration of magnetic minerals with coercivity values ~18.4 mT, whereas Caatinga, Amazon, and Atlantic biomes have a lower concentration of magnetic minerals and higher coercivity values of 24.4 mT, 27.7 mT and 23.9 mT, respectively. This result is consistent with known trends in pedogenic processes and are further evidence for the important role of pedogenic magnetite in Brazilian speleothems.

Future research on the fine-scale magnetic processes in karst systems would benefit from in-depth studies of soil profiles, constraining the physical and microbiological properties and periodically monitoring underlying caves, as is often done for oxygen and carbon isotopes studies. This approach would allow researchers to explore how the flux of magnetic particles into cave environments vary with time and seasonal across multiple biomes.

Acknowledgments

Chapter 3   Geomagnetic Field Recorded in Stalagmites

The following section (3.1) encompasses a published paper in "Proceedings of the National Academy of Sciences," where the first two authors share the primary authorship of the manuscript, as described in the published version. The supplementary material can be found on the online version of the journal. In this manuscript, I contributed to the study's design, sampling, measurements, paleomagnetism statistics and analysis, software development for relative paleointensity analysis, comparison with Africa data to test the recurrence of South Atlantic Anomaly and the draft and final form of the manuscript. The second study (section 3.2) expands the record of the Holocene for South America and has been submitted to 'Nature Communinations'. In this manuscript, I contributed to the study's design, sample preparation, measurements, paleomagnetism statistics and analysis, analysis of the geomagnetic power spectrum, draft and final form of the manuscript.

3.1 Speleothem record of geomagnetic South Atlantic Anomaly recurrence

Trindade, R.I.F., **Jaqueto, P.**, Terra-Nova, F., Brandt, D., Hartmann, G.A., Feinberg, J.M., Strauss, B.E., Novello, V.F., Cruz, F.W., Karmann, I., Cheng, H., Edwards, R.L., 2018. Speleothem record of geomagnetic South Atlantic Anomaly recurrence. Proceedings of the National Academy of Sciences, 201809197.

3.1.1   Abstract

The diminishing strength of the Earth's magnetic dipole over recent millennia is accompanied by the increasing prominence of the geomagnetic South Atlantic Anomaly (SAA), which spreads over the South Atlantic Ocean and South America. The longevity of this feature at millennial timescales is elusive because of the scarcity of continuous geomagnetic data for the region. Here we report a unique geomagnetic record for the last ~1500 years that combines the data of two well-dated stalagmites from Pau d'Alho cave, located close to the present-day minimum of the anomaly in central South America. Magnetic directions and relative paleointensity data for both stalagmites are generally consistent and agree with historical data from the last 500 years. Before 1500 CE the data adhere to the geomagnetic model ARCH3K.1, which is derived solely from archeomagnetic data. Our observations indicate

rapid directional variations (>0.1 °/yr) between ~860-960 CE and ~1450-1750 CE. A similar pattern of rapid directional variation observed from South Africa precedes the South American record by 224 ± 50 years. These results confirm that fast geomagnetic field variations linked to the SAA are a recurrent feature in the region, and the delay between continents possibly reflects the westward migration of the anomaly. We develop synthetic models of reversed magnetic flux patches at the core-mantle boundary and their expression at the Earth's surface. This model qualitatively resembles observational data, suggesting that the observed field behavior can result from the superposition between westward and southward moving, mid-latitude patches, combined with their expansion and intensification.

3.1.2   Significance Statement

Experimental and modeling evidence demonstrate the recurrence of the South Atlantic Anomaly. The areal growth of this geomagnetic anomaly accompanies the fast decay of the Earth's magnetic field, but its origin and longevity are still poorly understood given the scarcity of geomagnetic data in the southern hemisphere. We report a ~1500-year record with unprecedented resolution obtained close to the present-day minimum of the anomaly in South America from continuously grown cave speleothems. This unique record reveals rapid variations in direction and intensity of the local field as a function of the location and magnitude of the anomaly. Synthetic secular variation models show this feature reflects westward migration, expansion and intensification of reversed flux patches on the core-mantle boundary.

3.1.3   Introduction

The South Atlantic Anomaly (SAA) marks the position of the weakest geomagnetic field on Earth, and has long been recognized as a major sink for high-energy particles in the magnetosphere, with consequences for orbiting satellites, as well as telecommunication networks and transmission grids (Heirtzler, 2002). Historical geomagnetic data from ship-logs, magnetic observatories and more recently from satellites indicate that the SAA has been a prominent feature of the geomagnetic field since at least 1590 CE (Finlay et al., 2016b; Hartmann and Pacca, 2009; Thebault et al., 2015). These records indicate that the size of the anomaly has increased concomitant with increasing prominence (i.e., ever weakening field intensity), and the

anomaly has migrated continuously westward at a mean longitudinal speed of 0.17 ° yr^{-1}. Areal growth and intensity decay are linked to the first-order variations of the geomagnetic field, more specifically, the relative increase of non-dipole terms relative to the overall field geometry (Hartmann and Pacca, 2009; Pavon-Carrasco and De Santis, 2016) and the steady decay in the dipole moment itself at a rate of ~15 nT yr^{-1} (Finlay et al., 2016b; Jackson et al., 2000). These effects reflect deep Earth processes emanating from the core-mantle boundary where the proliferation of reverse flux patches (RFPs), particularly beneath the South Atlantic, causes a breakdown in symmetry in the advection sources of the axial dipole moment (Finlay et al., 2016b; Gubbins et al., 2006).

Reconstructing the SAA anomaly at the so-called archeomagnetic (or millennial) timescale is not trivial, mainly due to the scarcity of geomagnetic data in the southern hemisphere (Brown et al., 2015; Donadini et al., 2009). Besides recent advances in data acquisition (Hare et al., 2018; Poletti et al., 2016; Roperch et al., 2015; Tarduno et al., 2015a), the archeomagnetic datasets from Africa and South America that are essential for the reconstruction of the SAA evolution contribute respectively only 2.5 % and 2.8 % to the global geomagnetic database (Brown et al., 2015). Directional and intensity data recently obtained for Africa indicate relatively rapid directional changes (> 0.1 ° yr^{-1}) between ~400-550 CE, ~550-750 CE and ~1225-1550 CE accompanied by a fast decrease in intensity of -54 ± 36 nT yr^{-1} (Hare et al., 2018; Tarduno et al., 2015a). In comparison, a recent assessment of the archeomagnetic database for South America revealed only two intensity values before 1500 CE (Poletti et al., 2016). Most archeomagnetic data from South America is limited to historical lava flows and baked clay artifacts produced after the arrival of Europeans at 1500 CE. Several attempts to obtain archeomagnetic data from pre-Columbian archeological artifacts in Brazil and neighboring countries have been unsuccessful, mostly due to the incomplete baking of native ceramics (Hartmann et al., 2011). As a consequence, the only records of the geomagnetic field for South America at the millennial timescale are provided from studies of lake sediments (e.g., Escondido Lake (Gogorza et al., 2004)).

Baked-clay archeological artifacts and sediments are the classical archives used to reconstruct the geomagnetic field at millennial timescales. However, each of these records comes with caveats, particularly in recovering the Earth's field fluctuations at the centennial to millennial timescales. Baked clay archeological artifacts (and lavas) provide an absolute measure of the field intensity based on thermoremanent magnetization (Coe, 1967), but these materials

provide only episodic snapshots of the field. Sediments have the advantage of providing a continuous directional record of the local geomagnetic direction, but age uncertainties from sediments are typically on the order of hundreds to thousands years (Korte et al., 2011; Panovska et al., 2015). Sedimentary paleomagnetic records can also be afflicted by a delay between the age of sedimentation and the age of magnetization (Egli and Zhao, 2015; Nilsson et al., 2014; Roberts et al., 2013; Tauxe et al., 2006) or be obliterated by further diagenesis (Roberts, 2015). In addition, sediments can be affected by dewatering and compaction after remanence acquisition (Lascu and Feinberg, 2011; Tauxe and Kent, 2004), which produces shallower magnetic vectors. Speleothems, on the other hand, present several advantages over archeomagnetic and sedimentary archives by being usually continuous over thousands of years and readily dated at a very high precision by the radiometric ^{230}U-^{234}Th method (half-life of 245,000 years). As chemical precipitates, speleothems are not affected by post-depositional compaction effects (Lascu et al., 2016). Moreover, in contrast with soft sediments, the time lag between deposition of magnetic particles on the top of the stalagmite and remanence lock-in is very short, comprising hundreds of seconds at most (Dreybrodt and Scholz, 2011; Lascu and Feinberg, 2011; Latham et al., 1979; Morinaga et al., 1989), therefore ideally allowing the radiometric age obtained for each layer to be directly attributed to the remanence recorded in it.

Here we provide a ~1,500 years geomagnetic field record for central South America based on the magnetic remanence of two rapidly-grown and well-dated stalagmites. This high-resolution record reveals periods of rapid changes in the direction and intensity of the field out-of-phase with similar events in Africa (Hare et al., 2018). Then, synthetic models of migration, expansion and intensification of reversed magnetic flux patches are applied to test the mechanisms at the origin of the observed field variations.

3.1.4 Sampling and Dating of Pau d'Alho Stalagmites

Paleomagnetic and relative paleointensity data were obtained from two stalagmites from the Pau d'Alho cave system (15°12′20″ S, 56°48′41″ W), which is located near the present-day minima of the SAA, in Midwest Brazil. Samples Alho 06 and Alho 31 are cylindrical stalagmites, respectively 240 mm and 135 mm tall, with a nearly constant diameter of ~6 cm. The dominant mineralogy, determined by X-ray diffraction in both samples, is magnesian calcite

(~97%) with minor amounts of dolomite and quartz attributed to the detrital contribution from weathered dolomitic host rock. The internal structure is marked by a very regular stratigraphy of alternated millimetric layers of light grey to brownish calcite, with no evidence of hiatuses. Different strategies were used for their azimuthal orientation. Alho 31 was oriented in situ with a magnetic compass, and its declination was rotated by the azimuth measured during sampling, whereas Alho 06 had its declination rotated to the average declination of the IGRF model (-3.68 °) for the age of the youngest specimen (1932 CE ± 23 CE). The speleothem samples were cut into specimens consisting of thin slices of ~7 mm (Alho 06: 34 specimens) and ~5 mm (Alho 31: 27 specimens). U-Th dating shows mean growth rates of 0.169 ± 0.004 mm yr^{-1} (543 CE to 1932 CE) for Alho 06 (Novello et al., 2016) and 0.151 ± 0.008 mm yr^{-1} (1090 CE to 1922 CE) for Alho 31 (Figure 3-1, Table S1). These relatively high growth rates imply that each 7 mm or 5 mm specimen records a few decades of the geomagnetic field (~39 years for Alho 06 and ~32 years for Alho 31). Changes in growth rate are observed in both stalagmites, most pronouncedly at 30-50 mm from the top for Alho 06 and 40-75 mm from the top for Alho 31. The conversion of depth to age follows the model of Figure 1 and therefore takes these changes into account (see Methods). The most significant increase in accumulation rates observed in the two studied stalagmites occur in the interval between 1600 and 1820 CE, when precipitation was higher in the region associated with the Little Ice Age period (Novello et al., 2016). Both stalagmites ceased growth at the beginning of the last century, probably also due to changes in the hydrology of the cave resulting either from a dry period or by the blocking, in the epikarst, of the drip water supply to the speleothems.
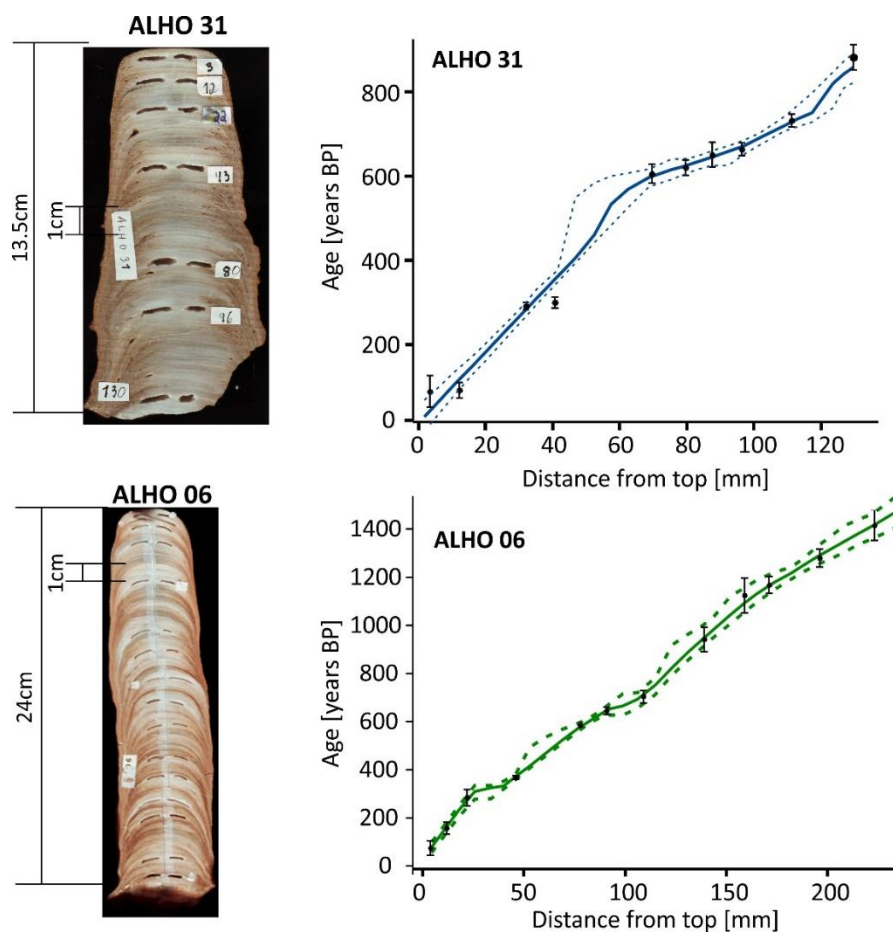
Figure 3-1: Stalagmites from Pau d'Alho cave (15°12′20″S, 56°48′41″W). Samples Alho 31 (upper) and Alho 06 (lower) with respective U-Th dating points and age-model. Dashed lines indicate 95% confidence calculated from Monte Carlo fitting of ensembles of straight lines.

3.1.5   Origin and Identification of Magnetic Minerals

The main magnetic mineral in both stalagmites is magnetite. Low temperature experiments on bulk samples show a Verwey transition (~120 K) in room-temperature saturation isothermal remanent curves (Figure S1). This transition is accentuated when analyzing the magnetic separates from the same samples (Figure S2). Goethite is also found, being identified by the characteristic separation of field cooling and zero-field cooling curves in both bulk samples and separates (Figures S1 and S2). The origin of magnetite can be inferred from coercivity unmixing analyses of anhysteretic remanent magnetization curves (ARM) (Figure S3) (Maxbauer et al., 2016b). ARM data in all previous studies of speleothems plot in the field of extracellular and pedogenic magnetite (Egli, 2004a), including stalagmites from Spain (Osete et al., 2012), Portugal (Font et al., 2014), South China (Zhu et al., 2017), Brazil (Jaqueto et al., 2016) and

different sectors of the United States (Bourne et al., 2015; Lascu and Feinberg, 2011) (Figure S4). In the Pau d'Alho cave, the magnetic mineralogy of soils above the cave was compared to the magnetic minerals present in the stalagmite (Jaqueto et al., 2016). Their similarity further reinforces a pedogenic origin for the magnetic particles deposited in the stalagmite, likely formed through dissimilatory iron-reduction in the soil (e.g., (Bourne et al., 2015; Jaqueto et al., 2016)). Type and size of magnetic minerals throughout the speleothems vary little and typically present, respectively for Alho 06 and Alho 31, median destructive fields (MDF) of ~16 mT and ~13 mT and dispersion parameter (DP) of ~0.29 and ~0.27 (Figure S2). First order reversal curves (FORC) for Alho 06 and Alho 31 indicate that magnetite grains are in the single-domain range without significant magnetic interaction (Figure S5).

3.1.6   Paleomagnetic Directions and Paleointensity

Detailed stepwise alternating field demagnetization (AF) of all specimens was performed in a superconducting rock magnetometer, followed by principal component analysis (see Methods). Specimen's volume varies from 1.08 to 2.61 cm^3 (mean of 1.79 cm^3). Initial magnetic moment of Alho 06 and Alho 31 are, on average, 2.8 x 10^{-9} A m² and 2.3 x 10^{-9} A m², respectively. This relatively high initial magnetization enabled useful directional data on a resolution of tens of years per specimen to be obtained in a commercial SQUID magnetometer, which in our case has a practical sensitivity higher than 6 x10^{-11} A m^2 (see Figure S6 and Supplementary information). Vector directions were calculated with an AF field range varying from 12 mT to 35 mT, which corresponds to 12% to 54% of the NRM (Figure 3-2). A magnetic remanence (< 10%) that persisted above an applied field of 120 mT is associated with goethite (Figure 3-2). Five specimens out of 61 displayed unstable behavior during demagnetization or maximum angular deviation (MAD) $\geq 20°$, and these specimens are not further discussed.
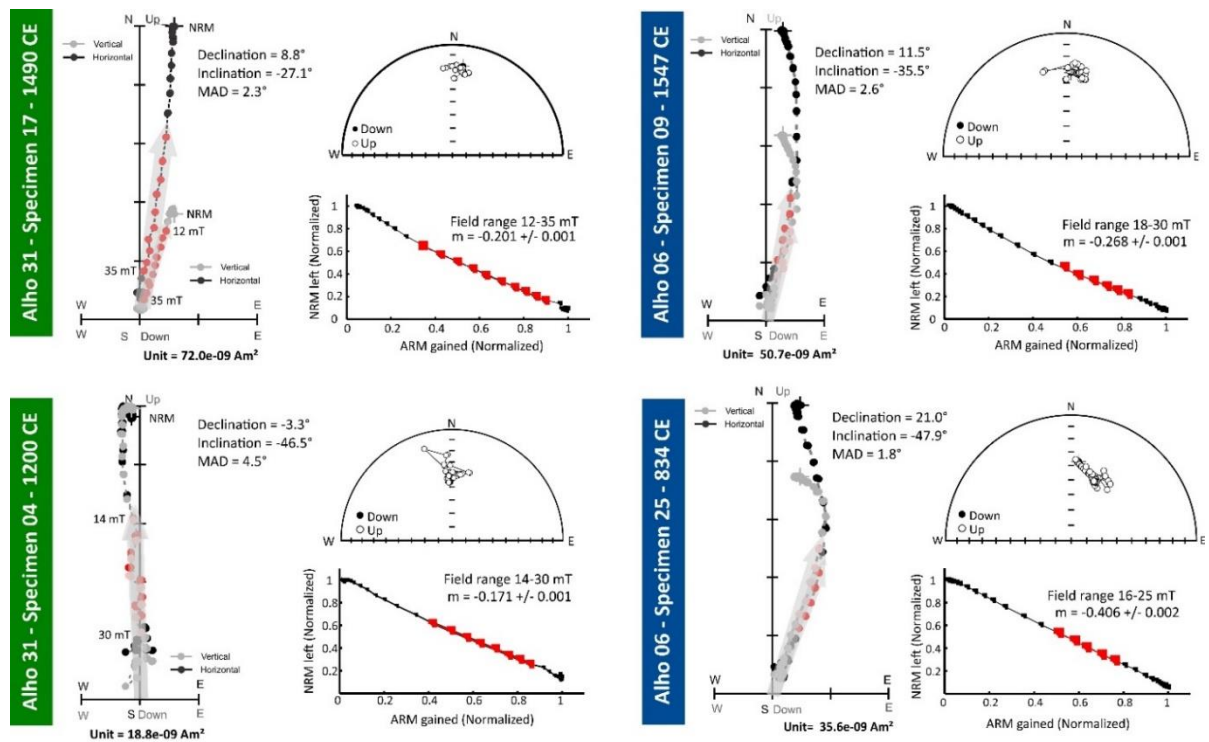
Figure 3-2: Examples of magnetic directions and relative paleointensities. Orthogonal vector plots and stereographic projections of alternating field demagnetization data, and respective relative paleointensity estimates for two specimens from each stalagmite (ages and specimen numbers are indicated). Gray arrows indicate the magnetic vectors obtained with principal component analysis (AF field range in red). Relative paleointensity was estimated following the pseudo-Thellier method (Tauxe et al., 1995), with m representing the slope of the curve ARM_{gained}-NRM_{left}.

The two stalagmites record deposition between ~1100 CE and ~1920 CE. Almost all magnetic declinations agree within error for this time period, whereas the magnetic inclinations show a ~10° difference between stalagmites (Figure 3-3, Table S2). One possibility to account for this systematic difference is the rolling of magnetic particles at the border of the stalagmite (Ponte et al., 2017). Magnetic grains in Alho 06 are arranged along an inclined plane as depicted from anisotropy of remanence measurements (Figure S7), suggesting that its specimens comprise the sloping border of the stalagmite. In contrast, magnetic grains in Alho 31 specimens (Figure S7) are arranged along the horizontal plane being thus immune to these effects. Other possibility would be a different degree of compaction between the stalagmites, but the average anisotropy degrees for Alho 06 and Alho 31 are 1.035 and 1.040, respectively, which imply compaction similar corrections of less than 2° for both stalagmites (Jackson et al., 1991).

The Alho 06 record covers a longer period of time starting at ~543 CE. Taking the entire record, magnetic declinations starting from 543 CE show two cycles of changing declination, with positive peaks at ~900 CE and ~1700 CE, and a negative peak at ~1200 CE. Declination has been decreasing since ~1700 CE. The magnetic inclination for the same stalagmite increases from ~543 CE until ~1100 CE, followed by a progressive decrease from about -40° to near 0° in recent times.

In addition to the directional data, the relative paleointensity was estimated for all specimens that presented MAD values lower than 20°. Paleointensity estimations were made across the same alternating field range used in the vectorial analysis (Figure 3-2). We retained only specimens whose standard error of the slope is less than 5% and the NRM fraction used in pseudo-Arai plots exceeds 25% (Table S2). The well-defined, straight pseudo-Arai plots obtained from our specimens corroborate the single-domain nature of the magnetic assemblage inferred from FORC curves, whereas curved pseudo-Arai diagrams would indicate the presence multidomain grains (Tauxe, 1993). There is a considerable variability of relative intensity estimates in these weakly magnetic rocks, particularly in the 1200-1400 CE interval for Alho 31 and at around 1600 CE for Alho 06. Notwithstanding, a general trend of geomagnetic field evolution for the past millennium is reproduced in the two stalagmites (Figure 3-3). The two curves also overlap the general pattern defined by the high quality archeointensity data for South America (Poletti et al., 2016), with marked intensity peaks at ~900 CE and ~1450 CE observed against a backdrop of decreasing field strength (Figure 3-3).
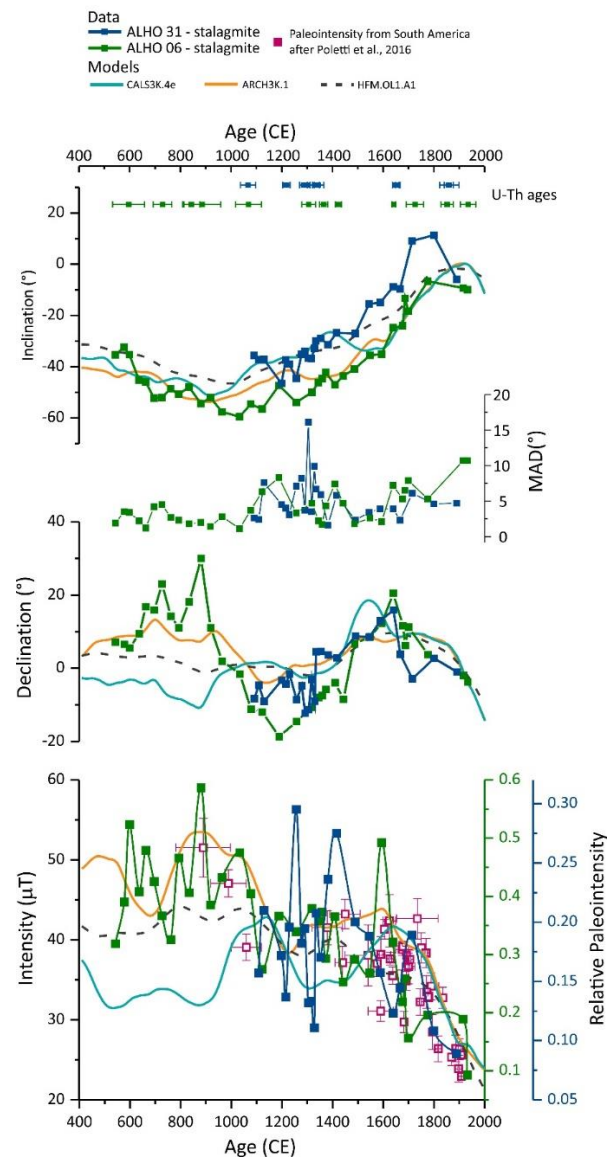
Figure 3-3: Continuous magnetic results and comparison with geomagnetic models. Radiometric ages (U-Th), magnetic declination, maximum angular deviation (MAD), magnetic inclination and relative paleointensity for specimens from Alho 31 (dark green) and Alho 06 (dark blue). Paleomagnetic results are compared to global geomagnetic field models for the Pau D'Alho cave location. CALS3k.4e (light blue) stands for "Continuous model from Archeomagnetic and Lake Sediment data" for the last 3 ka (Korte et al., 2011). Model ARCH3k.1 (orange) stands for "Archeomagnetic data" for the last 3 ka (Korte et al., 2009). Model HFM.OL1.A1 stands for "Holocene Field Model". This last model accounts for archaeomagnetic, lava flows and sedimentary data covering the past 10 ka, and is is less sensitive to outliers than CALS3k.4e yielding more stable estimates (Panovska et al., 2015). From 1840 to 1990 CE the three geomagnetic models are constrained by the *gufm1* model (Jackson et al., 2000). Also shown are the high quality South American archeointensity data from bricks, ceramics, tile and historic basalts for the last 700 years (pink squares and error bars), these data were relocated to the Pau d'Alho location for comparison (Poletti et al., 2016).

3.1.7 Stalagmite Record vs. Geomagnetic Field Models

Previous use of speleothems as recorders of the geomagnetic field has been focused on long-term variations or magnetic excursion events (Lascu et al., 2016; Latham et al., 1979). Here, we show that two well-dated, fast-grown stalagmites reproduce the field within error at a ~40 years resolution for the last 1500 years (Figure 3-3). The speleothem record matches both in direction and intensity the evolution of the field described by the geomagnetic models for recent times, when historical records are used to constrain the models HFM.OL1.A1, CALS3k.4e and ARCH3k.1 (Figure 3-3). Before 1200 CE the models diverge, most likely due to the different datasets on which they are based on (Panovska et al., 2015; Terra-Nova et al., 2016). It is noteworthy that field direction and intensity retrieved from the stalagmite data follow the ARCH3k.1 model (Korte et al., 2009), which was constructed solely from archeomagnetic data with no input from South America. Archeomagnetic data from South America for the 800-1200 CE obtained after the model was made are plotted in Figure 3 and corroborate the ARCH3k.1 model. In contrast, the other models (HFM.OL1.A1 and CALS3k.4e) include lake sediment data from Argentina that typically drive the model to lower intensities in the 400 CE to 1000 CE interval, a pattern that is not reproduced in our stalagmite data.

3.1.8 Rapid Directional Changes in South America and South Africa

A combined curve of paleosecular variation was constructed for the two stalagmites (Figure 3-4, Table S3). This curve traces a coherent loop that matches the ARCH3k.1 model within error for the Pau d'Alho location. The data describes a clockwise loop from ~570 CE to ~1450 CE, followed by a northward departure up to ~1700 CE and then a rapid westward migration until ~1920 CE. The validity of the stalagmite results is reinforced by the good match of the angular variation recorded in this archive compared to that of the geomagnetic model from the period between 1590 CE and 1900 CE (Figure 3-4), where the ARCH3k.1 model is constrained by the historical records (Jackson et al., 2000; Korte et al., 2009). Before 1590 CE, the variation observed on the stalagmite record is ~0.10 ° yr^{-1} until ~1450 CE, with a peak of 0.12 ° yr^{-1} at ~900 CE. After ~1450 CE, there is a general increase, with marked shifts at ~1500 CE and ~1700 CE.
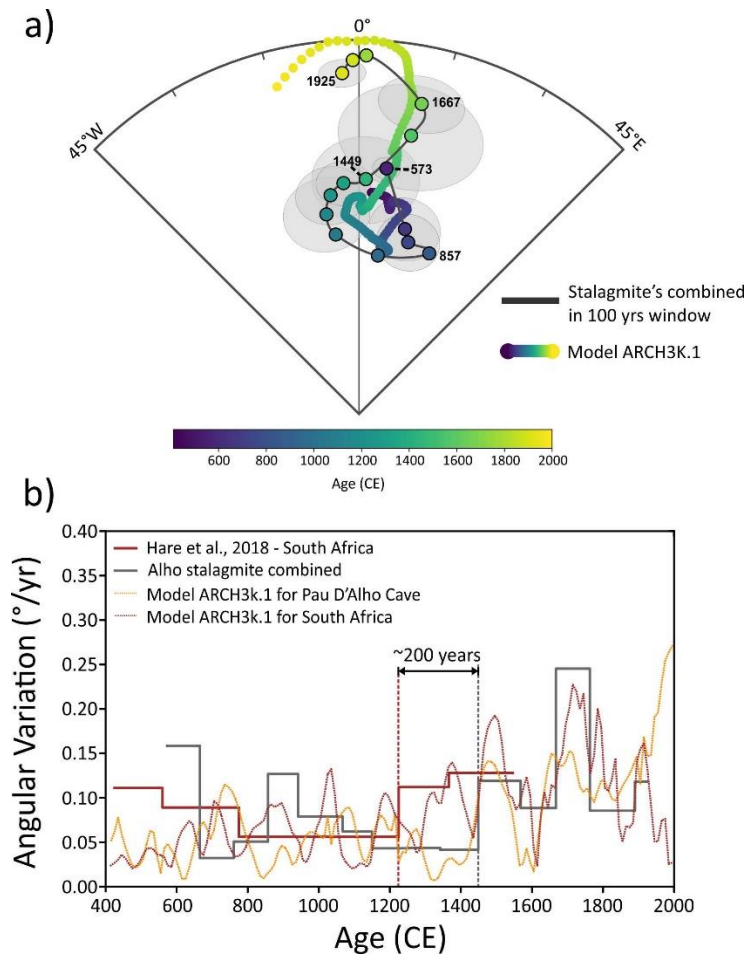
Figure 3-4: Geomagnetic secular variation. (a) Stereonet of 100 years window combined stalagmites directional data with 95% confidence ellipses with respective mean ages and comparison to model ARCH3k.1 (Korte et al., 2009); the color scale corresponds to age. (b) Angular variation of the field from South America (grey line) and South Africa (dark red line) (Hare et al., 2018); orange dashed line represents the model ARCH3k.1 for Pau d'Alho location and dark brown dashed line represents model ARCH3k.1 for the center of South Africa (Hare et al., 2018). Red (grey) bars indicate intervals with rapid directional variation in the geomagnetic field in South America (Africa).

The angular variation of Pau d'Alho stalagmites can be compared to that obtained from archeological burnt clay structures in South Africa (Hare et al., 2018). A meaningful coherence between them is observed from 1225 CE (South Africa) to 1449 CE (South America) where both paths increase their angular variation to ~0.13 ° yr^{-1} (Figure 3-4) with a time-lag of 224 ± 50 years. This result is validated by the ARCH3k.1 model in their respective locations for this period. Between ~1200 CE and ~600 CE the same trends are observed in stalagmite and burnt clay structures, with a decrease in South Africa from ~550 CE to ~750 CE and a similar decrease in South America from ~850 CE to ~1150 CE. Interestingly, the increase in directional changes recorded in Pau d'Alho stalagmites is accompanied by a decay in intensity values in the ARCH3k.1 model; this is observed at ~900 CE and at ~1450 CE. These rapid changes in

paleointensity were found in South Africa (Hare et al., 2018), again with a time lag of approximately 200 years between Africa and South America for the last period.

3.1.9   A Recurrent South Atlantic Anomaly?

The SAA may be a very ancient feature of the geomagnetic field (Tarduno et al., 2015a). According to Tarduno et al. (Tarduno et al., 2015a), a large and long-lived mantle heterogeneity stationed beneath Africa would control the preferential location of reverse flux patches (RFP) at the core-mantle boundary (CMB) by inducing local topographic roughness at the CMB making this region a preferential site for flux expulsion from the core. The tracking of RFPs throughout the last 3000 years using the available geomagnetic field models attests to the recurrence of reverse patches at specific regions and supports the hypothesis their link to mantle heterogeneities (Terra-Nova et al., 2016), but when kernel functions that link the location of reverse patches at depth to the location of the anomalies at the planet's surface are considered, a straightforward link between these features and the SAA has not been be established (Terra-Nova et al., 2017).

In order to test the mechanisms that would potentially contribute to the rapid field changes observed in South America and South Africa and the delay observed between the records at each side of the South Atlantic, we conducted a series of seven synthetic tests of secular variation (SV) (Figure 3-5, Table S4) over a 400 years timespan. In these tests, advection is given by westward and southward drift, stretching is represented by expansion of RFP and diffusion by its intensification (see details in the Supporting material and in Table S4).
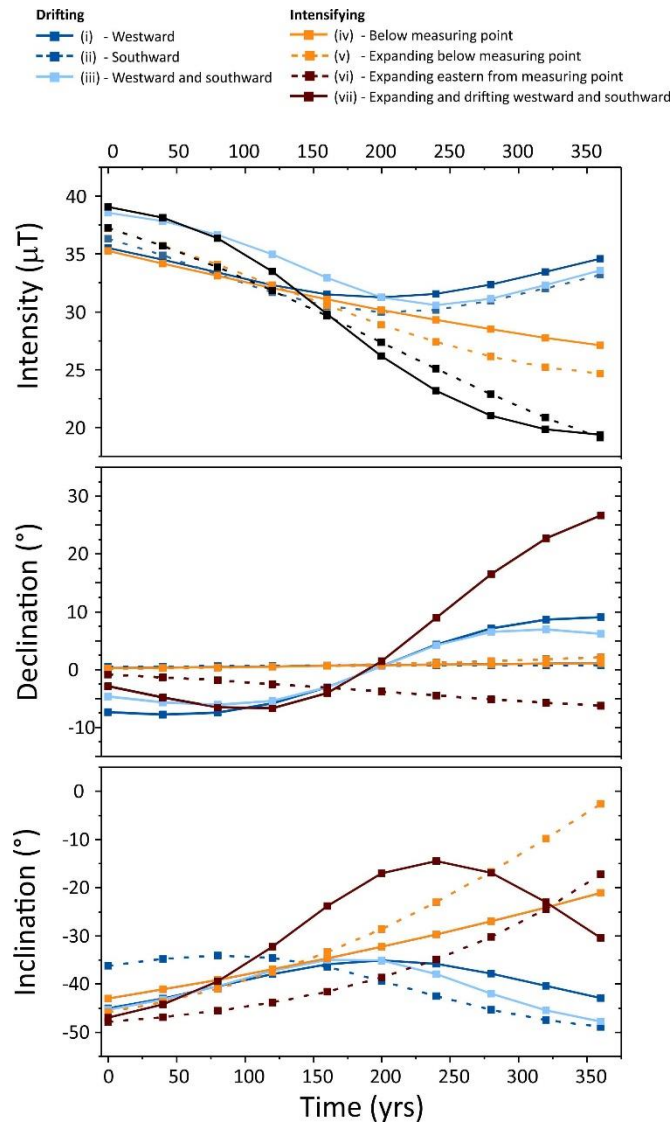
Figure 3-5: Secular variation scenarios. (i) in blue for westward drift, (ii) in red for southward drift, (iii) in purple for westward coupled with southward drift, (iv) in green for intensification, (v) in black for intensification and expansion, (vi) in orange for eastern intensification and expansion and (vii) in navy for all SV mechanisms. Dashed lines denote the snapshot where an RFP is just below the measuring point, navy dashed line overwrite purple dashed line. Note that for westward drift (blue curve) there is a mirror effect whereas for SV scenarios with southward drift a faster decay is observed as RFP approaches and slower enhancing is observed as it goes away. These effects are not seen when all SV mechanism are applied due to its large influence time (navy lines).

Westward drift of an RFP is the most efficient mechanism for rapid changes of declination (scenario i, Figure 3-5). Pure southward drift and pure intensification effects can be neglected as sole mechanisms behind the observed variations (scenarios ii and iv in Figure 3-5 and Table S4). Intensification of an RFP coupled with its expansion is more efficient if the RFP grows eastwards than just below the measuring point. In contrast, scenarios that combine expansion and intensification of an RFP are more effective in changing inclination than those involving westward drift. Note that apart from westward drift all SV scenarios produce sharper changes in inclination than in declination. Field intensity decreases in all tested SV

scenarios, but those involving exclusively advection of an RFP were the least efficient. Intensification works better when coupled with expansion and when the RFP is not below the measuring point. Finally, when all SV mechanisms are combined the directional and intensity changes are the most pronounced. Of the scenarios considered, this is the only one where rapid intensity decay and sharp directional changes occur and are shifted in time (Figure 3-5 and Table S4). Usually, the fastest intensity decay can be thought as the result of the arrival of the anomaly and the rapid changes in declination correspond to when the center of the anomaly is the closest to the measuring point.

The synthetic scenarios are simple approximations of the field and lack the complexity of the Earth's actual magnetic field. But these models do give insights into how an RFP can alter the geomagnetic record and what to expect in a measuring point where an RFP region is prominent as over the South Atlantic Ocean. In our analysis, westward drift alone does not suffice to explain the rapid changes observed. Westward drift is by far the main source of observed sharp changes in declination, but intensification and expansion of RFPs are needed to produce the abrupt variations of inclination and the rapid decay of intensity also seen in our observations. Moreover, in a scenario where changes in inclination are more pronounced than in declination the SV needs more than a zonal source of field. Our results suggest that upwelling structures and diffusion were present at least as early as ~1450 CE in the South Atlantic region, and possibly as early as ~860 CE. Therefore, a weak field anomaly at the South Atlantic is expected to be recurrent as previously suggested by Tarduno et al. (2015) and Hare et al. (2018). In addition, our results indicate that the anomaly cannot be locked into the South Atlantic region since a westward drift is an essential component of its time-evolution.

3.1.10 Materials and Methods

U-Th dating. Radiometric dating was carried out at the Minnesota Isotope Laboratory using a multi-collector inductive plasma mass spectrometer (MC-ICO-MS, Thermo-Finnigan NEP-TUNE)(Cheng et al., 2013). Ten new U-Th ages were obtained for Alho 31 sample (Table S1). Ages for Alho 06 were compiled from Novello et al. (Novello et al., 2016). Age-models and corresponding 95% confidence limits were obtained through Monte Carlo fitting of ensembles of straight lines with the software StalAge (Scholz and Hoffmann, 2011).

Paleomagnetic and paleointensity measurements. Remanent measurements were carried out in Laboratório de Paleomagnetismo of Universidade de São Paulo (USPmag). Remanence was measured in a 755-1.65 2G Enterprises DC SQUID magnetometer (noise level ~10^{-11} Am²) with coupled alternating field (AF) and direct current coil in a u-channel system. An analysis of the practical sensitivity of the equipment using the acetate tray is provided in the Supplementary information. The specimens were submitted to stepwise AF demagnetization along 30 steps up to 140 mT. Directions were analyzed using principal component analysis (Kirschvink, 1980). The criterion for direction acceptance was a maximum angular deviation (MAD) below 20°. Relative paleointensity estimates followed the pseudo-Thellier method (Tauxe, 1993). The anhysteretic remanent magnetization has been preferred over the saturation isothermal remanent magnetization to calculate the relative paleointensity estimates (Lerner et al., 2017). Specimens were submitted to a direct field of 0.05 mT along the same AF steps used in the demagnetization. The slope of the ARM_{gained}-NRM_{left} curve was calculated using the line fitting method of (Coe, 1967). Acceptance criteria were: (1) standard error of the slope less than 5%, (2) fraction of the NRM used in line fitting above 25% and (3) MAD of the corresponding vector below 20°.

Anisotropy of anhysteretic remanence. This procedure investigates the preferred orientation of ferromagnetic minerals. All specimens were previously demagnetized (120 mT); then a weak magnetization was acquired with a direct current field (0.5 mT) simultaneously with a decaying alternating field (peak at 100 mT). A total of six orthogonal positions were used and the induced anhysteretic remanence was measured in a superconducting rock magnetometer. The tensor is represented as magnitude ellipsoid in a lower hemisphere, equal area plot, with principal axis lengths (K_{max}, K_{int}, K_{min}) equal to the corresponding eigenvalues (Jackson et al., 1991). The mean tensor was calculated using Jelinek and Kropácek statistics (Jelínek and Kropáček, 1978).

Magnetic mineralogy. Pau d'Alho bulk samples were subjected to ARM acquisition curves with a direct current field of 0.05 mT superposed by an alternating field in 33 steps up to 120 mT. The magnetization curves were analyzed using the software MAXUNMIX (Maxbauer et al., 2016b). Hysteresis and First-Order Reversal Curve (FORC) were performed in a Princeton Measurements Corporation vibrating sample magnetometer (VSM). The procedure for obtaining the FORC diagram was a variable-resolution that enables high-resolution analysis (Zhao et al., 2015). The procedure was adopted in both stalagmites after adjustment of hysteresis

curves through the software XFORC (Zhao et al., 2017), the generated script for the measurement with variable-resolution uses discrete averaging time of 200 ms. In addition, low-temperature experiments were performed on bulk samples and magnetic extracts. Magnetic extraction was performed following the procedure described by Strehlau et al. (2014), which consists in dissolving the carbonate and then separate the resulting residue into a magnetic "extract" using a Nd-magnet and a weaker magnetic "remainder". In practice, the extract will preferentially contain strongly magnetic minerals such as magnetite and maghemite, while the remainder will contain comparatively weaker magnetic phases such as hematite and goethite or extremely fine grained magnetite. Measurements were performed in a Quantum Designs Magnetic Properties Measurement System (MPMS-5S) housed in the Institute for Rock Magnetism (IRM) at the University of Minnesota (Strehlau et al., 2014). They consisted of room-temperature saturation isothermal remanent magnetization (RTSIRM) and field-cooling-zero-field cooling (FC-ZFC). RTSIRM corresponds to a cooling-heating cycle at null field from room temperature 300 K down to 10 K after the initial application of a direct field of 2.5 T at room temperature. Another experiment comprises two parts. The field cooling (FC) cycle consists of applying a direct field of 2.5 T from 300 K to 10 K and then measure the remanence during warming back to room temperature with null field, while the zero-field cooling (ZFC) cycle consists of cooling in null field until 10 K, then applying a 2.5 T direct field at 10 K and warming the sample back to room temperature while measuring the remanence.

Geomagnetic angular variation. The directional variation of the geomagnetic record was evaluated using data from both stalagmites combined in a running mean with 100 years of interval (Fisher, 1953). The angular rate was calculated by the ratio of the angular distance between each point of the path and the corresponding interval of time. The error of angular rate was calculated using the propagation of the 63% of confidence angle (α_{63}) as the angular error for each mean and the standard deviation of the ages from the grouped directions (Hare et al., 2018) (Table S3).

Synthetic models. To test plausible scenarios for recurrent weak field intensity and rapid field variations at the South Atlantic region, we performed synthetic tests of simple radial field configurations at the core-mantle boundary and estimated their effects on the Earth's surface using appropriate kernel functions (Terra-Nova et al., 2017). The synthetic fields were built from a background axial dipole field superimposed by local patches modeled by gaussians (Amit, 2014; Terra-Nova et al., 2017). Fluxes were set to maintain $\int_S B_r dS = 0$. In our

synthetic secular variation scenarios, advection is given by westward and southward drift, stretching by expansion and diffusion by intensification of reverse flux patches (RFP). Westward drift value used was the classical one of 0.2 ° yr^{-1} (Bullard et al., 1950). Southward drift is 0.15 ° yr^{-1} based on the evolution of the Patagonia RFP from 1930 until 1970 in the geomagnetic model *gufm1* (Jackson et al., 2000; Terra-Nova et al., 2017). Intensification is based on values of reversed flux intensification on the southern hemisphere during the historical period (Olson and Amit, 2006). Expansion scenarios use estimations of reversed flux area growth from 1880-1990 CE (Metman et al., 2018).

Acknowledgments

Author contributions

RIFT, PJ, FWC and IK conceived the work. PJ and VN collected the sample. VN, HC and RLE dated the stalagmites. RIFT, PJ, DB and GAH did paleomagnetic analysis and interpretation. BES and JMF did rock magnetic experiments. FTN produced synthetic secular variation scenarios. RIFT and PJ wrote the first version of the work and all authors contributed to the final manuscript.

3.2 Stalagmite paleomagnetic record of a quiet mid-to-late Holocene field activity in central South America

Plinio Jaqueto, Ricardo I.F. Trindade, Filipe Terra-Nova, Joshua M. Feinberg, Valdir F. Novello, Nicolas Stríkis, Peter Schroedl, Vitor Azevedo, Beck E. Strauss, Francisco W. Cruz, Hai Cheng, R. Lawrence Edwards. Stalagmite paleomagnetic record of a quiet mid-to-late Holocene field activity in central South America. Submitted to Nature Communications.

3.2.1   Abstract

Speleothems can provide high-quality continuous records of the direction and relative paleointensity of the geomagnetic field, combining high precision dating (with U-Th method) and rapid lock-in of their detrital magnetic particles during calcite precipitation. Paleomagnetic results for a mid-to-late Holocene stalagmite from Dona Benedita Cave in central Brazil encompasses ~2150 years (3147 BP to 5306 BP, constrained by 14 U-Th ages) of paleomagnetic record from 58 samples (resolution of ~39 years). This dataset reveals angular variations of less than 0.06°/yr and a relatively steady paleointensity record (after calibration with geomagnetic field model) contrasting with the fast variations observed in younger speleothems from the same region under influence of the South Atlantic Anomaly. These results point to a quiescent period of the geomagnetic field during the mid-to-late Holocene in the area now comprised by the South Atlantic Anomaly, suggesting an intermittent or an absent behavior at the multi-millennial timescale.

3.2.2   Introduction

Direct observations of the geomagnetic field since the mid-19th century revealed a low-intensity region in the South Atlantic. This South Atlantic Anomaly (SAA) is nowadays the most prominent expression of the non-dipolar field on Earth's surface (Amit et al., 2021; Constable et al., 2016). Centennial-scale reconstructions of the SAA are fundamental for a complete knowledge of the origin and persistence of such important geomagnetic feature. Nevertheless, the most common materials used to track the variations of the past geomagnetic field are archeological artifacts, volcanic rocks, and sediments. These can be divided into two main

classes (Donadini et al., 2009). The first type comprises archeological and volcanic materials which acquire thermal magnetic remanence upon cooling. They provide spot readings of the field's absolute paleointensity estimates and directional data when the original orientation of archeological structures and rocks can be assessed, but they rarely provide continuous stratigraphic records. The second material type comprises sediments, and their natural magnetism is acquired during deposition or after (post-depositional magnetic remanence). Sediments provide a continuous variation of the geomagnetic field, being good recorders of its directional behavior, and may also provide relative paleointensity estimates if certain conditions are satisfied (Tauxe, 1993). However, their age may not correspond to the age of remanence acquisition due to the time difference between sedimentation and the lock-in of magnetic particles in sedimentary strata (Korte and Constable, 2006; Tauxe, 1993).

A combination of records from archeological artifacts, volcanic rocks, and sediments is used to construct geomagnetic field models. Due to their time coverage, sedimentary records are key to understanding the geomagnetic field's time evolution at the centennial to millennial timescales (Gonzalez-Lopez et al., 2021). For example, these models reveal a persistent and dominant westward drift at high latitudes (Nilsson et al., 2020) and a dominant 1350 years cycle in the dipole tilt variation for the past 9,000 years (Nilsson et al., 2011). It has also been shown for the last 10,000 years that the southern hemisphere has a weaker average field strength than the northern hemisphere. Furthermore, the Atlantic hemisphere has more active secular variation than the Pacific hemisphere (Constable et al., 2016). Nevertheless, data coverage is described as a limiting factor when attempting more refined models, especially to understand short-time variations at high resolution in the southern hemisphere (Constable et al., 2016; Gonzalez-Lopez et al., 2021; Korte et al., 2011; Panovska et al., 2015).

One material that offers good global coverage and can be used for studies at the centennial to millennial timescale is cave speleothems (Lascu and Feinberg, 2011). Directional data from speleothems have been preferentially used to study the timing and structure of geomagnetic field excursions when the virtual geomagnetic pole locally departs more than 45° from its time-average position (Chou et al., 2018; Lascu et al., 2016; Osete et al., 2012; Pozzi et al., 2019). Also, speleothems are also a promising material to study the recent secular variation of the geomagnetic field at high temporal resolution (Ponte et al., 2018; Trindade et al., 2018; Zanella et al., 2018). In particular, a speleothem from central South America covering the last 1500 years demonstrated high rates of angular variation (>0.1°/yr.) and intensity drops with a

time lag of ~200 years when compared to equivalent events in South Africa (Hare et al., 2018; Tarduno et al., 2015). These records were interpreted as a result of the recurrence of the South Atlantic Anomaly as it migrates westward (and southward), combined with its expansion and intensification. Here we present a paleomagnetic study of a speleothem from Dona Benedita cave, in central Brazil, with ages within 3000-6000 BP. This study reports new U-Th ages, paleomagnetic directions, relative paleointensity and an assessment of the magnetic mineralogy of one well-dated speleothem, expanding the record of the geomagnetic field in central Brazil to ~6000 BP.

3.2.3   Results

3.2.3.1 Sampling and U-Th dating

Dona Benedita cave (20.57°S, 56.72°W) is located in Central-western Brazil (Figure 3-6), along the karst of Serra da Bodoquena that comprises carbonate and terrigenous rocks from the Corumbá Group (Neoproterozoic) (Sallun and Karmann, 2007). The present-day climate in the study area is humid tropical with an average temperature between 22 °C and 24 °C, with a five-month-long dry season during the austral winter (MJJAS) and annual rainfall of ~1419 mm (Sallun and Karmann, 2007). The vegetation is dominated by woodland and savannah forests that correspond to the Brazilian Cerrado Biome.

The stalagmite DBE50 from Dona Benedita cave was available in the collection of the Instituto de Geociências, Universidade de São Paulo. The sample is a fragment of a candle-like stalagmite 417 mm in height (Figure 3-6). A total of 58 paleomagnetic specimens were cut using a diamond wire saw to avoid loss of material. The average size of the specimens is ~6.9 mm in height, ~14.7 mm in length, and ~11.1 mm in width. The specimen's sizes were chosen to maximize the noise-to-signal ratio and avoid the layers' curvature on the speleothem's border. For the magnetic mineralogy study, powder samples of ~0.03g were prepared. The stalagmite DBE50 covers ~2159 years, from 3147 BP to 5306 BP, with an average specimen resolution of ~39 years (Figure 3-6). The high ^{232}Th content of the speleothem, with an average of ~9963 ppt is a result from its high fluvial detrital content. This value provides a low ^{230}Th/^{232}Th ratio with an average of ~ 3.4×10^{-5}; typical U-Th dating assumes an initial ^{230}Th/^{232}Th ratio of $4.4 \times 10^{-6} \pm 2.2 \times 10^{-6}$ (Cheng et al., 2013). The low values found for ^{230}Th/^{232}Th ratios in this speleothem are expected in a sample with visible clay and silt layers

(Figure 3-6) and imply a relatively high error in age determinations (2σ error of ~434 years). From the 14 U-Th analyses, 6 points were discarded in the geochronology model due to age inversions (where an older age is stratigraphically above a younger age) (Supplementary Table 1), and the main age model was generated with the remaining age estimations using the software COPRA.
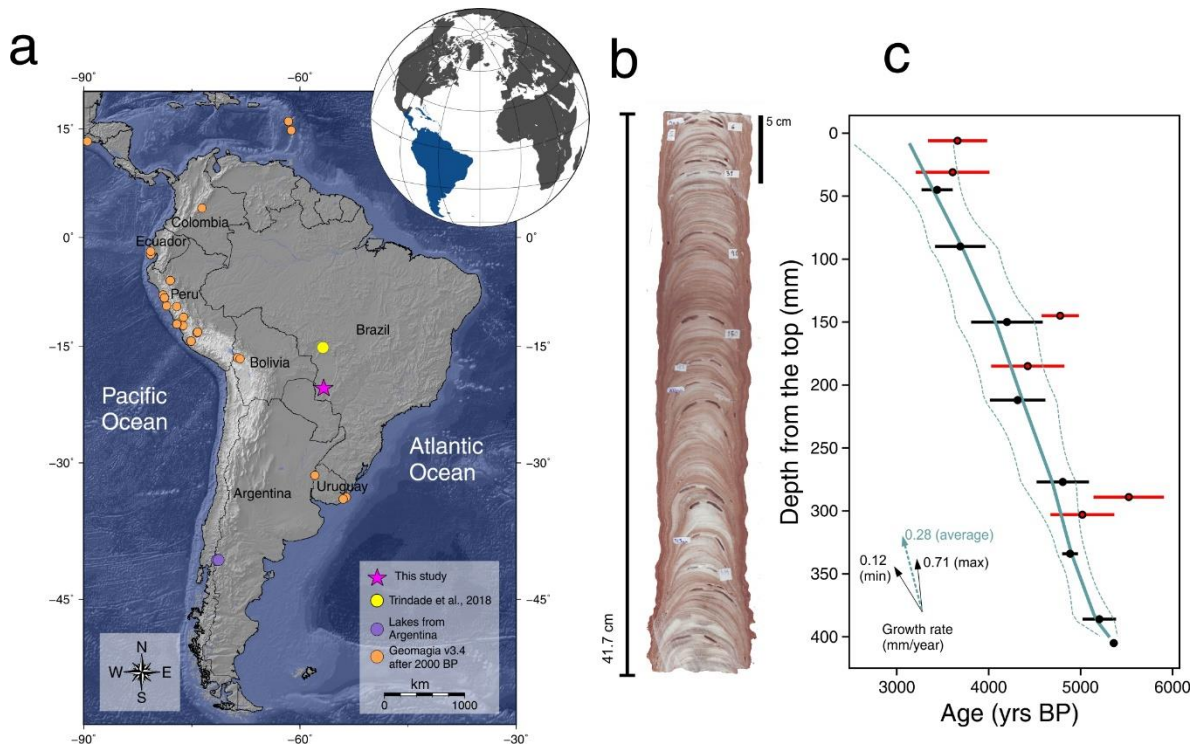

Figure 3-6: (a) Location of Dona Benedita cave (pink star) and Pau d'Alho cave (Trindade et al., 2018) (yellow circle). Also represented are the records from lakes (purple circle) (Gogorza et al., 2006; Gogorza et al., 2004), archeointensity and volcanic rocks (orange circles) for ages after 2000 BP available in the GEOMAGIA50 database v3.4 (Brown et al., 2015). (b) Stalagmite DBE50 from Dona Benedita cave and (c) age model obtained through U/Th dating; data in red are inverse ages that were discarded in the age model. The solid cyan line represents the age model obtained with the COPRA algorithm (Breitenbach et al., 2012) and dashed lines represent 95% confidence intervals. Arrows represent growth-rates with minimum and maximum values in solid black and average value in dashed cyan.

3.2.3.2 Rock Magnetism

Rock magnetic low-temperature experiments included field-cooled (FC) and zero field-cooled (ZFC) measurements, and room-temperature saturation remanent magnetization (RTSIRM) were performed in magnetic extracts obtained from the samples. In addition, bulk rock samples were submitted to stepwise anhysteretic remanence (ARM) acquisition, and the corresponding curves were deconvolved to identify different magnetic components.

 ZFC-FC experiments show that fine particles dominate the magnetic signal, as the FC data are higher than their ZFC equivalents (Figure 3-7). They also indicate the presence of goethite by the separation between curves at all temperatures (Strauss et al., 2013). The presence of superparamagnetic magnetite is suggested by a drop in remanence between (10 K and 50 K) (Ozdemir et al., 1993). Previous studies in the same region have interpreted the magnetic minerals present in speleothems in this tropical-subtropical karst system as soil-derived (Jaqueto et al., 2021; Jaqueto et al., 2016), and the presence of superparamagnetic minerals is consistent with other studies of soil magnetism (Jordanova, 2017). The Verwey transition (~120 K) is suppressed in FC-ZFC curves, but this phenomenon can be attributed to the maghemitization of the original magnetite particles (Ozdemir and Dunlop, 2010).
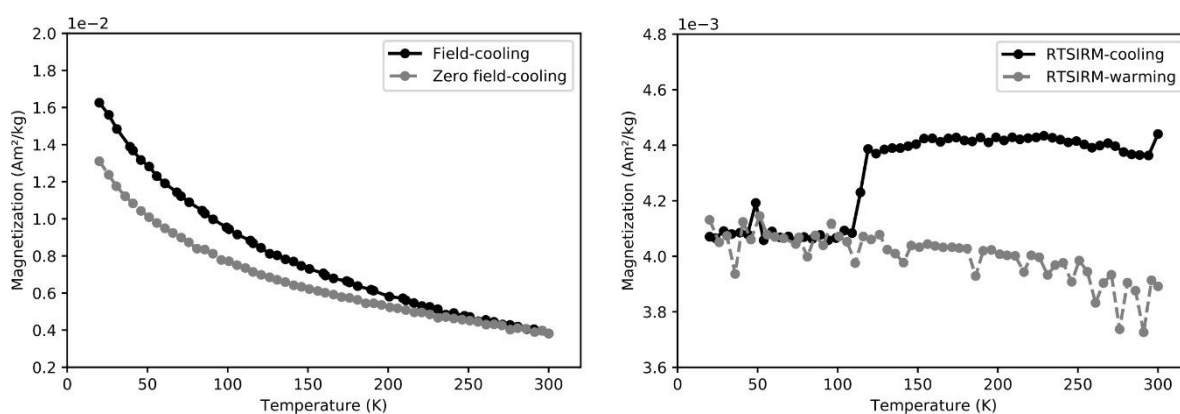

Figure 3-7: Magnetic mineralogy from magnetic extracts of stalagmite DBE50; *(left)* Curves of Field-cooling (2.5 T) (black circles) and Zero-field cooling (gray circles) measured on warming; *(right)* Curve of room temperature saturation isothermal remanent magnetization (RTSIRM); the Verwey transition (~120 K) which is characteristic of magnetite is signaled by the drop observed in the cooling curve (black circles).

The presence of magnetite is confirmed in RTSIRM experiments by the Verwey transition as a prominent drop in magnetization at ~120 K during cooling (Figure 3-7). The presence of partially oxidized magnetite and pure stoichiometric magnetite suggests a core-shell structure, with a magnetite core and a maghemite shell, a common feature of magnetic particles found in soils (Ahmed and Maher, 2018; Ge et al., 2014).

Finally, the median destructive field (MDF) of ARM for sample DBE50 (Jaqueto et al., 2021) shows values of ~16 mT (low-coercivity) and a dispersion parameter of ~0.28, consistent with extracellular magnetite of pedogenic origin according to the scheme of (Egli, 2004b), also

supporting the transport of these particles from the soil in the epikarst into the cave through drip water. This pedogenic magnetic fingerprint has also been found in other speleothems (Bourne et al., 2015; Jaqueto et al., 2016; Zhu et al., 2017).

3.2.3.3 Paleomagnetim

Paleomagnetic directions were isolated after AF demagnetization between steps 8 mT and 30 mT (Figure 3-8, Supplementary Table 2). The magnetic stability of the characteristic component can be asserted by its internal coherence and by the low values of maximum angular deviation (MAD) and deviation of the angle (DANG) (Tauxe and Staudigel, 2004). The mean MAD found was ~3.8° and the mean DANG was ~2.8° (Figure 3-8). Compared to the MAD, the lower value of DANG indicates that the characteristic magnetic component points to the origin (Heslop and Roberts, 2016). The inclinations show good agreement with the expected Geocentric Axial Dipole for the site location (inclination -36.9°). The fisher mean values obtained for the declination was -5.2°, and for the inclination was -41.7° for an $\alpha_{95} \sim 2.0°$ and N=58 (Figure 3-8, Supplementary Table 2).

The results were then plotted with their age correspondence and compared with different geomagnetic models after rotation of the declinations to the mean declination of model CALS10k.2 (Constable et al., 2016) for the same period (Figure 3-8). The geomagnetic models chosen for comparison comprise the period covered by our data: CALS10k.2 (Constable et al., 2016), HFM.OL1.A1 (Constable et al., 2016), pfm9k.1a (Nilsson et al., 2014), SHA.DIF.14k (Pavon-Carrasco et al., 2014) and BIGMUDI4k.1 (Arneitz et al., 2019), the last one being the most updated but limited to the last 4000 years (Figure 3-8).
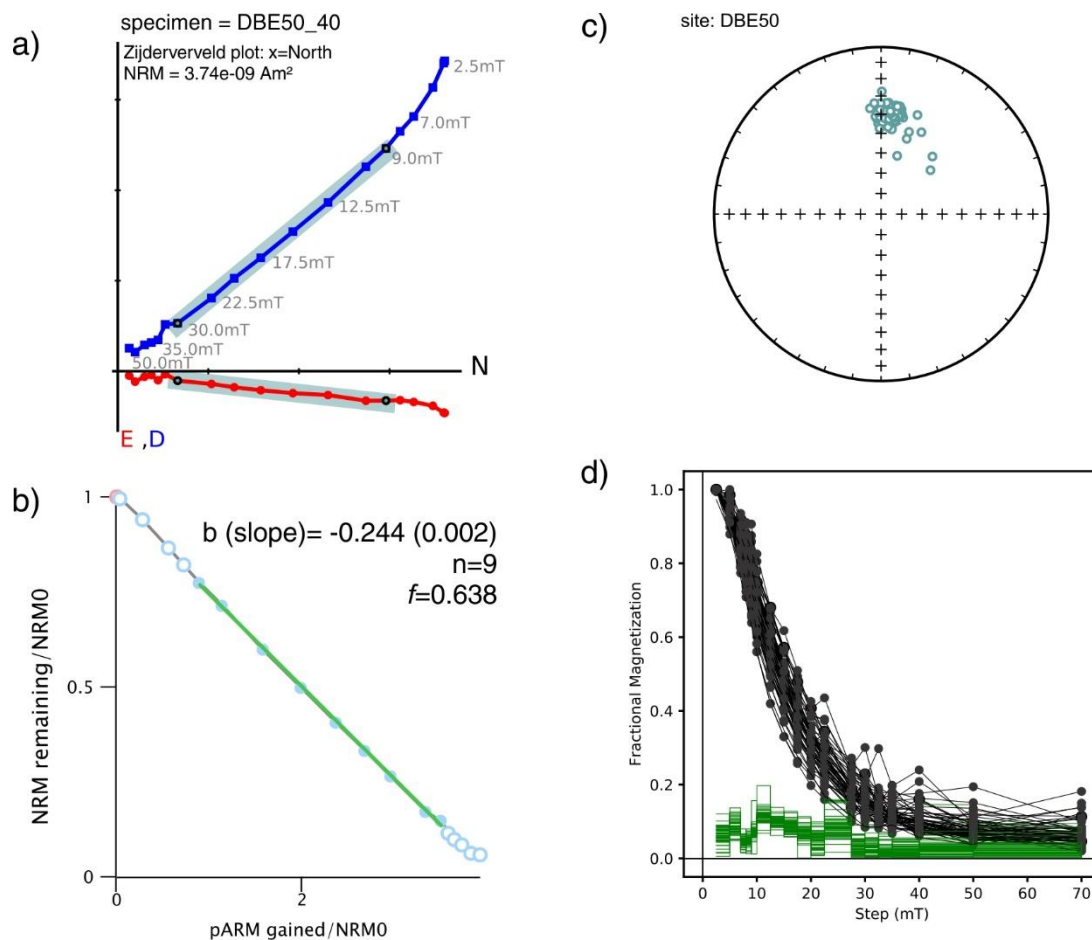
Figure 3-8: Paleomagnetic results of DBE50 stalagmite; (a) orthogonal plot for specimen DBE50_40, with respective horizontal (red) and vertical (blue) components and the characteristic direction in cyan shade (from 9 mT to 30 mT). Directional data was obtained using the PMAGPY software (Tauxe et al., 2016). (b) Relative paleointensity for the same specimen calculated with the pseudo-Thellier technique (Tauxe et al., 1995) along the same steps (n=9), corresponding to a magnetization fraction of 63% (f=0.63). The slope of the Arai-plot was obtained in Paleointensity.org software (Beguin et al., 2020). (c) Equal area plot of characteristic directions for all specimens of the DBE50 stalagmite (in-situ). (d) Demagnetization plot obtained after stepwise alternating field up to 70 mT for all DBE50 specimens (black curves), and their respective gradient (green lines) showing the preponderant contribution of magnetic fraction with remnant coercivity between 10 mT and 30 mT.
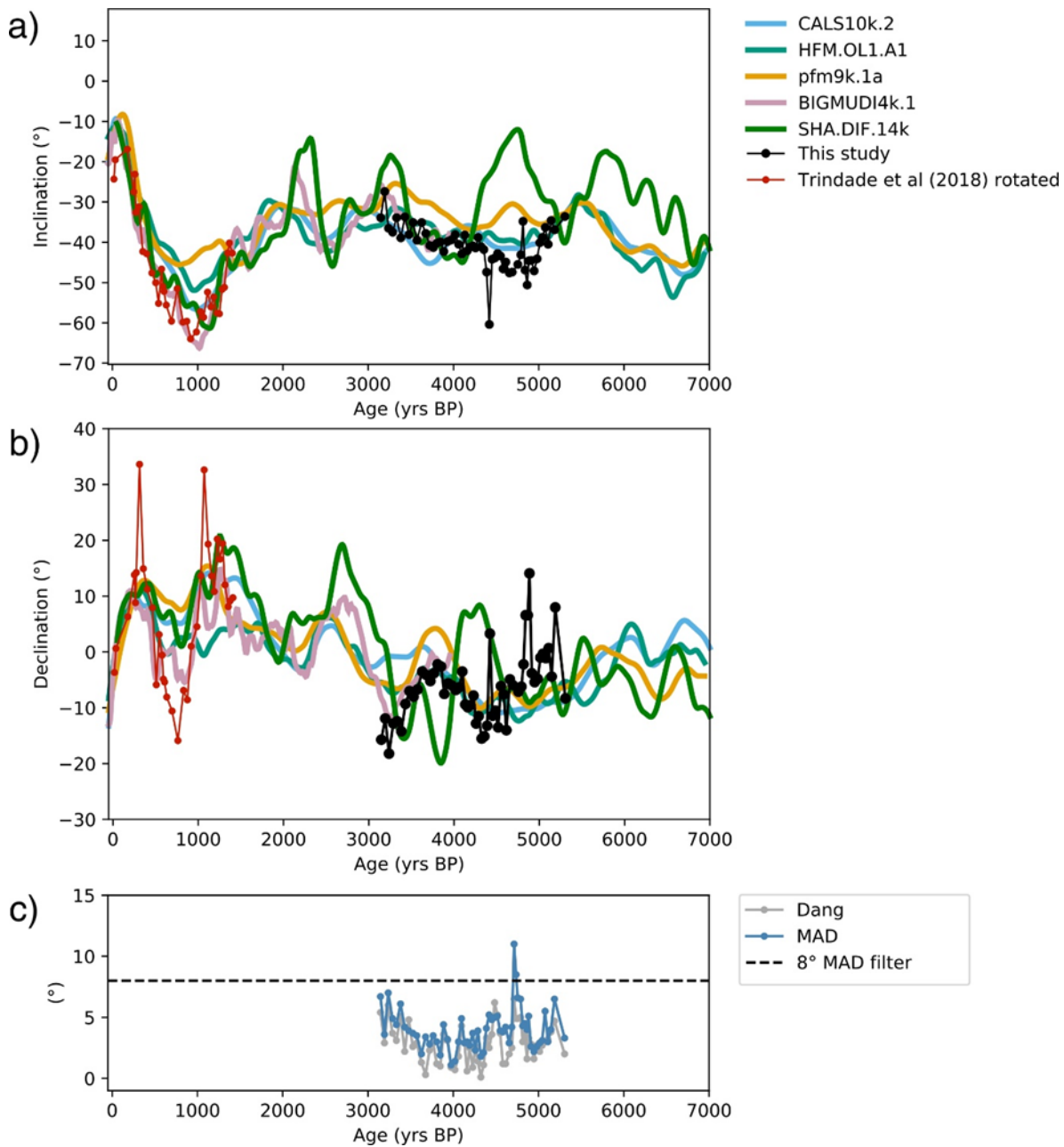
Figure 3-9: Magnetic direction data for stalagmite DBE50 (black dots): (a) inclination, (b) declination, (c) maximum angular deviation (MAD) and Deviation angle (DANG). Also represented are the following geomagnetic models for the location of Dona Benedita cave: CALS10k.2 (light blue curve), HFM.OL1.A1 (green curve), pfm9k.1a (gold curve), BIGMUDI4k.1 (light pink curve), SHA.DIF.14k (dark green curve). Results obtained for stalagmite ALHO6 (Pau D'Alho cave, red dots) were relocated to the DBE50 site location. An 8° filter (dashed line) was applied for MAD values of DBE50 specimens.

Magnetic directions show good agreement with the models. Magnetic inclination (Figure 3-9) shows a decrease from -35° to -50° at the beginning of the record (5500 BP to 5000 BP), following the trend of models CALS10k.2 and HFM.OL1.A1, although inclination from the stalagmite is about 10° lower than these models between 5500 to 4500 BP. The model pfm9k.1a presents higher values for inclination than the speleothem but keeps the same tendency,

except for a peak at ~4800 BP. The model SHA.DIF.14k differs significantly from the data and other models with peaks of low inclination at ~3200 and ~4800 BP. After ~5000 BP, the speleothem record shows a linear increase of inclination from -50° to -30° until 3000 BP (Figure 3-9), which agrees with the tendency of all models and remarkably matches the BIG-MUDI4k.1 (from 4000 BP onwards). Declination results (Figure 3-9) shows a westward trend at the beginning of the stalagmite record, between 5500 BP to 4200 BP, which is not in perfect agreement with the geomagnetic models that tend to be flat at the same time interval. Then, a short-term (800 years) eastward trend is observed from 4500 BP to 3800 BP, followed by a westward trend from 3800 BP to 3000 BP. This pattern agrees with the amplitudes observed in the BIGMUDI4k.1 model and follows the HFM.OL1.A1 as well, but it is not predicted by the CALS10k.2 or the SHA.DIF.14k models.

The relative paleointensity (RPI) estimates were obtained through the pseudo-Thellier method from an average fraction of 0.58 ±0.07 of the natural remanence encompassing eight steps. The best-fit (slope of Arai diagram) mean value was -0.19 ±0.01 (Figure 3-10, Supplementary Table 2). These results were then normalized by multiplying the absolute value of the slopes by the median value of 197.5 (See Methods for further information). Then, a cubic spline with 75 years knot was calculated to plot the RPI curve for the DBE50 stalagmite (Figure 3-10). The RPI results present a high variability compared to the geomagnetic field models. However, they are compatible with the range of absolute GEOMAGIA50.v3.4 datapoints (Brown et al., 2015) within a 2000 km radius from the cave location (Figure 3-10). A decrease in intensity at the beginning of the stalagmite record from 5500 BP to 4500 BP is observed, followed by a higher intensity peak between 4500 BP and 4000 BP, and finally, a higher variability (also observed on few data points from the database) towards lower intensities from 4000 BP to 3100 BP. The average trend defined by the speleothem record agrees with the models between 5500 BP and 3500 BP. Nevertheless, it is significantly lower for the younger record segment between 3500 BP and 3000 BP.
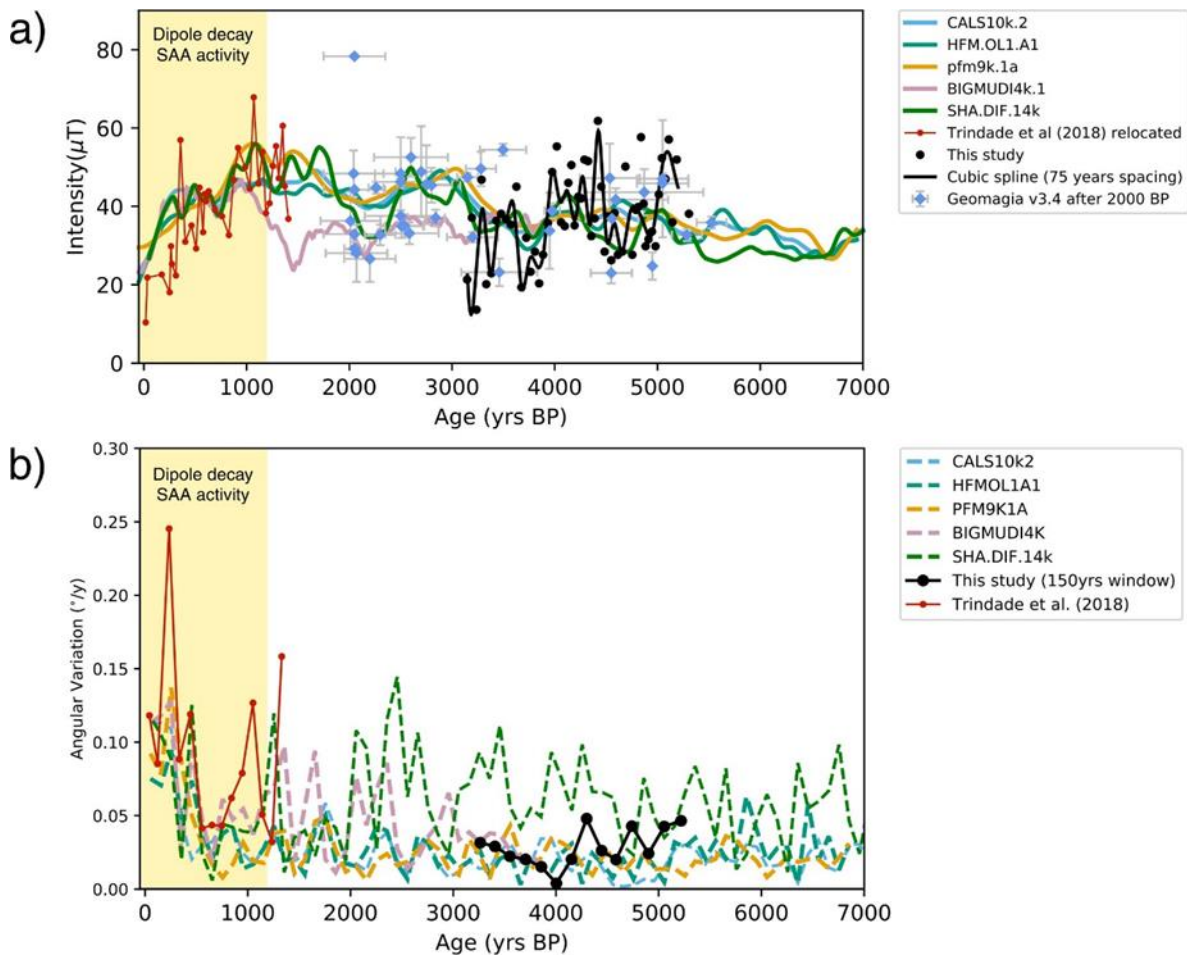
Figure 3-10: Geomagnetic field variations in central Brazil. (a) Relative paleointensity data for stalagmite DBE50 (black dots) and cubic spline fit for 75 years knots (black curve). Models: CALS10k.2 (light blue curve), HFM.OL1.A1 (green curve), pfm9k.1a (gold curve), BIGMUDI4k.1 (light pink curve), SHA.DIF.14k (dark green curve). Results from ALHO6 (Pau D'Alho cave; (Trindade et al., 2018) relocated to the Dona Benedita cave coordinates are shown in red dots. Absolute intensity (blue dots) and respective errors (bars) within a ~2000 km radius from Dona Benedita cave were obtained from Geomagia v3.4 (Brown et al., 2015). (b) Angular variation within a 150 yrs window for directions from Dona Benedita stalagmite (black dots) and Pau d'Alho cave stalagmite (red dots) showing the contrasting behavior before and after the geomagnetic dipole decay and the likely onset of SAA (yellow shade).

3.2.4   Discussion

The DBE50 speleothem contains tiny amounts of partially oxidized magnetite in a core-shell structure likely originated from the pedogenic process in the soil above the cave, and also some amount of goethite, as found in other examples worldwide (Bourne et al., 2015; Jaqueto et al., 2021; Jaqueto et al., 2016; Lascu and Feinberg, 2011; Trindade et al., 2018; Zhu et al., 2017). In contrast to lake sediments, the magnetization acquisition in speleothems is faster, and they seem to be spared of post-deposition effects (Lascu and Feinberg, 2011). As a result, the relation between radiometric dating and the age of magnetization acquisition is also more

straightforward. The homogeneity of the magnetic mineralogy observed in this case and other speleothem favor more robust relative paleointensity estimations. The high-quality directional and paleointensity record of DBE50 expands the previous records of Pau d'Alho cave speleothems collected in the same region (Trindade et al., 2018). These younger speleothems covered the last 1500 yrs and revealed fast geomagnetic field variations linked to the SAA and recurring similar features (Figure 3-9 and Figure 3-10) with angular velocities higher than 0.1°/yr in two different time intervals at ~1050 BP and ~500 BP (Figure 3-10). In contrast, the DBE50 stalagmite data reported here show no significant drops in intensity and the angular velocities are lower than 0.06°/yr for the whole interval between 3147 BP and 5306 BP. This low angular variability is predicted by almost all models, except for the SHA.DIF.14k (Figure 3-10). Taken together, the DBE50 results express a low secular variation activity in the mid-to-late Holocene in central South America (Figure 3-10). Therefore, it suggests the configuration that enabled the recurrent appearance of low intensity and strongly non-dipolar anomalies like the South Atlantic Anomaly was not being expresses at the Earth's surface in the region at that time.

The South Atlantic Anomaly is usually attributed to the motion and intensification of geomagnetic reverse flux patches (RFPs) at the core-mantle boundary (CMB) (Olson and Amit, 2006; Tarduno et al., 2015b; Terra-Nova et al., 2019; Terra-Nova et al., 2017). These features arise from the expulsion of toroidal field lines by diffusion due to flow upwelling at the top of the core (Bloxham, 1986). Normal flux patches (NFPs), on the other hand, arise from the concentration of poloidal field lines by downwelling at the edge of the tangent cylinder (Olson et al., 1999). Furthermore, geomagnetic flux patches are responsible for a significant North-South hemispherical asymmetry in the advective sources of the axial dipole moment observed nowadays (Finlay et al., 2016a; Olson and Amit, 2006). Ideally, in a pure axial dipole field, the minimum intensity is located along the geographic equator. However, the contribution of non-axial dipole field components may lead to a departure from this ideal case resulting in complex field morphologies, i.e., a weaker dipole field may result in a more prominent contribution of localized non-dipolar features such as RFPs and NFPs, leading to a significant dislocation of the field minima away from the geographic equator.

To assess the evolution of RFPs and NFPs through the last 10,000 years, we identified these features in models CALS10k.2, HFM.OL1.A1 and pfm9k.1a. Similar work was conducted for the last 3,000 years for NFPs (Amit et al., 2011) and for RFPs (Terra-Nova et al., 2015,

2016). Figure 3-11 shows our results for model CALS10k.2 (other models in Figure 3-13 and Figure 3-14). A marked contrast is observed in the occurrence of RFPs for three different time intervals (Figure 3-11). Interval #1 (50-2150 BP), which comprises the time of the South Atlantic Anomaly and other similar recurrent features, shows several RFPs in the southern hemisphere. The simultaneous tracking of the SAA minimum and RFPs and NFPs through time showed the position, motion, and amplitude of the anomaly are highly influenced by the interplay between three persistent geomagnetic flux patches: an RFP below southern South America, the South Pacific high-latitude NFP and a low-latitude intense NFP near Africa (Terra-Nova et al., 2017). These flux patches are tracked in the considered models (Figure 3-11). Interval #2 (3000-5100 BP), which corresponds to the time interval covered by the DBE50 record reported here, shows much fewer RFPs, with almost all of them in the northern hemisphere (Figure 3-11). Finally, in interval #3 (6500-8600 BP), the RFPs are more frequent, mainly located at higher latitudes in the southern hemisphere and mid-to-high latitudes in the northern hemisphere (Figure 3-11). Results obtained from models HFM.OL1.A1 (Figure 3-13) and pfm9k.1a (Figure 3-14) also show these same contrasting concentrations of RFPs between the time intervals considered.
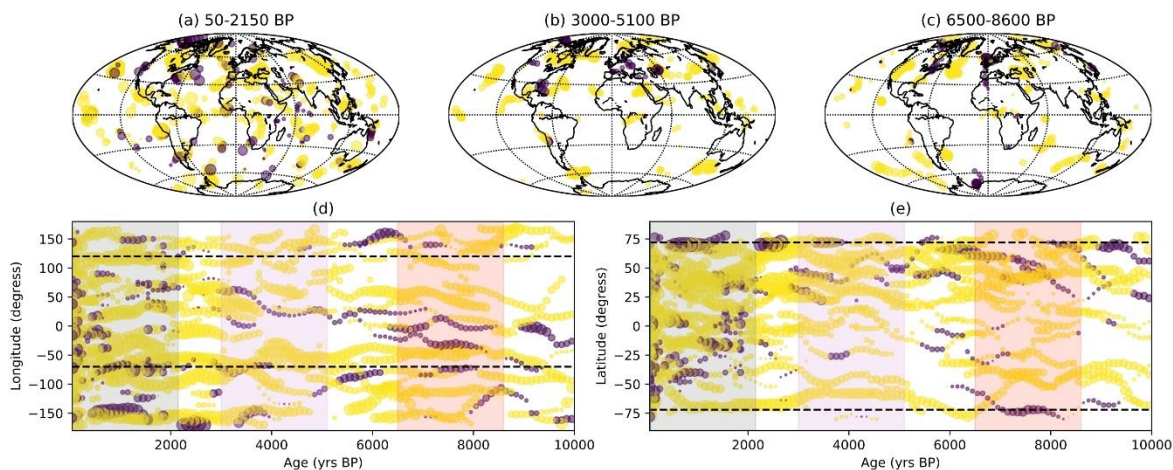

Figure 3-11: Tracking of normal (NFP) and reverse (RFP) flux patches at the core mantle boundary for model CALS10k.2 (Constable et al., 2016). (a-c) the location of NFP (yellow) and RFP (purple) for time intervals #1 (a, 50-2150 BP), #2 (b, 3000-5100 BP), #3 (c, 6500-8600 BP). (d) longitudinal evolution of NFP (yellow circles) and RFP (purple circles); dashed lines indicate the azimuth of the positive peak of shear wave velocity in the mantle (Masters et al., 2000), rectangle shades correspond to interval #1 (light grey), #2 (light purple), #3 (light red) (e) latitudinal evolution of NFP (yellow circles) and RFP (purple circles); dashed lines indicate the expected latitude of the tangent cylinder in the northern and southern hemispheres. The size of purple and yellow circles is proportional to the intensity of the flux patch. Also, the Dona Benedita results comprehends the second interval.

In all models, intense NFPs are observed throughout the past 10,000 years follow the azimuthal positions coincident with the positive peak of shear wave velocity anomalies at the

lowermost mantle (Figure 3-11) in the seismic model (Masters et al., 2000), reinforcing the strong mantle control on these features as previously signaled (Gubbins, 2003). In latitude, the normal flux-patches are limited by the expected coordinates for the tangent cylinder at 72º (Figure 3-11).

We can now consider the role of the dipole strength and the non-dipole components to the variability of the field for the considered time intervals. Figure 3-12 shows the spectral power of the dipole and non-dipole components from models CALS10k.2, HFM.OL1.A1 and pfm9k.1a. Interval #1 shows a continuous decrease of the dipole concomitant to a general increase of the non-dipole components, expressed by a relatively high non-dipole/dipole ratio of ~0.02 (Figure 3-12), which is likely the source of the high angular variations observed in the past two millennia. In contrast, interval #2, shows the lowest non-dipole/dipole ratios of the time intervals considered (Figure 3-12) and corresponds to the low angular variations recorded in Dona Benedita speleothem (Figure 3-10). In interval #3, all analyzed models show a non-dipole/dipole ratio increase to values higher than 0.02 (Figure 3-12). The DBE50 record, therefore, covers a time of quiet field activity in the South Atlantic and South America, which coincides with an interval of limited occurrence of RFPs in the southern hemisphere, when the non-dipole field components were less prominent regarding the total field. Generally, our results suggest that the occurrence of South Atlantic-like features along the mid-latitude belt of the South Atlantic is an intermittent phenomenon whose expression at the surface depends on the ratio between the dipole to non-dipole field components, as it determines the existence of the reversed flux in the southern hemisphere. This is in agreement with the intermittent SAA-like feature in a model of the geomagnetic field spanning 30–50 ka (Brown et al., 2018) and with the strongly time-dependent nature of the SAA area shape and center for the historical and modern field (Amit et al., 2021).
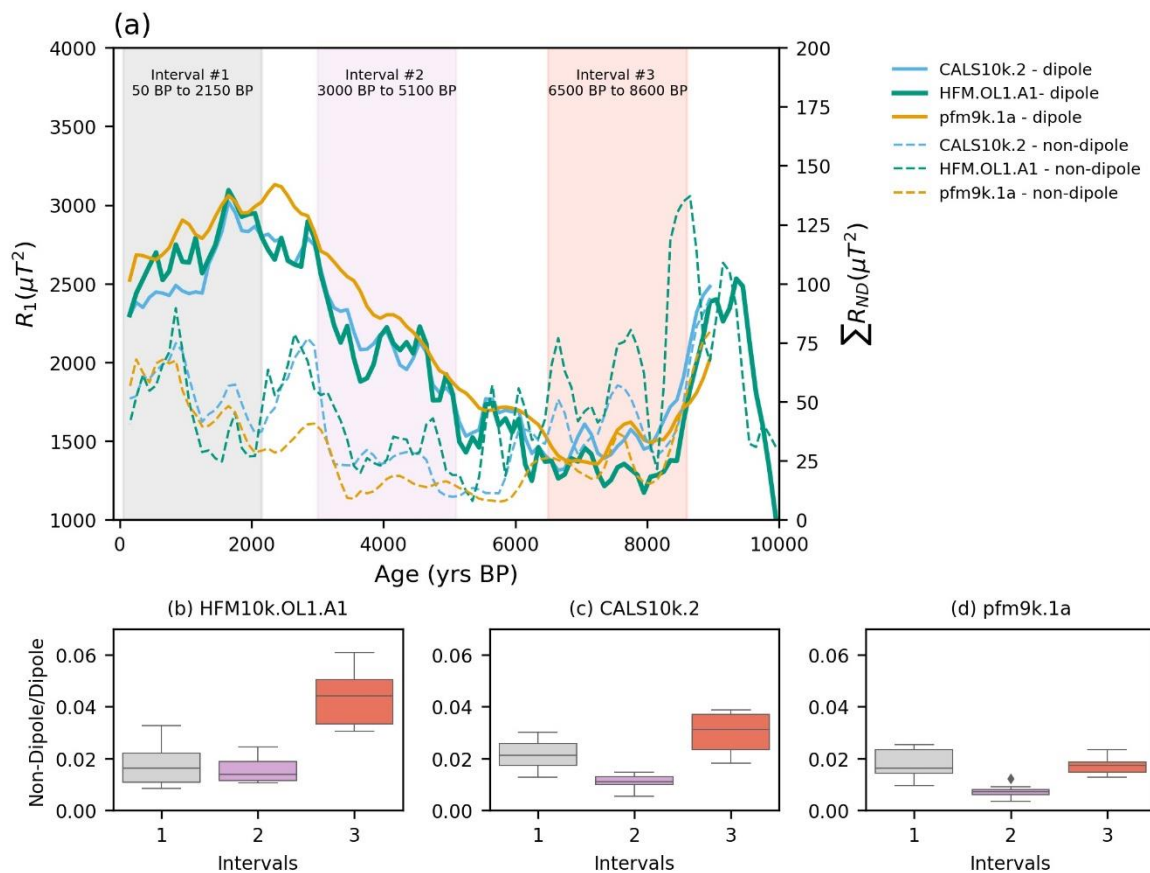
Figure 3-12: (a) Energy at Earth's surface of dipole and non-dipole moments for the past 10,000 years for models CALS10k.2 (light blue curve), HFM.OL1.A1 (green curve), pfm9k.1a (gold curve), with selected time intervals #1 (50-2150 BP, light grey), #2 (3000-5100 BP, light purple) and #3 (6500-8600 BP, light red). (b-d) boxplots for non-dipole to dipole ratios for time intervals #1, #2 and #3 for models (b) HFM.OL1.A1 (Constable et al., 2016), (c) CALS10k.2 (Constable et al., 2016) and (d) pfm9k.1a (Nilsson et al., 2014). The energy of the dipole and non-dipole and its subsequent ratio was calculated from the gauss coefficients of the models up to 10 degrees (Lowes, 1974).

3.2.5   Methods

3.2.5.1 U-Th dating and age model

Radiometric dating by the U-Th method was done at the Isotope Laboratory of the University of Minnesota (USA) and Xi'an Jiaotong University (China). A total of 14 new U-Th ages were obtained from powder samples (~100 mg) following stratigraphic horizons of the speleothem. The chemical procedure for separation of uranium (U) and thorium (Th) follows the procedure described in (Edwards et al., 1987b), and the analysis was performed in a multi-collector inductively coupled plasma mass spectrometer [NEPTUNE (Thermo-Finnigan)], following the methodology described in (Cheng et al., 2013). The final age model for DBE50

stalagmites was calculated using the software COPRA, and a linear interpolation method was adopted (Breitenbach et al., 2012).

3.2.5.2 Low-temperature remanence experiments

Stalagmites usually have a low content of magnetic minerals, so the preferred method for low-temperature experiments is to first separate the magnetic mineralogy from the carbonate matrix (Strauss et al., 2013; Strehlau et al., 2014). It consists of dissolving the carbonate in a mildly acidic buffer solution (pH ~4), followed by a flask extraction method using a Nd magnet and an orbital shaker to extract the magnetic minerals (Strehlau et al., 2014).

The extracted magnetic minerals were used in two protocols to measure low-temperature magnetic properties in a Quantum Design Magnetic Properties Measurement System (MPMS-XL) with a sensitivity of ~10^{-11} Am² at the Institute for Rock Magnetism (IRM) at the University of Minnesota. The first protocol consisted of applying a 2.5 T field during cooling from room temperature to 10 K (Field Cooled (FC)). The magnetic moment was then measured in 5 K steps during warming up to room temperature. After this cycle, the specimen was cooled up to 10 K without a field, and a 2.5 T field was imparted at 10 K (Zero Field Cooled (ZFC)), then the magnetic moment was measured in 5 K steps during warming up to room temperature. This protocol has been used to identify the presence of goethite (separation between FC-ZFC curves), low-temperature magnetic transitions, like the Verwey transition ~120 K for magnetite and Morin transition ~260 K for hematite, and also as a grain-size indicator for magnetite and its oxidation state (Jaqueto et al., 2016; Ozdemir and Dunlop, 2010; Strauss et al., 2013). The second protocol is the room-temperature saturation isothermal remanent magnetization (RTSIRM), where a pulsed field of 2.5 T was applied at room temperature, and the remanence was measured during cooling (300 K to 10 K) and warming (10 K to 300 K) at 5 K steps. The RTSIRM protocol examines those magnetic minerals that hold remanence at room temperature. It is sensitive to stoichiometric magnetite (Verwey transition) and its oxidation state (Ozdemir and Dunlop, 2010; Strauss et al., 2013). Also, goethite has been recognized by the increase in magnetization as the temperature cools by a factor of two in RTSIRM experiments (Lascu and Feinberg, 2011).

3.2.5.3 Paleomagnetism

Rock magnetic experiments were carried at the Institute for Rock Magnetism (IRM) at the University of Minnesota in a magnetically shielded room with a noise field of less than 100 nT. Remanence measurements were made in a u-channel superconducting magnetometer (2G enterprises) with an inline alternating field demagnetization device, with a noise field of less than $\sim 3.0 \times 10^{-11}$ Am². Demagnetization and acquisition of anhysteretic remanent magnetization (ARM) were carried in 25 steps up to 70 mT. For the ARM acquisition, a steady field of 0.05 mT was applied concomitant to an alternating field following the pseudo-Thellier protocol (Tauxe et al., 1995).

The analysis of directions was made with the PmagPy software (Tauxe et al., 2016) to obtain the characteristic remanent magnetization direction (ChRM) using a routine for principal component analysis (PCA) (Kirschvink, 1980). For relative paleointensity estimates, the slope obtained with ARM_{gained} by NRM_{left} (Arai plot) was calculated using the line fitting method with the software Paleointensity.org (Beguin et al., 2020). Because the sample was not azimuthally oriented in the field, the procedure adopted to reorient it was to calculate the fisher mean for the directional results and compare with the geomagnetic field model CALS10k.1b for the same period, then the difference in mean declination between them was used to rotate the declination results.

To compare the relative paleointensity (RPI) results with the absolute paleointensity record, the data were normalized following the calibration method used in the CALS7k.2 model (Korte and Constable, 2006), by multiplying the median ratio of the geomagnetic field model CALS10k.1b by the slope of the pseudo-Thellier method. The angular variation was calculated using a running mean with a 150 years window (encompassing an average of three specimens) for the angular distance between the directions divided by the time interval (Hare et al., 2018; Trindade et al., 2018).

3.2.5.4 Identification of magnetic flux-patches at the core-mantle boundary

We identified the center of flux patches, both normal (NFP) and reversed (RFP), in geomagnetic field models CALS10k.2, HFM.OL1.A1 (Constable et al., 2016) and pfm9k.1a (Nilsson et al., 2014) by defining the local maxima and minima of the radial magnetic field at the core-

mantle boundary. Following a methodology previously used in archeomagnetic field models (Terra-Nova et al., 2015), we assigned a patch as normal or reversed based on its polarity to the axial dipole and its relative position to the magnetic equator. However, here we used a different approach for the identification of the magnetic equator. We identified all null-curves of the radial magnetic field at the core-mantle boundary and assigned the magnetic equator to the one present at least once in all longitudes. This updated method is more robust than the previous strategy and fails only if the magnetic equator reaches the geographic poles. Also, no filtering technique was applied as it is different to previous geomagnetic patches identifications (Amit et al., 2011; Terra-Nova et al., 2015).

Competing interests

The authors declare no competing interests.

Data availability

All data obtained in this study is available on the MAGIC database (https://earthref.org/MagIC/16957/24ed868e-7417-489d-9b6b-cca90bfca6ca).

Acknowledgments
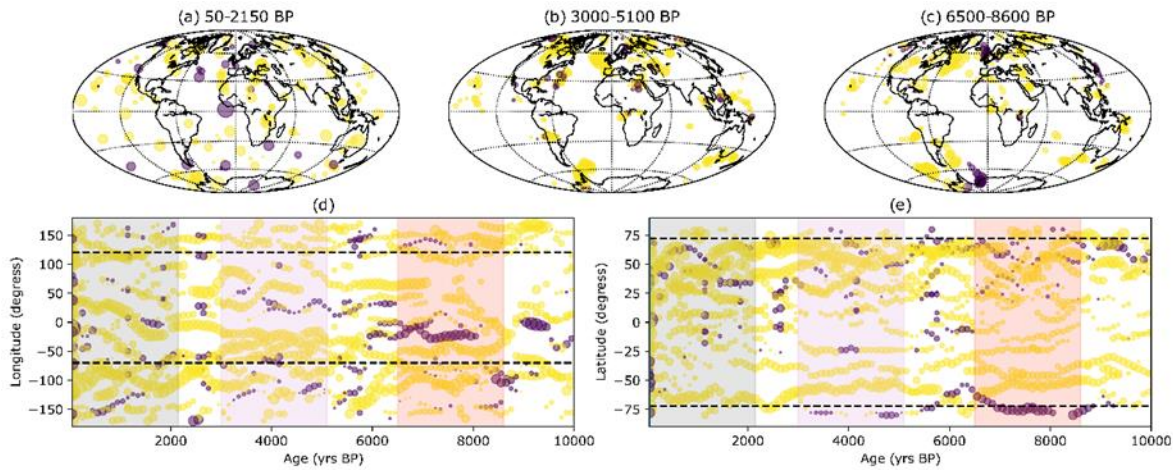
3.2.6 Article supplementary figures

Figure 3-13: Tracking of normal (NFP) and reverse (RFP) flux patches at the core mantle boundary for model HFM.OL1.A1 (Constable et al., 2016)(a-c) the location of NFP (yellow) and RFP (purple) for time intervals #1 (a, 50-2150 BP), #2 (b, 3000-5100 BP), #3 (c, 6500-8600 BP). (d) longitudinal evolution of NFP (yellow circles) and RFP (purple circles); dashed lines indicate the azimuth of the positive peak of shear wave velocity in the mantle (Masters et al., 2000), rectangle shades correspond to interval #1 (light grey), #2 (light purple), #3 (light red) (e) latitudinal evolution of NFP (yellow circles) and RFP (purple circles); dashed lines indicate the expected latitude of the tangent cylinder in the northern and southern hemispheres. The size of purple and yellow circles is proportional to the intensity of the flux patch.

Figure 3-14: Tracking of normal (NFP) and reverse (RFP) flux patches at the core mantle boundary for model pfm9k.1a (Nilsson et al., 2014) (a-c) the location of NFP (yellow) and RFP (purple) for time intervals #1 (a, 50-2150 BP), #2 (b, 3000-5100 BP), #3 (c, 6500-8600 BP). (d) longitudinal evolution of NFP (yellow circles) and RFP (purple circles); dashed lines indicate the azimuth of the positive peak of shear wave velocity in the mantle (Masters et al., 2000)(Masters et al., 2000), rectangle shades correspond to interval #1 (light grey), #2 (light purple), #3 (light red) (e) latitudinal evolution of NFP (yellow circles) and RFP (purple circles); dashed lines indicate the expected latitude of the tangent cylinder in the northern and southern hemispheres. The size of purple and yellow circles is proportional to the intensity of the flux patch.
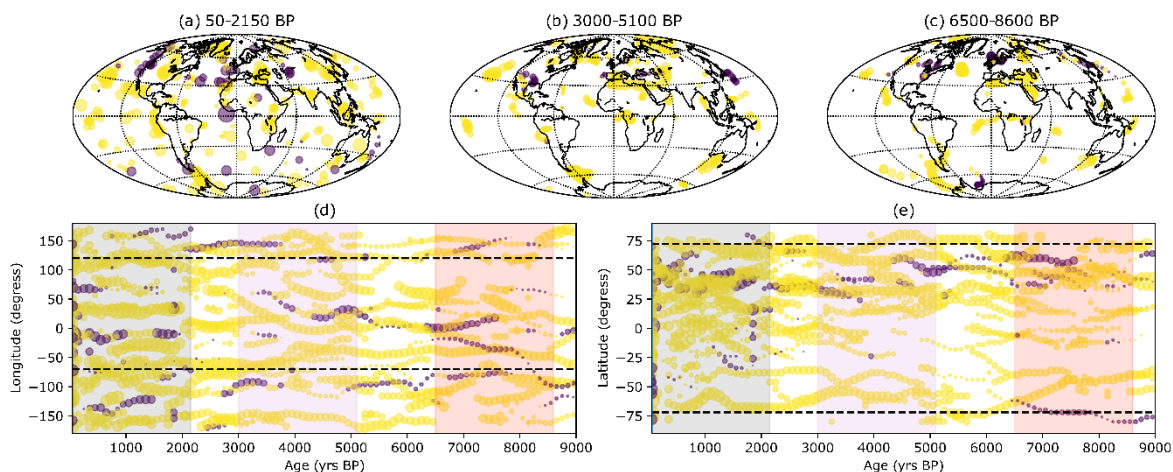
Chapter 4   Conclusions and perspectives

This thesis provides insight into the origin of magnetic minerals in speleothems and how these materials record the geomagnetic field variations. The main contribution and prospects for this topic of research are summarized below.

4.1 Karst environment and the origin of magnetic minerals

Early research in speleothem magnetism was limited to single-site studies focused on interpreting the variation of the magnetic content through time. This thesis presented a more comprehensive view of the magnetic mineralogy present in the (sub-)tropical karst system (Chapter 2). It consists of a collection of stalagmites from 22 different cave locations with various latitudes and biomes, which were later compared to soil and host carbonate in two specific sites.

The obtained results showed the dominance of low-coercivity minerals (>90%) in the magnetic signal, which corroborates previous stalagmite studies. Also, a high Spearman's rank correlation was obtained between different rock magnetic concentration parameters (mass-normalized magnetic susceptibility, natural remanent magnetization, anhysteretic remanent magnetization, and isothermal remanent magnetization). The observed correlation strengthens the interpretation of the magnetic signal as originated from the low-coercivity minerals, such as magnetite and maghemite derived from pedogenic processes in soils overlying karst systems and that those processes affecting pedogenic enhancement are pervasive in tropical zones. This relationship was also confirmed by comparing soil and host carbonate in specific sites where the dominant magnetic coercivity in the stalagmites resembles the soil but not the host carbonate. Another comparison between biomes and the speleothem magnetism database was made since the different biomes could directly affect the production of pedogenic magnetite and its local rainfall regimes. From this analysis, the Cerrado biome showed the highest concentration of magnetic minerals when compared to Caatinga, Atlantic, and Amazon biomes. This relationship can reflect the higher seasonality in Cerrado that promotes pedogenic magnetite formation and its transport through more recurrent wet and dry cycles when compared to others.

The construction of a speleothem magnetism database with good coverage in South America presented in this thesis provides a framework for future high-resolution studies using rock magnetism techniques in stalagmites. Furthermore, it facilitates interpreting the main magnetic signal as a relationship between soil formation and transport into the cave system, avoiding the interpretation of carbonate weathering and/or allochthonous sediments. Although, we bear in mind that each karst and cave system (even the same cave hall) have their own formation and development that could capture specific depositional/climatic signals.

A more sophisticated solution for high-resolution studies of magnetic signals nowadays is magnetic microscopy technology. This technique has already started to be used in stalagmites (Feinberg et al., 2020; Fu et al., 2021; Fukuyo et al., 2021). The use of magnetic microscopy would enable a better understanding of the magnetic signal in each layer (annual to sub-annual scale). It also has the potential to achieve the same or better resolution than isotopic and trace-elements investigations. However, it is worth noting that acquiring magnetic maps is very time consuming and can therefore be prohibitive for studies of an entire karst system. These new technologies could be combined with regular discrete samples in stalagmites for specific objectives. Also, to better constrain the seasonality variation, it is suggested that annual cave monitoring focusing on magnetic mineralogy should be done to improve the interpretation and separation of the different signals that can compose each stalagmite layer.

4.2 Earth's magnetic field record of stalagmites

A significant contribution of this thesis is the stalagmite record of the Earth's Magnetic Field retrieved from two caves from Brazil (Chapter 3). These are the first reported records using stalagmites for the southern hemisphere and provide good coverage for South America for the last 6,000 years.

The first study encompasses two stalagmites from the Pau d'Alho cave system in central Brazil (Trindade et al., 2018). These stalagmites provided a 1500-year record from ~1930 CE to ~500 CE with an average resolution of ~35 years per specimen. The paleomagnetic direction and relative paleointensity obtained showed a reliable record of the past inclination and declination compared to the geomagnetic field models that incorporate archeomagnetic, lava flows, and sedimentary data. The Pau D'Alho cave is located in an area of influence of the South

Atlantic Anomaly. The obtained record was able to test whether the anomaly has a recurrent feature beyond the instrumental era. The observed values of angular variation demonstrated two distinct periods with fast variation (higher than 0.10°/yr) in 860 to 960 CE and 1450 to 1750 CE. These variations match the records in South Africa with a westward time lag of ~200 years (Hare et al., 2018). These fast variations expressed in the geomagnetic field at the surface are linked to mantle heterogeneities beneath South Africa, a preferred location for re-versed flux patches at the core-mantle boundary, making this region a site for flux expulsion from the core. Synthetic models to account for the directional and intensity variations ob-served in our data showed that westward drift is the primary source of changes in declination, but also intensification and expansion of reversed flux patches are needed to reproduce the observed inclination and the decay of intensity. Also, this record showed that speleothems of-fer an alternative for archeomagnetic, lava flow and lake sediment data, where continuous di-rectional variation can be obtained without the difficulties of lock-in deposition commonly found on sedimentary strata.

A second study was conducted in a cave in Serra da Bodoquena karst area in central Brazil. The stalagmite DBE50 from Dona Benedita cave (20.57°S, 56.72°W) encompasses ~2159 years, from 3147 BP to 5306 BP, with an average specimen resolution of ~39 years. This sample showed a steady geomagnetic field for this period, which contrasts with the behavior of the last 1500 years as expressed in the first study (Trindade et al., 2018). Although few studies from South America were incorporated in the construction of the geomagnetic models, the inclination results obtained in Dona Benedita have a good correspondence with most available models. The low variability recorded in the DBE50 stalagmite can be an indicator of the dominance of dipole sources for this period. After calculating the angular variation rates, the values are lower than 0.06°/yr. It is the lowest variation on the whole Holocene for the re-gion, reinforcing the low activity of non-dipole sources at this location as also expressed by the ratio of non-dipole by dipole sources in geomagnetic field models.

To summarize, speleothems are excellent archives of the Earth's magnetic field and may al-low high-resolution (multidecadal) directional studies, especially for South America, where little data is available (<5% of the globe). Also, the possibility of using a superconducting quantum interference device microscope could enable annual resolution for these records and provide an unprecedented directional data variation for South America and other parts of the globe. As the speleothem magnetism record expands, it will be possible to constrain the

influence of heterogeneities in the core-mantle boundary expressed at the Earth's surface, and high-quality regional field models could be constructed.

Chapter 5   References

Ahmed, I.A.M., Maher, B.A., 2018. Identification and paleoclimatic significance of magnetite nanoparticles in soils. Proceedings of the National Academy of Sciences of the United States of America 115, 1736-1741.

Amit, H., 2014. Can downwelling at the top of the Earth's core be detected in the geomagnetic secular variation? Physics of the Earth and Planetary Interiors 229, 110-121.

Amit, H., Korte, M., Aubert, J., Constable, C., Hulot, G., 2011. The time-dependence of intense archeomagnetic flux patches. Journal of Geophysical Research-Solid Earth 116.

Amit, H., Terra-Nova, F., Lezin, M., Trindade, R.I., 2021. Non-monotonic growth and motion of the South Atlantic Anomaly. Earth Planets and Space 73.

Arneitz, P., Egli, R., Leonhardt, R., Fabian, K., 2019. A Bayesian iterative geomagnetic model with universal data input: Self-consistent spherical harmonic evolution for the geomagnetic field over the last 4000 years. Physics of the Earth and Planetary Interiors 290, 57-75.

Baldini, J.U.L., Lechleitner, F.A., Breitenbach, S.F.M., van Hunen, J., Baldini, L.M., Wynn, P.M., Jamieson, R.A., Ridley, H.E., Baker, A.J., Walczak, I.W., Fohlmeister, J., 2021. Detecting and quantifying palaeoseasonality in stalagmites using geochemical and modelling approaches. Quaternary Science Reviews 254.

Balsam, W.L., Ellwood, B.B., Ji, J.F., Williams, E.R., Long, X.Y., El Hassani, A., 2011. Magnetic susceptibility as a proxy for rainfall: Worldwide data from tropical and temperate climate. Quaternary Science Reviews 30, 2732-2744.

Beguin, A., Paterson, G.A., Biggin, A.J., de Groot, L.V., 2020. Paleointensity.org: An Online, Open Source, Application for the Interpretation of Paleointensity Data. Geochemistry Geophysics Geosystems 21.

Bloemendal, J., King, J.W., Hall, F.R., Doh, S.J., 1992. Rock magnetism of late Neogene and Pleistocene deep-sea sediments- relationship to sediment source, diagenetic processes, and sediment lithology. Journal of Geophysical Research-Solid Earth 97, 4361-4375.

Bloxham, J., 1986. THE EXPULSION OF MAGNETIC-FLUX FROM THE EARTHS CORE. Geophysical Journal of the Royal Astronomical Society 87, 669-678.

Bosch, R.F., White, W.B., 2004. Lithofacies and Transport of Clastic Sediments in Karstic Aquifers. Springer US, Boston, MA, pp. 1-22.

Bosch, R.F., White, W.B., 2018. Lithofacies and Transport for Clastic Sediments in Karst Conduits. Karst Groundwater Contamination and Public Health: Beyond Case Studies, 277-281.

Bourne, M.D., Feinberg, J.M., Strauss, B.E., Hardt, B., Cheng, H., Rowe, H.D., Springer, G., Edwards, R.L., 2015. Long-term changes in precipitation recorded by magnetic minerals in speleothems. Geology 43, 595-598.

Breitenbach, S.F.M., Rehfeld, K., Goswami, B., Baldini, J.U.L., Ridley, H.E., Kennett, D.J., Prufer, K.M., Aquino, V.V., Asmerom, Y., Polyak, V.J., Cheng, H., Kurths, J., Marwan, N., 2012. COnstructing Proxy Records from Age models (COPRA). Climate of the Past 8, 1765-1779.

Brown, M., Korte, M., Holme, R., Wardinski, I., Gunnarson, S., 2018. Earth's magnetic field is probably not reversing. Proceedings of the National Academy of Sciences of the United States of America 115, 5111-5116.

Brown, M.C., Donadini, F., Nilsson, A., Panovska, S., Frank, U., Korhonen, K., Schuberth, M., Korte, M., Constable, C.G., 2015. GEOMAGIA50.v3: 2. A new paleomagnetic database for lake and marine sediments. Earth Planets and Space 67, 19.

Bullard, E.C., Freedman, C., Gellman, H., Nixon, J., 1950. THE WESTWARD DRIFT OF THE EARTHS MAGNETIC FIELD. Philosophical Transactions of the Royal Society of London Series a-Mathematical and Physical Sciences 243, 67-92.

Campos, J., Cruz, F.W., Ambrizzi, T., Deininger, M., Vuille, M., Novello, V.F., Strikis, N.M., 2019. Coherent South American Monsoon Variability During the Last Millennium Revealed Through High-Resolution Proxy Records. Geophysical Research Letters 46, 8261-8270.

Chen, Q., Zhang, T.W., Wang, Y.T., Zhao, J.X., Feng, Y.X., Liao, W., Wang, W., Yang, X.Q., 2019. Magnetism Signals in a Stalagmite From Southern China and Reconstruction of Paleorainfall During the Interglacial-Glacial Transition. Geophysical Research Letters 46, 6918-6925.

Cheng, H., Edwards, R.L., Shen, C.C., Polyak, V.J., Asmerom, Y., Woodhead, J., Hellstrom, J., Wang, Y.J., Kong, X.G., Spotl, C., Wang, X.F., Alexander, E.C., 2013. Improvements in Th-230 dating, Th-230 and U-234 half-life values, and U-Th isotopic measurements by multi-collector inductively coupled plasma mass spectrometry. Earth and Planetary Science Letters 371, 82-91.

Chou, Y.M., Jiang, X.Y., Liu, Q.S., Hu, H.M., Wu, C.C., Liu, J.X., Jiang, Z.X., Lee, T.Q., Wang, C.C., Song, Y.F., Chiang, C.C., Tan, L.C., Lone, M.A., Pan, Y.X., Zhu, R.X., He, Y.Q., Chou, Y.C., Tan, A.H., Roberts, A.P., Zhao, X., Shen, C.C., 2018. Multidecadally resolved polarity oscillations during a geomagnetic excursion. Proceedings of the National Academy of Sciences of the United States of America 115, 8913-8918.

Coe, R.S., 1967. DETERMINATION OF PALEO-INTENSITIES OF EARTHS MAGNETIC FIELD WITH EMPHASIS ON MECHANISMS WHICH COULD CAUSE NON-IDEAL BEHAVIOR IN THELLIERS METHOD. Journal of Geomagnetism and Geoelectricity 19, 157-&.

Constable, C., Korte, M., Panovska, S., 2016. Persistent high paleosecular variation activity in southern hemisphere for at least 10 000 years. Earth and Planetary Science Letters 453, 78-86.

Cruz, F.W., Burns, S.J., Karmann, I., Sharp, W.D., Vuille, M., Cardoso, A.O., Ferrari, J.A., Dias, P.L.S., Viana, O., 2005. Insolation-driven changes in atmospheric circulation over the past 116,000 years in subtropical Brazil. Nature 434, 63-66.

Cruz, F.W., Burns, S.J., Karmann, I., Sharp, W.D., Vuille, M., Ferrari, J.A., 2006. A stalagmite record of changes in atmospheric circulation and soil processes in the Brazilian subtropics during the Late Pleistocene. Quaternary Science Reviews 25, 2749-2761.

Donadini, F., Korte, M., Constable, C.G., 2009. Geomagnetic field for 0-3 ka: 1. New data sets for global modeling. Geochemistry Geophysics Geosystems 10, 28.

Dreybrodt, W., 1999. Chemical kinetics, speleothem growth and climate. Boreas 28, 347-356.

Dreybrodt, W., Eisenlohr, L., Madry, B., Ringer, S., 1997. Precipitation kinetics of calcite in the system $CaCO_3$-H_2O-CO_2: The conversion to CO_2 by the slow process $H^+ + HCO_3^- \rightarrow CO_2 + H_2O$ as a rate limiting step. Geochimica Et Cosmochimica Acta 61, 3897-3904.

Dreybrodt, W., Scholz, D., 2011. Climatic dependence of stable carbon and oxygen isotope signals recorded in speleothems: From soil water to speleothem calcite. Geochimica Et Cosmochimica Acta 75, 734-752.

Edwards, R.L., Chen, J.H., Wasserburg, G.J., 1987a. ^{238}U- ^{234}U- ^{230}Th- ^{232}Th systematics and the precise measurement of time over the past 500,000 years. Earth and Planetary Science Letters 81, 175-192.

Edwards, R.L., Chen, J.H., Wasserburg, G.J., 1987b. U-238 U-234-TH-230-TH-232 SYSTEMATICS AND THE PRECISE MEASUREMENT OF TIME OVER THE PAST 500000 YEARS. Earth and Planetary Science Letters 81, 175-192.

Egli, R., 2004a. Characterization of individual rock magnetic components by analysis of remanence curves, 1. Unmixing natural sediments. Studia Geophysica Et Geodaetica 48, 391-446.

Egli, R., 2004b. Characterization of individual rock magnetic components by analysis of remanence curves. 2. Fundamental properties of coercivity distributions. Physics and Chemistry of the Earth 29, 851-867.

Egli, R., Lowrie, W., 2002. Anhysteretic remanent magnetization of fine magnetic particles. Journal of Geophysical Research-Solid Earth 107, 21.

Egli, R., Zhao, X., 2015. Natural remanent magnetization acquisition in bioturbated sediment: General theory and implications for relative paleointensity reconstructions. Geochemistry Geophysics Geosystems 16, 995-1016.

Evans, M., Heller, F., 2003. Environmental magnetism: principles and applications of enviromagnetics. Elsevier.

Fairchild, I.J., Baker, A., 2012. Speleothem science : from process to past environments. Wiley, Hoboken, N.J.

Fairchild, I.J., Smith, C.L., Baker, A., Fuller, L., Spotl, C., Mattey, D., McDermott, F., Eimp, 2006. Modification and preservation of environmental signals in speleothems. Earth-Science Reviews 75, 105-153.

Fassbinder, J.W.E., Stanjek, H., Vali, H., 1990. Occurence of magnetic bacteria in soil. Nature 343, 161-163.

Feinberg, J.M., Lascu, I., Lima, E.A., Weiss, B.P., Dorale, J.A., Alexander, E.C., Edwards, R.L., 2020. Magnetic detection of paleoflood layers in stalagmites and implications for historical land use changes. Earth and Planetary Science Letters 530, 115946.

Finlay, C.C., Aubert, J., Gillet, N., 2016a. Gyre-driven decay of the Earth's magnetic dipole. Nature Communications 7.

Finlay, C.C., Aubert, J., Gillet, N., 2016b. Gyre-driven decay of the Earth's magnetic dipole. Nature Communications 7, 8.

Fisher, R., 1953. DISPERSION ON A SPHERE. Proceedings of the Royal Society of London Series a-Mathematical and Physical Sciences 217, 295-305.

Fohlmeister, J., Voarintsoa, N.R.G., Lechleitner, F.A., Boyd, M., Brandtstatter, S., Jacobson, M.J., Oster, J.L., 2020. Main controls on the stable carbon isotope composition of speleothems. Geochimica Et Cosmochimica Acta 279, 67-87.

Font, E., Veiga-Pires, C., Pozo, M., Carvallo, C., Neto, A.C.D., Camps, P., Fabre, S., Mirao, J., 2014. Magnetic fingerprint of southern Portuguese speleothems and implications for paleomagnetism and environmental magnetism. Journal of Geophysical Research-Solid Earth 119, 7993-8020.

Fu, R.R., Hess, K., Jaqueto, P., Novello, V.F., Kukla, T., Trindade, R.I.F., Strikis, N.M., Cruz, F.W., Ben Dor, O., 2021. High-Resolution Environmental Magnetism Using the Quantum Diamond Microscope (QDM): Application to a Tropical Speleothem. Frontiers in Earth Science 8.

Fukuyo, N., Oda, H., Yokoyama, Y., Clark, G., Yamamoto, Y., 2021. High spatial resolution magnetic mapping using ultra-high sensitivity scanning SQUID microscopy on a speleothem from the Kingdom of Tonga, southern Pacific. Earth Planets and Space 73.

Garreaud, R.D., Vuille, M., Compagnucci, R., Marengo, J., 2009. Present-day South American climate. Palaeogeography Palaeoclimatology Palaeoecology 281, 180-195.

Ge, K.P., Williams, W., Liu, Q.S., Yu, Y., 2014. Effects of the core-shell structure on the magnetic properties of partially oxidized magnetite grains: Experimental and micromagnetic investigations. Geochemistry Geophysics Geosystems 15, 2021-2038.

Gogorza, C.S.G., Irurzun, M.A., Chaparro, M.A.E., Lirio, J.M., Nunez, H., Bercoff, P.G., Sinito, A.M., 2006. Relative paleointensity of the geomagnetic field over the last 21,000 years BP from sediment cores, Lake El Trebol (Patagonia, Argentina). Earth Planets and Space 58, 1323-1332.

Gogorza, C.S.G., Lirio, J.M., Nunez, H., Chaparro, M., Bertorello, H.R., Sinito, A.M., 2004. Paleointensity studies on holocene-pleistocene sediments from Lake Escondido, Argentina. Physics of the Earth and Planetary Interiors 145, 219-238.

Gonzalez-Lopez, A., Campuzano, S.A., Molina-Cardin, A., Pavon-Carrasco, F.J., De Santis, A., Osete, M.L., 2021. Characteristic periods of the paleosecular variation of the Earth?s magnetic field during the Holocene from global paleoreconstructions. Physics of the Earth and Planetary Interiors 312.

Goree, W.S., Fuller, M., 1976. MAGNETOMETERS USING RF-DRIVEN SQUIDS AND THEIR APPLICATIONS IN ROCK MAGNETISM AND PALEOMAGNETISM. Reviews of Geophysics 14, 591-608.

Gornitz, V., 2009. Paleoclimate Proxies, An Introduction, in: Gornitz, V. (Ed.), Encyclopedia of Paleoclimatology and Ancient Environments. Springer Netherlands, Dordrecht, pp. 716-721.

Gubbins, D., 2003. Thermal Core-Mantle Interactions: Theory and Observations, Earth's Core: Dynamics, Structure, Rotation, pp. 163-179.

Gubbins, D., Jones, A.L., Finlay, C.C., 2006. Fall in Earth's magnetic field is erratic. Science 312, 900-902.

Hare, V.J., Tarduno, J.A., Huffman, T., Watkeys, M., Thebe, P.C., Manyanga, M., Bono, R.K., Cottrell, R.D., 2018. New Archeomagnetic Directional Records From Iron Age Southern Africa (ca. 425-1550 CE) and Implications for the South Atlantic Anomaly. Geophysical Research Letters 45, 1361-1369.

Hartmann, A., Baker, A., 2017. Modelling karst vadose zone hydrology and its relevance for paleoclimate reconstruction. Earth-Science Reviews 172, 178-192.

Hartmann, A., Goldscheider, N., Wagener, T., Lange, J., Weiler, M., 2014. Karst water resources in a changing world: Review of hydrological modeling approaches. Reviews of Geophysics 52, 218-242.

Hartmann, G.A., Afonso, M.C., Trindade, R.I.F., 2011. Preliminary Results of Magnetic Archaeointensity Measurements in Brazil. Springer Berlin Heidelberg, Berlin, Heidelberg, pp. 495-499.

Hartmann, G.A., Pacca, I.G., 2009. Time evolution of the South Atlantic Magnetic Anomaly. Anais Da Academia Brasileira De Ciencias 81, 243-255.

Hatfield, R.G., 2014. Particle Size-Specific Magnetic Measurements as a Tool for Enhancing Our Understanding of the Bulk Magnetic Properties of Sediments. Minerals 4, 758-787.

Heirtzler, J.R., 2002. The future of the South Atlantic anomaly and implications for radiation damage in space. Journal of Atmospheric and Solar-Terrestrial Physics 64, 1701-1708.

Heslop, D., 2015. Numerical strategies for magnetic mineral unmixing. Earth-Science Reviews 150, 256-284.

Heslop, D., Roberts, A.P., 2013. Calculating uncertainties on predictions of palaeoprecipitation from the magnetic properties of soils. Global and Planetary Change 110, 379-385.

Heslop, D., Roberts, A.P., 2016. Analyzing paleomagnetic data: To anchor or not to anchor? Journal of Geophysical Research-Solid Earth 121, 7742-7753.

Hu, P., Heslop, D., Viscarra Rossel, R.A., Roberts, A.P., Zhao, X., 2019. Continental-scale magnetic properties of surficial Australian soils. 103028.

Inokuchi, H., Morinaga, H., Yaskawa, K., 1981. PRELIMINARY-REPORT ON PALEOMAGNETISM OF CAVE DEPOSIT. Journal of Geomagnetism and Geoelectricity 33, 325-327.

Jackson, A., Jonkers, A.R.T., Walker, M.R., 2000. Four centuries of geomagnetic secular variation from historical records. Philosophical Transactions of the Royal Society of London Series a-Mathematical Physical and Engineering Sciences 358, 957-990.

Jackson, M.J., Banerjee, S.K., Marvin, J.A., Lu, R., Gruber, W., 1991. DETRITAL REMANENCE, INCLINATION ERRORS, AND ANHYSTERETIC REMANENCE ANISOTROPY - QUANTITATIVE MODEL AND EXPERIMENTAL RESULTS. Geophysical Journal International 104, 95-103.

Jaqueto, P., Trindade, R.I.F., Feinberg, J.M., Carmo, J., Novello, V.F., Stríkis, N.M., Cruz, F.W., Shimizu, M.H., Karmann, I., 2021. Magnetic Mineralogy of Speleothems From Tropical-Subtropical Sites of South America. Frontiers in Earth Science 9.

Jaqueto, P., Trindade, R.I.F., Hartmann, G.A., Novello, V.F., Cruz, F.W., Karmann, I., Strauss, B.E., Feinberg, J.M., 2016. Linking speleothem and soil magnetism in the Pau d'Alho cave (central South America). Journal of Geophysical Research-Solid Earth 121, 7024-7039.

Jelínek, V., Kropáček, V., 1978. Statistical processing of anisotropy of magnetic susceptibility measured on groups of specimens. Studia Geophysica et Geodaetica 22, 50-62.

Jordanova, N., 2017. Soil Magnetism: Applications in Pedology, Environmental Science and Agriculture. Soil Magnetism: Applications in Pedology, Environmental Science and Agriculture, 1-445.

Kirschvink, J.L., 1980. THE LEAST-SQUARES LINE AND PLANE AND THE ANALYSIS OF PALEOMAGNETIC DATA. Geophysical Journal of the Royal Astronomical Society 62, 699-718.

Korte, M., Constable, C., Donadini, F., Holme, R., 2011. Reconstructing the Holocene geomagnetic field. Earth and Planetary Science Letters 312, 497-505.

Korte, M., Constable, C.G., 2006. On the use of calibrated relative paleointensity records to improve millennial-scale geomagnetic field models. Geochemistry Geophysics Geosystems 7.

Korte, M., Donadini, F., Constable, C.G., 2009. Geomagnetic field for 0-3 ka: 2. A new series of time-varying global models. Geochemistry Geophysics Geosystems 10, 24.

Lachniet, M.S., 2009. Climatic and environmental controls on speleothem oxygen-isotope values. Quaternary Science Reviews 28, 412-432.

Lascu, I., Feinberg, J.M., 2011. Speleothem magnetism. Quaternary Science Reviews 30, 3306-3320.

Lascu, I., Feinberg, J.M., Dorale, J.A., Cheng, H., Edwards, R.L., 2016. Age of the Laschamp excursion determined by U-Th dating of a speleothem geomagnetic record from North America. Geology 44, 139-142.

Latham, A.G., Ford, D.C., Schwarcz, H.P., Birchall, T., 1989. SECULAR VARIATION FROM MEXICAN STALAGMITES - THEIR POTENTIAL AND PROBLEMS. Physics of the Earth and Planetary Interiors 56, 34-48.

Latham, A.G., Schwarcz, H.P., Ford, D.C., 1980. PALEOMAGNETISM AND DATING OF LATE PLEISTOCENE STALAGMITES FROM ENGLAND AND MEXICO. Geophysical Journal of the Royal Astronomical Society 61, 212-212.

Latham, A.G., Schwarcz, H.P., Ford, D.C., 1986a. SECULAR VARIATION STUDIES FROM VANCOUVER ISLAND STALAGMITES. Geophysical Journal of the Royal Astronomical Society 85, 258-259.

Latham, A.G., Schwarcz, H.P., Ford, D.C., 1986b. THE PALEOMAGNETISM AND U-TH DATING OF MEXICAN STALAGMITE, DAS2. Earth and Planetary Science Letters 79, 195-207.

Latham, A.G., Schwarcz, H.P., Ford, D.C., Pearce, G.W., 1979. Paleomagnetism of stalagmite deposits. Nature 280, 383-385.

Lean, C.B., Latham, A.G., Shaw, J., 1995. Palaeosecular variation from a Vancouver-Island stalagmite and comparison with contemporary North-American records. Journal of Geomagnetism and Geoelectricity 47, 71-87.

Lerner, G.A., Smirnov, A.V., Surovitckii, L.V., Piispa, E.J., 2017. Nonheating methods for absolute paleointensity determination: Comparison and calibration using synthetic and natural magnetite-bearing samples. Journal of Geophysical Research-Solid Earth 122, 1614-1633.

Lowes, F.J., 1974. Spatial Power Spectrum of the Main Geomagnetic Field, and Extrapolation to the Core. Geophysical Journal International 36, 717-730.

Maher, B.A., 1998. Magnetic properties of modern soils and Quaternary loessic paleosols: paleoclimatic implications. Palaeogeography Palaeoclimatology Palaeoecology 137, 25-54.

Maher, B.A., 2011. The magnetic properties of Quaternary aeolian dusts and sediments, and their palaeoclimatic significance. Aeolian Research 3, 87-144.

Maher, B.A., Taylor, R.M., 1988. Formation of ultrafine-grained magnetite in soils. Nature 336, 368-370.

Maher, B.A., Thompson, R., 1999. Quaternary climates, environments, and magnetism. Cambridge University Press, Cambridge, UK ; New York.

Masters, G., Laske, G., Bolton, H., Dziewonski, A., 2000. The Relative Behavior of Shear Velocity, Bulk Sound Speed, and Compressional Velocity in the Mantle: Implications for Chemical and Thermal Structure, Earth's Deep Interior: Mineral Physics and Tomography From the Atomic to the Global Scale, pp. 63-87.

Maxbauer, D.P., Feinberg, J.M., Fox, D.L., 2016a. Magnetic mineral assemblages in gills and paleosols as the basis for paleoprecipitation proxies: A review of magnetic methods and challenges. Earth-Science Reviews 155, 28-48.

Maxbauer, D.P., Feinberg, J.M., Fox, D.L., 2016b. MAX UnMix: A web application for unmixing magnetic coercivity distributions. Computers & Geosciences 95, 140-145.

Maxbauer, D.P., Feinberg, J.M., Fox, D.L., Nater, E.A., 2017. Response of pedogenic magnetite to changing vegetation in soils developed under uniform climate, topography, and parent material. Scientific Reports 7, 10.

Metman, M.C., Livermore, P.W., Mound, J.E., 2018. The reversed and normal flux contributions to axial dipole decay for 1880-2015. Physics of the Earth and Planetary Interiors 276, 106-117.

Meyer, K.W., Feng, W.M., Breecker, D.O., Banner, J.L., Guilfoyle, A., 2014. Interpretation of speleothem calcite delta C-13 variations: Evidence from monitoring soil CO2, drip water, and modern speleothem calcite in central Texas. Geochimica Et Cosmochimica Acta 142, 281-298.

Morinaga, H., Inokuchi, H., Yaskawa, K., 1985. PALEOMAGNETISM AND PALEOTEMPERATURE OF A STALAGMITE. Journal of Geomagnetism and Geoelectricity 37, 823-828.

Morinaga, H., Inokuchi, H., Yaskawa, K., 1986. MAGNETIZATION OF A STALAGMITE IN AKIYOSHI PLATEAU AS A RECORD OF THE GEOMAGNETIC SECULAR VARIATION IN WEST JAPAN. Journal of Geomagnetism and Geoelectricity 38, 27-44.

Morinaga, H., Inokuchi, H., Yaskawa, K., 1989. Paleomagnetism of Stalagmites (Speleothems) in SW Japan. Geophysical Journal-Oxford 96, 519-528.

Nilsson, A., Holme, R., Korte, M., Suttie, N., Hill, M., 2014. Reconstructing Holocene geomagnetic field variation: new methods, models and implications. Geophysical Journal International 198, 229-248.

Novello, V.F., Cruz, F.W., McGlue, M.M., Wong, C.I., Ward, B.M., Vuille, M., Santos, R.A., Jaqueto, P., Pessenda, L.C.R., Atorre, T., Ribeiro, L., Karmann, I., Barreto, E.S., Cheng, H., Edwards, R.L., Paula, M.S., Scholz, D., 2019. Vegetation and environmental changes in tropical South America from the last glacial to the Holocene documented by multiple cave sediment proxies. Earth and Planetary Science Letters 524.

Novello, V.F., da Cruz, F.W., Vuille, M., Campos, J., Strikis, N.M., Apaestegui, J., Moquet, J.S., Azevedo, V., Ampuero, A., Utida, G., Wang, X.F., Paula-Santos, G.M., Jaqueto, P., Pessenda, L.C.R., Breecker, D.O., Karmann, I., 2021. Investigating delta C-13 values in stalagmites from tropical South America for the last two millennia. Quaternary Science Reviews 255.

Novello, V.F., Vuille, M., Cruz, F.W., Strkis, N.M., de Paula, M.S., Edwards, R.L., Cheng, H., Karmann, I., Jaqueto, P.F., Trindade, R.I.F., Hartmann, G.A., Moquet, J.S., 2016. Centennial-scale solar forcing of the South American Monsoon System recorded in stalagmites. Scientific Reports 6, 8.

Olson, D.M., Dinerstein, E., Wikramanayake, E.D., Burgess, N.D., Powell, G.V.N., Underwood, E.C., D'Amico, J.A., Itoua, I., Strand, H.E., Morrison, J.C., Loucks, C.J., Allnutt, T.F., Ricketts, T.H., Kura, Y., Lamoreux, J.F., Wettengel, W.W., Hedao, P., Kassem, K.R.,

2001. Terrestrial ecoregions of the worlds: A new map of life on Earth. Bioscience 51, 933-938.

Olson, P., Amit, H., 2006. Changes in earth's dipole. Naturwissenschaften 93, 519-542.

Olson, P., Christensen, U., Glatzmaier, G.A., 1999. Numerical modeling of the geodynamo: Mechanisms of field generation and equilibration. Journal of Geophysical Research-Solid Earth 104, 10383-10404.

Openshaw, S., Latham, A., Shaw, J., 1997. Speleothem palaeosecular variation records from China: Their contribution to the coverage of Holocene palaeosecular variation data in east Asia. Journal of Geomagnetism and Geoelectricity 49, 485-505.

Osete, M.L., Martin-Chivelet, J., Rossi, C., Edwards, R.L., Egli, R., Munoz-Garcia, M.B., Wang, X.F., Pavon-Carrasco, F.J., Heller, F., 2012. The Blake geomagnetic excursion recorded in a radiometrically dated speleothem. Earth and Planetary Science Letters 353, 173-181.

Ozdemir, O., Dunlop, D.J., 2010. Hallmarks of maghemitization in low-temperature remanence cycling of partially oxidized magnetite nanoparticles. Journal of Geophysical Research-Solid Earth 115.

Ozdemir, O., Dunlop, D.J., Moskowitz, B.M., 1993. THE EFFECT OF OXIDATION ON THE VERWEY TRANSITION IN MAGNETITE. Geophysical Research Letters 20, 1671-1674.

Panovska, S., Korte, M., Finlay, C.C., Constable, C.G., 2015. Limitations in paleomagnetic data and modelling techniques and their impact on Holocene geomagnetic field models. Geophysical Journal International 202, 402-418.

Pavon-Carrasco, F.J., De Santis, A., 2016. The South Atlantic Anomaly: The Key for a Possible Geomagnetic Reversal. Frontiers in Earth Science 4, 1-9.

Pavon-Carrasco, F.J., Osete, M.L., Torta, J.M., De Santis, A., 2014. A geomagnetic field model for the Holocene based on archaeomagnetic and lava flow data. Earth and Planetary Science Letters 388, 98-109.

Perkins, A.M., 1996. Observations under electron microscopy of magnetic minerals extracted from speleothems. Earth and Planetary Science Letters 139, 281-289.

Perkins, A.M., Maher, B.A., 1993. Rock magnetic and paleomagnetic studies of British speleothems. Journal of Geomagnetism and Geoelectricity 45, 143-153.

Poletti, W., Trindade, R.I.F., Hartmann, G.A., Damiani, N., Rech, R.M., 2016. Archeomagnetism of Jesuit Missions in South Brazil (1657-1706 AD) and assessment of the South American database. Earth and Planetary Science Letters 445, 36-47.

Ponte, J.M., Font, E., Veiga-Pires, C., Hillaire-Marcel, C., 2018. Speleothems as Magnetic Archives: Paleosecular Variation and a Relative Paleointensity Record From a Portuguese Speleothem. Geochemistry Geophysics Geosystems 19, 2962-2972.

Ponte, J.M., Font, E., Veiga-Pires, C., Hillaire-Marcel, C., Ghaleb, B., 2017. The effect of speleothem surface slope on the remanent magnetic inclination. Journal of Geophysical Research-Solid Earth 122, 4143-4156.

Pozzi, J.P., Rousseau, L., Falgueres, C., Mahieux, G., Deschamps, P., Shao, Q.F., Kachi, D., Bahain, J.J., Tozzi, C., 2019. U-Th dated speleothem recorded geomagnetic excursions in the Lower Brunhes. Scientific Reports 9.

Regattieri, E., Zanchetta, G., Isola, I., Zanella, E., Drysdale, R.N., Hellstrom, J.C., Zerboni, A., Dallai, L., Tema, E., Lanci, L., Costa, E., Magri, F., 2019. Holocene Critical Zone dynamics in an Alpine catchment inferred from a speleothem multiproxy record: disentangling climate and human influences. Scientific Reports 9.

Ribeiro, J., Sano, S., Macedo, J., da Silva, J., 1983. Os principais tipos fisionômicos da região dos cerrados. v. 21, Planaltina. Boletim de Pesquisa, EMBRAPA/CPAC.

Roberts, A.P., 2015. Magnetic mineral diagenesis. Earth-Science Reviews 151, 1-47.

Roberts, A.P., Hu, P.X., Harrison, R.J., Heslop, D., Muxworthy, A.R., Oda, H., Sato, T., Tauxe, L., Zhao, X., 2019. Domain State Diagnosis in Rock Magnetism: Evaluation of Potential Alternatives to the Day Diagram. Journal of Geophysical Research-Solid Earth 124, 5286-5314.

Roberts, A.P., Tauxe, L., Heslop, D., 2013. Magnetic paleointensity stratigraphy and high-resolution Quaternary geochronology: successes and future challenges. Quaternary Science Reviews 61, 1-16.

Rochette, P., Mathe, P.E., Esteban, L., Rakoto, H., Bouchez, J.L., Liu, Q.S., Torrent, J., 2005. Non-saturation of the defect moment of goethite and fine-grained hematite up to 57 Teslas. Geophysical Research Letters 32.

Roperch, P., Chauvin, A., Lara, L.E., Moreno, H., 2015. Secular variation of the Earth's magnetic field and application to paleomagnetic dating of historical lava flows in Chile. Physics of the Earth and Planetary Interiors 242, 65-78.

Ruddiman, W.F., 2008. Earth's climate : past and future, 2nd ed. W.H. Freeman, New York.

Sallun, W., Karmann, I., 2007. Geomorphological map of the Serra da Bodoquena karst, west-central Brazil. Journal of Maps, 282-295.

Schmidt, V., Gunther, D., Hirt, A.M., 2006. Magnetic anisotropy of calcite at room-temperature. Tectonophysics 418, 63-73.

Scholz, D., Hoffmann, D.L., 2011. StalAge - An algorithm designed for construction of speleothem age models. Quaternary Geochronology 6, 369-382.

Strauss, B.E., Strehlau, J.H., Lascu, I., Dorale, J.A., Penn, R.L., Feinberg, J.M., 2013. The origin of magnetic remanence in stalagmites: Observations from electron microscopy and rock magnetism. Geochemistry Geophysics Geosystems 14, 5006-5025.

Strehlau, J.H., Hegner, L.A., Strauss, B.E., Feinberg, J.M., Penn, R.L., 2014. SIMPLE AND EFFICIENT SEPARATION OF MAGNETIC MINERALS FROM SPELEOTHEMS AND OTHER CARBONATES. Journal of Sedimentary Research 84, 1096-1106.

Tarduno, J.A., Watkeys, M.K., Huffman, T.N., Cottrell, R.D., Blackman, E.G., Wendt, A., Scribner, C.A., Wagner, C.L., 2015a. Antiquity of the South Atlantic Anomaly and evidence for top-down control on the geodynamo. Nature Communications 6, 6.

Tarduno, J.A., Watkeys, M.K., Huffman, T.N., Cottrell, R.D., Blackman, E.G., Wendt, A., Scribner, C.A., Wagner, C.L., 2015b. Antiquity of the South Atlantic Anomaly and evidence for top-down control on the geodynamo. Nature Communications 6.

Tauxe, L., 1993. SEDIMENTARY RECORDS OF RELATIVE PALEOINTENSITY OF THE GEOMAGNETIC-FIELD - THEORY AND PRACTICE. Reviews of Geophysics 31, 319-354.

Tauxe, L., Kent, D.V., 2004. A simplified statistical model for the geomagnetic field and the detection of shallow bias in paleomagnetic inclinations: Was the ancient magnetic field dipolar? Timescales of the Paleomagnetic Field 145, 101-115.

Tauxe, L., Pick, T., Kok, Y.S., 1995. Relative paleointensity in sediments - a pseudo-Thellier approach. Geophysical Research Letters 22, 2885-2888.

Tauxe, L., Shaar, R., Jonestrask, L., Swanson-Hysell, N.L., Minnett, R., Koppers, A.A.P., Constable, C.G., Jarboe, N., Gaastra, K., Fairchild, L., 2016. PmagPy: Software package for paleomagnetic data analysis and a bridge to the Magnetics Information Consortium (MagIC) Database. Geochemistry Geophysics Geosystems 17, 2450-2463.

Tauxe, L., Staudigel, H., 2004. Strength of the geomagnetic field in the Cretaceous Normal Superchron: New data from submarine basaltic glass of the Troodos Ophiolite. Geochemistry Geophysics Geosystems 5.

Tauxe, L., Steindorf, J.L., Harris, A., 2006. Depositional remanent magnetization: Toward an improved theoretical and experimental foundation. Earth and Planetary Science Letters 244, 515-529.

Terra-Nova, F., Amit, H., Choblet, G., 2019. Preferred locations of weak surface field in numerical dynamos with heterogeneous core-mantle boundary heat flux: consequences for the South Atlantic Anomaly. Geophysical Journal International 217, 1179-1199.

Terra-Nova, F., Amit, H., Hartmann, G.A., Trindade, R.I.F., 2015. The time dependence of reversed archeomagnetic flux patches. Journal of Geophysical Research-Solid Earth 120, 691-704.

Terra-Nova, F., Amit, H., Hartmann, G.A., Trindade, R.I.F., 2016. Using archaeomagnetic field models to constrain the physics of the core: robustness and preferred locations of reversed flux patches. Geophysical Journal International 206, 1890-1913.

Terra-Nova, F., Amit, H., Hartmann, G.A., Trindade, R.I.F., Pinheiro, K.J., 2017. Relating the South Atlantic Anomaly and geomagnetic flux patches. Physics of the Earth and Planetary Interiors 266, 39-53.

Thebault, E., Finlay, C.C., Beggan, C.D., Alken, P., Aubert, J., Barrois, O., Bertrand, F., Bondar, T., Boness, A., Brocco, L., Canet, E., Chambodut, A., Chulliat, A., Coisson, P., Civet, F., Du, A., Fournier, A., Fratter, I., Gillet, N., Hamilton, B., Hamoudi, M., Hulot, G., Jager, T., Korte, M., Kuang, W., Lalanne, X., Langlais, B., Leger, J.M., Lesur, V., Lowes, F.J., Macmillan, S., Mandea, M., Manoj, C., Maus, S., Olsen, N., Petrov, V., Ridley, V., Rother, M., Sabaka, T.J., Saturnino, D., Schachtschneider, R., Sirol, O., Tangborn, A., Thomson, A., Toffner-Clausen, L., Vigneron, P., Wardinski, I., Zvereva, T., 2015. International Geomagnetic Reference Field: the 12th generation. Earth Planets and Space 67, 19.

Trindade, R.I.F., Jaqueto, P., Terra-Nova, F., Brandt, D., Hartmann, G.A., Feinberg, J.M., Strauss, B.E., Novello, V.F., Cruz, F.W., Karmann, I., Cheng, H., Edwards, R.L., 2018. Speleothem record of geomagnetic South Atlantic Anomaly recurrence. Proceedings of the National Academy of Sciences, 201809197.

Whitmore, T.C., Prance, G.T., 1987. Biogeography and Quaternary history in tropical America. Clarendon Press.

Wong, C.I., Breecker, D.O., 2015. Advancements in the use of speleothems as climate archives. Quaternary Science Reviews 127, 1-18.

Xie, S.C., Evershed, R.P., Huang, X.Y., Zhu, Z.M., Pancost, R.D., Meyers, P.A., Gong, L.F., Hu, C.Y., Huang, J.H., Zhang, S.H., Gu, Y.S., Zhu, J.Y., 2013. Concordant monsoon-driven postglacial hydrological changes in peat and stalagmite records and their impacts on prehistoric cultures in central China. Geology 41, 827-830.

Zanella, E., Tema, E., Lanci, L., Regattieri, E., Isola, I., Hellstrom, J.C., Costa, E., Zanchetta, G., Drysdale, R.N., Magri, F., 2018. A 10,000 yr record of high-resolution Paleosecular Variation from a flowstone of Rio Martino Cave, Northwestern Alps, Italy. Earth and Planetary Science Letters 485, 32-42.

Zhu, Z.M., Feinberg, J.M., Xie, S.C., Bourne, M.D., Huang, C.J., Hu, C.Y., Cheng, H., 2017. Holocene ENSO-related cyclic storms recorded by magnetic minerals in speleothems of central China. Proceedings of the National Academy of Sciences of the United States of America 114, 852-857.